2020

Visualizing Protease Activation, Retrochmp3 Activity, and VPR Recruitment During HIV-1 Assembly

Kate Bredbenner

VISUALIZING PROTEASE ACTIVATION, RETROCHMP3 ACTIVITY, AND VPR RECRUITMENT DURING HIV-1 ASSEMBLY

A Thesis Presented to the Faculty of
The Rockefeller University
in Partial Fulfillment of the Requirements for
the degree of Doctor of Philosophy

by
Kate Bredbenner
June 2020

VISUALIZING PROTEASE ACTIVATION, RETROCHMP3 ACTIVITY, AND VPR RECRUITMENT DURING HIV-1 ASSEMBLY

Kate Bredbenner, Ph.D.
The Rockefeller University 2020

This thesis covers my contributions to the field of HIV-1 assembly and the field of science communication. Over the course of my studies, I have determined when the HIV-1 protease becomes active during the assembly of new virions, elucidated the mechanism by which the protein retroCHMP3 has an antiviral function, and examined the kinetics of recruitment of the HIV-1 accessory protein Vpr. I have also added significantly to science communication research through a study which evaluated the effectiveness of science summary methods.

HIV-1 virions assemble at the plasma membrane of infected cells. The assembly of new viruses is driven by the HIV-1 Gag structural polyprotein and involves a number of viral and host proteins to produce infectious virions. Although many of these factors have been studied extensively, there are still steps during viral assembly that have yet to be fully characterized.

In Chapter 2 of this thesis, I will discuss my study of the activation of the HIV-1 protease which is necessary for infectious particle production. Previous research has suggested that protease becomes active prior to scission of the particle from the cell, but there was no study which specifically measured protease activation and its cleavage of Gag during the assembly process. The timing of protease activation and Gag cleavage directly affects particle morphology and infectivity. Using polarization TIRF microscopy, I have directly measured protease activation and Gag cleavage. My results suggest that protease becomes active prior to recruitment of the host ESCRT proteins and scission from the cell.

Chapter 3 of this thesis describes my work on the protein retroCHMP3, which was performed in collaboration with Sundquist lab at the University of Utah. The retroCHMP3 protein was originally found in squirrel monkeys and is a truncated and mutated version of the endogenous CHMP3 ESCRT protein. Data from the Sundquist lab shows that retroCHMP3 inhibits the budding of many ESCRT-dependent viruses, including HIV-1, while not preventing essential ESCRT-dependent cell functions such as cytokinesis. To determine the mechanism of retroCHMP3, I used TIRF imaging to show that retroCHMP3 alters ESCRT recruitment to sites of HIV-1 assembly. This altered recruitment suggests that a delay in scission occurs when retroCHMP3 is present in cells. My results also suggest that there is a loss of HIV-1 proteins back into the cell due to protease activation as assayed by loss of fluorescence. As a confirmation of these results, I show that this loss of fluorescence was rescued by genetic inactivation of the protease. We suspect that the retroCHMP3 alteration of ESCRT function affects viral budding more than cellular events like cytokinesis due to the need for viruses to assemble quickly to avoid cellular defense mechanisms and loss of viral proteins from protease activation.

My final contribution to the HIV-1 field is a study of the recruitment kinetics of the HIV-1 accessory protein Vpr. My study of Vpr will also be presented in Chapter 3 of this thesis. Vpr is a protein which increases infectivity in infected animals and humans. It is packaged specifically into virions through interactions with the Gag protein. Through simultaneous TIRF imaging of Gag and Vpr, I was able to show that Vpr has a delayed accumulation compared to Gag, suggesting that Vpr is not bound to Gag before coming to the membrane. This work hints at possible interactions between Vpr and the host ESCRT proteins which have recruitment sites close to the Vpr recruitment site.

Finally, Chapter 4 of this thesis will show my findings regarding the effectiveness of different science summaries. Science summaries like video abstracts, graphical abstracts, and plain language summaries all help with accessibility of research papers. To study the efficacy of each of those summaries, I created a survey which showed participants video abstracts, graphical abstracts, plain language summaries, and academic abstracts from two HIV-1 research papers. My findings suggested that video abstracts and plain language summaries are both effective ways to summarize scientific research while graphical abstracts and academic abstracts are not as effective.

After presenting all of my work in Chapters 2-4, I will discuss the implications and immediate future directions of each contribution I have made. These discussions will be in Chapter 5 of this thesis.

For the family I was given,
the family I have made,
and the friends I'll cherish always

Acknowledgments

No work is accomplished alone, and the work I'm presenting in this thesis is no exception. I have many co-workers, family, and friends to thank for supporting me through my life and through my PhD.

Firstly, thanks to every member of the Simon Lab past and present. Whether we did experiments together, talked about life, or I bothered you to submit your information to Bagel and Birthdays, you are a key part of my success. A special thanks to Xiao for helping me plan the student retreat (oof), keeping my feline companion alive, and being a great person to have a drink with. Thanks to Joan, Gabriella, and Melissa for reading my thesis and providing feedback. Thanks also to Joan for taking a chance on imaging HIV with me. It's a great feeling when you have one of your co-workers become such a close friend. At work and outside of it, I'm lucky to have you. My knowledge of HIV-1 and how to do any of my experiments all comes from Marina, Dan, and Michelle. Working with you three was a dream. Thanks to Marcello for being a wizard with funding and for keeping the lab stocked, and of course to Sandy for his mentorship and support through the years. I would never have been able to start a YouTube career and do research on science communication in addition to my bench work in any other lab but Sandy's. His strong understanding of not only how important the research is, but how important it is to be able to explain and share it is something every researcher should have.

I would also like to thank the Dean's Office for accommodating my strange requests and for helping me become the best possible graduate student I could be. I would also like to thank Paul Bieniasz and Vanessa Ruta for many challenging conversations over the years which have always pushed me to make my research better than it was before. To my wonderful collaborators, Lara Rheinemann and Wes Sundquist, you have shown me what a successful and open collaboration in science looks like. It was an honor to work with both of you and I will carry the lessons I have learned from you forward into my next career.

Next I would like to thank my family. Thanks to my wonderful parents Mary and Rusty. You both inspire me to find happiness wherever it might be and to not worry about what other people might think. To my grandparents Bunny, Doug, Mary, and David. I treasure the time we have spent together, and I think about you all often. To my 7 uncles, 5 aunts, and 18 cousins, growing up with you helped make me the person I am today. You are the best family I could ask for. Finally, to my new-found family the Brennas and Firestones. I was already the luckiest person with the Browns and Bredbenners in my life, but now I have more than I ever thought possible.

This acknowledgements section would not be complete without thanking my friends. To my wonderful Rochester friends who taught me the meaning of Meliora. With every year that goes by, our friendships are indeed ever better. To my Rockefeller friends who have been right there by my side for this crazy PhD rollercoaster, our

shared struggles have only made us closer and your support has meant everything. And finally, thanks to my assorted NYC friends. We met in all kinds of places through all kinds of connections and my world is a much richer and fuller place because of you.

Last, but of course not least, thank you to my life partner Jonathan. We met when we were 19 and stupid. I had no idea then that you would be the best part of my life, but you really are unquestionably the absolute best part. You've given me countless laughs and pep talks, and you're a wonderful father to our cat, Nova. There is nothing that I can't do without you there by my side holding me up. Even get a PhD.

Table of Contents

Acknowledgments ..... **iv**
Table of Contents ..... **vi**
List of Figures ..... **viii**
List of Tables ..... **x**
List of Abbreviations ..... **xi**
Chapter 1 Introduction **1**
1.1 HIV-1 Life Cycle 2
1.1.1 General Overview 2
1.1.2 Assembly of HIV-1 at the Plasma Membrane 2
Gag 2
HIV-1 Genome 3
ESCRTs 4
Pol 5
Vif, Nef, and Vpr 6
Tat, Rev, and Vpu 7
1.2 Role of Protease and Maturation 8
1.2.1 Role of Protease in the HIV-1 Life Cycle 8
1.2.2 Structure and Function of Protease 8
1.2.3 Regulation of Protease 11
1.3 retroCHMP3 11
1.4 TIRF Imaging 13
1.4.1 General TIRF Overview 13
1.4.2 Polarized TIRF Overview 13
1.5 Summarizing Scientific Work 14
Chapter 2 Measuring Protease Activation and Gag Cleavage **16**
2.1 Past attempts to measure protease activation and Gag cleavage 17
2.1.1 FRET 17
2.1.2 Cleavage-sensitive reporters 21
2.2 Measuring Gag cleavage with Anisotropy 26
2.2.1 Anisotropy is compatible with TIRF Imaging 26
2.2.2 Anisotropy can detect structural differences in HIV-1 VLPs 28
2.2.3 HIV-1 Protease activation occurs during assembly of new particles 36
Chapter 3 Further Characterization of Events during Assembly **39**
3.1 retroCHMP3 interacts with ESCRTs during assembly 40
3.1.1 retroCHMP3 has antiviral activity without cellular toxicity 40
3.1.2 retroCHMP3 affects the recruitment of ESCRT proteins to HIV-1 assembly sites 43
3.2 Vpr co-assembles with Gag 51
3.2.1 Vpr is incorporated into VLPs 51
3.2.2 Vpr co-assembles with GagPol 54
Chapter 4 How to summarize a graduate career studying HIV-1 ..... **57**
4.1 Brief Methods for Study 58
4.2 Survey Participants and Preferences 58

4.3 Video and Plain Language Summaries are the most effective regardless of Career 62
4.4 Strong correlations exist between reported learning preferences and summary ranks 65
4.5 Reported understanding and comprehension show strong correlations for Takata et al. summaries 68
Chapter 5 Implications and Future Directions 71
5.1 Gag Cleavage Discussion 72
5.2 retroCHMP3 Discussion 75
5.3 Vpr Discussion 77
5.4 Discussion of how to summarize a graduate career studying HIV-1 78
Chapter 6 Materials and Methods 80
6.1 Cell Maintenance 81
6.2 VLP Collection 81
6.3 Biochemistry 81
6.4 Imaging 82
6.5 Image Processing, Plotting, and Statistics 83
6.5.1 Vpr 83
6.5.2 retroCHMP3 83
6.5.3 Protease 84
FRET Imaging 84
Anisotropy Assemblies 84
Anisotropy VLPs 85
Anisotropy Control Cells 85
6.6 Plasmids 86
6.6.1 Vpr Plasmids 86
6.6.2 retroCHMP3 Plasmids 88
6.6.3 Protease Plasmids 90
FRET 90
Cleavage-sensitive reporters 92
Anisotropy 94
6.7 Protease Inhibitors 96
6.8 Survey Methods 96
6.8.1 Science Summary Design 96
6.8.2 Survey Design 98
6.8.3 Survey Recruitment 103
6.8.4 Survey Analysis 104
References 105

List of Figures

Chapter 1

Figure 1.1 Diagram of HIV-1 assembly at the plasma membrane 3
Figure 1.2 Diagram of ESCRT Recruitment 5
Figure 1.3 Schematic of HIV-1 GagPol 6
Figure 1.4 Crystal structure of HIV-1 protease 10
Figure 1.5 Schematic of CHMP3 variants 12

Chapter 2

Figure 2.1 FRET efficiencies of different pairings 18
Figure 2.2 Schematic of FRET constructs 19
Figure 2.3 Western blot of VLPs with FRET constructs 20
Figure 2.4 FRET efficiencies of Syngag constructs 21
Figure 2.5 Schematic of cleavage-sensitive reporters 23
Figure 2.6 Western blot of ZipGFP cleavage 24
Figure 2.7 Western blot of FPX system cleavage 25
Figure 2.8 Anisotropy of control constructs 27
Figure 2.9 Anisotropy at different TIRF angles with control constructs 28
Figure 2.10 Schematic of GagPol anisotropy contructs 29
Figure 2.11 Westerns of GagPol anisotropy constructs 31
Figure 2.12 Anisotropy of VLPs 32
Figure 2.13 Intensity and anisotropy of GagPol-mEGFP-MA VLPs with decreasing TIRF angles 33
Figure 2.14 Intensity and anisotropy of GagPol-mEGFP-DC VLPs with decreasing TIRF angles 34
Figure 2.15 77/70 degree intensity ratio of VLPs 35
Figure 2.16 Intensity and anisotropy of GagPol-mEGFP-MA during assembly .. 37
Figure 2.17 Intensity and anisotropy of GagPol-mEGFP-DC during assembly .. 38

Chapter 3

Figure 3.1 retroCHMP3 affects viral budding 41
Figure 3.2 retroCHMP3 is non-toxic 42
Figure 3.3 CHMP4B recruitment with and without retroCHMP3 45
Figure 3.4 VPS4A recruitment with and without retroCHMP3 47
Figure 3.5 Fluorescence is lost in assemblies with retroCHMP3 50
Figure 3.6 Schematic of GagPol plasmids 51
Figure 3.7 Vpr is packaged specifically into VLPs 53
Figure 3.8 GagPol with and without the LXXLF mutation 55
Figure 3.9 Assembly traces of GagPol and Vpr 56

Chapter 4

Figure 4.1 Participant reported preferences 61
Figure 4.2 All data from all summaries 63
Figure 4.3 Correlations between reported preference and summary values 67
Figure 4.4 Heat maps of reported undersatnding versus comprehension score 69

Chapter 5

Figure 5.1 New diagram of HIV-1 protease activation 72

Chapter 6

Figure 6.1 Flowchart of survey assignment and pooling 99

List of Tables

Chapter 4

Table 4.1 Participant numbers for Cohn et al. and Takata et al. 59

Chapter 6

Table 6.1 Primary antibodies used in this work 82
Table 6.2 Primers for Vpr constructs 87
Table 6.3 Primers for retroCHMP3 constructs 89
Table 6.4 Primers for FRET protease constructs 91
Table 6.5 Primers for cleavage-sensitive reporter constructs 93
Table 6.6 Primers for protease anisotropy constructs 95
Table 6.7 Readability of published abstracts and plain language summaries for Cohn et al. and Takata et al. 97
Table 6.8 Follow up questions for Cohn et al. and Takata et al. 101

List of Abbreviations

MA	Matrix
CA	Capsid
SP1	Spacer Peptide 1
NC	Nucleocapsid
SP2	Spacer Peptide 2
PR	Protease
RT	Reverse Transcriptase
IN	Integrase
FRET	Förster resonance energy transfer
FPX	Fluorescent protein exchange
TIRF	Total internal reflection fluorescence
VLPs	Virus-like particles
XFP	Example fluorescent protein
WT	Wild-type
PI-WT	Protease inhibited wild-type
EOM	electrooptic modifier
nt/nts	nucleotide/nucleotides
RRE	Rev response element
LoG	Laplacian of Gaussian

Chapter 1
Introduction

The main focus of this thesis is on determining the kinetics of a variety of viral and host factors that are involved in the genesis of new HIV-1 viruses. It also has a secondary focus on how scientists should summarize their research. This introductory chapter will describe the lifecycle of HIV-1 and how new viruses are assembled in addition to discussing how we as scientists summarize our research.

I will begin this chapter by broadly introducing the HIV-1 lifecycle before narrowing down to an in-depth view of the viral and host proteins involved in the assembly of new particles. This introduction will provide necessary information for Chapter 3 of this thesis. Chapter 3 will show my contributions to our knowledge about the HIV-1 accessory protein Vpr and also include the characterization of a newly discovered protein called retroCHMP3 which works by interactions with the host ESCRT proteins.

Following the overview of the HIV-1 lifecycle, I will introduce what is known about the HIV-1 protease and its importance in creating fully infectious viruses. This section will provide background information necessary for Chapter 2 of this thesis. Chapter 2 will discuss past attempts to characterize the kinetics of protease activation and Gag cleavage, along with a successful attempt to measure protease activation and Gag cleavage using polarized TIRF microscopy.

After the discussion of HIV-1, I will give an overview of our total internal reflection fluorescence (TIRF) microscopy setup and the advantages of using TIRF to study HIV-1 assembly, which will be a key part of the data presented in Chapters 2 and 3. I will also introduce the special form of TIRF with polarization which will be important for my study of the protease in Chapter 2.

Finally, I will close this introductory chapter by discussing how to effectively summarize scientific research, like the HIV-1 research presented in this thesis. Chapter 5 of this thesis is my attempt to determine which methods for summarizing scientific research are the most efficient. This work was done to lower the activation energy for scientists, publishers, and editors to connect the research done in labs to the outside world.

1.1 HIV-1 Life Cycle

1.1.1 General Overview

HIV-1 affects over 30 million people around the globe and more than a million people in the United States alone (UNAIDS, 2019). The virus replicates by targeting the immune cells of its human host and inserting its genetic material into the DNA of the infected cell. The immune cells that are prone to infection are vital to immune system function including CD4+ helper T cells, macrophages, and dendritic cells (Cavrois et al., 2007; Fontenot et al., 2009; Kahn and Walker, 1998; Yu et al., 2008). In advanced stages of HIV-1 infection, patients enter a condition called acquired immunodeficiency syndrome, also known as AIDS, which is characterized by a failure of the immune system to protect from opportunistic pathogens and cancers.

HIV-1 is part of the retrovirus family, and it has an envelope and two copies of its single-stranded positive-sense RNA genome. On the outside of each HIV-1 virus are several copies of the Env proteins, gp120 and gp41, which bind to the CD4 receptor along with either the CCR5 or CXCR4 co-receptor (Feng et al., 1996; Kahn and Walker, 1998; Maddon et al., 1986). Two copies of the HIV-1 RNA genome are packaged and protected within a capsid conical shell, which prevents the RNA from being degraded in the cytosol (Gamble et al., 1997).

After entry into the cell, the HIV-1 RNA must be reverse transcribed into DNA and inserted into the DNA of its host. HIV-1 has a virally encoded reverse transcriptase which reverse transcribes the HIV-1 RNA to DNA (Varmus, 1988), and an integrase which integrates the newly reverse transcribed viral DNA into the host DNA (Brown et al., 1989). Once the viral DNA is inserted, the cell host machinery begins to transcribe the HIV-1 DNA. Some of the newly transcribed HIV-1 RNA remains whole to be packaged into new viruses, but other HIV-1 RNAs are spliced to be translated into protein to drive HIV-1 assembly (Stoltzfus, 2009).

1.1.2 Assembly of HIV-1 at the Plasma Membrane

Gag

Chapters 2 and 3 of this thesis focus on events that take place during the process of HIV-1 assembly. Assembly of new viruses takes place at the plasma membrane of the infected cell (Jouvenet et al., 2006). HIV-1 encodes for the Gag structural polyprotein which drives assembly by polymerizing to create a spherical bud. Gag consists of four proteins and two spacer peptides. The four proteins are matrix (MA), capsid (CA), nucleocapsid (NC), and p6 (Figure 1.1A). The first spacer peptide (SP1) is between CA and NC, and the second spacer peptide (SP2) is between NC and p6.

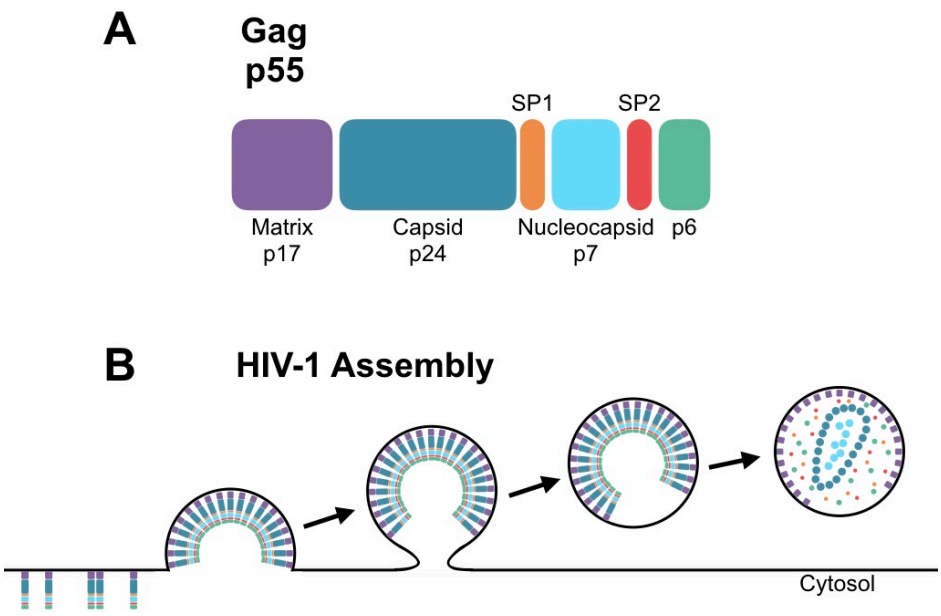

Figure 1.1 Diagram of HIV-1 assembly at the plasma membrane
HIV-1 Gag (p55) is shown in **A** with each domain labelled with name and size. A diagram of HIV-1 assembly at the plasma membrane is shown in **B**.

The Gag polyprotein is targeted to the plasma membrane by myristoylation of MA (Gottlinger et al., 1989; Mammano et al., 1995) and polymerization is driven mainly by interactions between CA (Gamble et al., 1997) (Figure 1.1B). After a threshold of Gag is reached in the cytosol, assembly of new HIV-1 viruses begins. It takes 5-25 minutes between the arrival of the HIV-1 genome and assembly of the Gag protein, and each virus contains an estimated 2400 Gag polyproteins (Carlson et al., 2008; Jouvenet et al., 2008; Jouvenet et al., 2009).

HIV-1 Genome

The nucleating force for Gag assembly is the HIV-1 RNA which comes to the plasma membrane along with a few attached Gag polyproteins (Jouvenet et al., 2009). The NC domain in Gag is responsible for binding and directing the packaging of two viral RNAs per virion (Bieniasz, 2009). NC binds to the 120-nt ψ sequence on the HIV-1 RNA in the 5' untranslated region of the HIV-1 genome (Clever et al., 1995; Harrison and Lever, 1992; Lever et al., 1989; Luban and Goff, 1994). This ψ sequence is interrupted during splicing of HIV-1 RNA to create transcripts that code for the Env and other accessory proteins. This interruption leads to only full-length HIV-1 RNA being packaged into virions. Both Gag and GagPol are translated from unspliced HIV-1 RNA, but the other HIV-1 proteins are translated from over 50 identified mRNA splice variants (Stoltzfus, 2009).

In addition to the ψ sequence, the HIV-1 RNA has binding sites for several other accessory proteins. The TAR hairpin at nts 1-55 is the binding site of Tat, and the Rev response element (RRE) at nts 7362-7596 is the binding site for Rev. Rev binds to the RRE and allows for export of unspliced HIV-1 mRNA from the nucleus (Chang and Sharp, 1989; Fischer et al., 1995). The genome also has a primer-binding site at nts 182-199 that is necessary for initiation of reverse transcription and a dimerization site at nts 248-271 that helps with packaging of two genomic RNAs.

ESCRTs

After recruitment of the genomic viral RNA and near completion of the Gag shell, host ESCRT proteins are recruited to sites of assembly via domains in p6 to help the new particle scission from the cell (Morita et al., 2011). Host ESCRT proteins are found in groups 0-III and sequential recruitment of the ESCRT components allows for membrane scission in various cellular contexts. ESCRT-mediated scission occurs during cytokinesis, during membrane repair, and during membrane budding (Hurley, 2015). HIV-1 hijacks the ESCRT complexes to help with membrane scission during viral budding, but not all members of the ESCRT pathway are necessary (Figure 1.2). ESCRT-I/TSG101 and Alix both bind directly to the p6 domain of Gag (Morita et al., 2011). The PTAP motif recruits TSG101 (Garrus et al., 2001; Martin-Serrano et al., 2001) and the YPXL motif recruits Alix (Fisher et al., 2007; Martin-Serrano et al., 2003; Strack et al., 2003; Von Schwedler et al., 2003). TSG101 and Alix then recruit members of the ESCRT-III complex. ESCRT-III members CHMP2 (either A or B variant) and CHMP4B are necessary for scission (Morita et al., 2011). ESCRT-III members CHMP1 and CHMP3 are thought to help viral scission but are mostly dispensable for the process (Morita et al., 2011).

All ESCRT-III members have five alpha-helix core structures, and they form rings or spirals within the neck of the budding virion to help provide the motive force for scission (Cashikar et al. 2014; Fabrikant et al., 2009; Johnson et al., 2018; Lata et al., 2008; Morita et al., 2011; Wollert et al. 2009). Finally, the hexameric AAA+ ATPase VPS4A/B is required to either come to recycle the ESCRT-III components or to help actively remodel them for scission (Cashikar et al. 2014; Fabrikant et al., 2009; Johnson et al., 2018; Lata et al., 2008; Saksena et al., 2009; Wollert et al. 2009). The exact interactions between VPS4A/B and the ESCRT-III components are still an active area of investigation. Without recruitment of TSG101, Alix, ESCRT-III proteins, and VPS4A/B, HIV-1 viruses are not able to leave the cell (Morita et al., 2011).

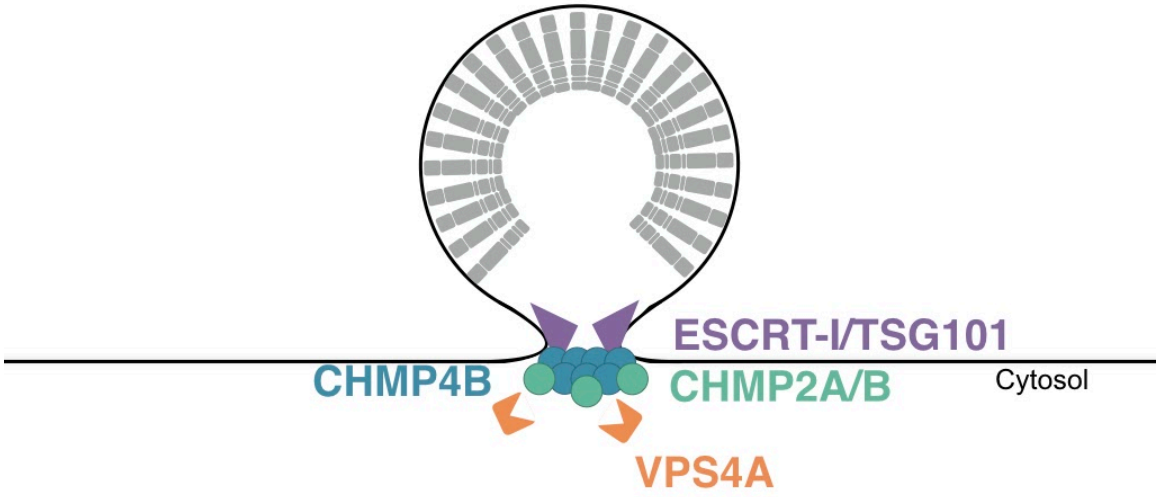

Figure 1.2 Diagram of ESCRT recruitment
A diagram of ESCRT recruitment to sites of assembly. ESCRT-I is recruited first followed by CHMP4B and CHMP2A/B. Finally, VPS4A is recruited to disassemble/remodel the complex.

Pol

In addition to the Gag polyprotein, there are also the three Pol proteins. The three Pol proteins are protease (PR), reverse transcriptase (RT), and integrase (IN), and they are produced as a single polyprotein when a -1 ribosomal frameshift occurs during the translation of Gag mRNA (Figure 1.3). The -1 ribosomal frameshift is mediated by a pseudoknot combined with a slippage site within SP2, meaning that GagPol polyproteins contain MA, CA, SP1, NC, PR, RT, and IN proteins in that order (Cassan et al., 1994; Jacks et al., 1988). The slippage to create GagPol happens during 5% of translations which leads to a 1:20 ratio of GagPol:Gag (Cassan et al., 1994; Jacks et al., 1988). Much like Gag, GagPol is directed to the membrane via a myristoylation of MA and the polymerization is driven via CA interactions. Unlike Gag, GagPol also contains the Pol proteins which are each known to dimerize or form higher order multimers. However, it has been reported that the stability of protease dimerization while it is attached to the rest of Gag is weaker than free protease dimers (Louis et al., 1999).

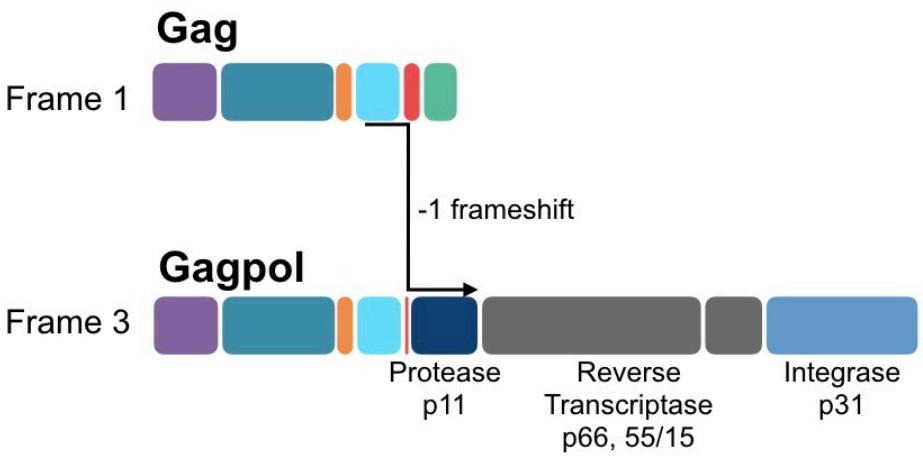

Figure 1.3 Schematic of HIV-1 GagPol
This schematic shows Gag in frame 1 and the Pol proteins in frame 3. In 5% of translations, the ribosome slips back 1 nucleotide and moves from translating Gag in frame 1 to Pol in frame 3 creating the GagPol polyprotein.

Vif, Nef, and Vpr

In addition to the Gag and Pol proteins, there are six other accessory proteins. Three of these six are found in the released viruses. These three are Vif, Nef, and Vpr. Vif is a 192-amino acid protein that binds to the host defense protein APOBEC3G and facilitates its degradation through polyubiquitination (Kao et al., 2003; Liu et al., 2004; Marin et al., 2003; Sheehy et al., 2002; Sheehy et al., 2003; Yu et al., 2003). APOBEC3G functions as a cytidine deaminase which induces hypermutation of the viral cDNA when Vif is not present (Harris et al., 2003; Lecossier et al., 2003; Mangeat et al., 2003; Zhang et al., 2003). It has also been reported that Vif is incorporated into viruses through interactions with the HIV-1 RNA (Khan et al., 2001).

Nef is a 206-amino acid protein involved in reducing the cellular level of CD4 to prevent repeat infection by another HIV-1 virus (Aiken et al., 1994; Luo et al., 1996; Schwartz et al., 1995). It has also been reported to have several other possible functions in intracellular trafficking, where it helps with viral release and infectivity, but this is an ongoing area of research (Pereira and daSilva, 2016). Like MA, Nef is myristoylated and it is suspected that Nef is incorporated into viruses through its membrane interactions (Bentham et al., 2006; Bukovsky et al., 1997; Pandori et al., 1996; Welker et al., 1996; Welker et al., 1998).

Vpr is a 96-amino acid protein that is not required for infection in cell culture, but it has been shown to have an impact on infection rates in macaques (Gibbs et al., 1995; Hirsch et al., 1998). It is packaged into viruses through interaction with the LXXLF motif on p6 (Jenkins et al., 2001; Kondo and Gottlinger, 1996), and it has proposed functions including influences on nuclear entry of viral proteins (Gallay et al., 1996; Heinzinger et al., 1994) and induction of G2/M cell cycle arrest or cell apoptosis (Chang et al., 2004;

Hrimech et al., 1999; Poon et al., 1998), but this is still an active area of investigation. In Chapter 3.2 of this thesis, I will talk about my contributions to our knowledge about Vpr. Because Vpr is packaged through interaction with Gag, it has been a frequent choice for inserting proteins into HIV-1 particles in-trans. Previous researchers have used Vpr to deliver PR, IN, and RT into virions outside of their typical packing as fusions to Gag (Bouyac-Bertoia et al., 2001; Fletcher et al., 1997; Liu et al., 1997; Wu et al., 1996; Wu et al., 1997). Other researchers have packaged the TEV protease or GFP into virions using Vpr (Campbell et al., 2007; Desai et al., 2015; Jones and Padilla-Parra, 2015; Muthumani et al., 2004; Votteler et al., 2016). Chapter 3.2 will discuss my work using an mEGFP-Vpr to look at the kinetics of Vpr recruitment compared to Gag.

Tat, Rev, and Vpu

The final three proteins encoded by HIV-1 are Tat, Rev, and Vpu. Tat and Rev both play roles in gene regulation. Tat enhances the processivity of polymerases transcribing HIV-1 DNA (Feinberg et al., 1991). As previously mentioned, Rev binds the RRE site in the Env coding region and helps with nuclear export (Chang and Sharp, 1989; Fischer et al., 1995). Finally, Vpu counteracts the host protein Tetherin, which prevents newly budded viruses from leaving the cell periphery (McNatt et al., 2013; Neil et al., 2008).

In order for successful assembly to occur, all of these viral and host proteins must work together in concert. Removal or mutation of any one protein can result in failure to replicate or the production of non-infectious particles (Abram and Parniak, 2005; Chiang et al., 2010; Mohammed et al., 2011; Yu et al., 1998). HIV-1 is also polycistronic and requires protease cleavage of its proteins in order to create an infectious particle. This proteolytic cleavage is often cited as a reason that many HIV-1 mutations result in failure to bud (Bendjennat and Saffarian, 2016; Huang et al., 1995; Karacostas et al., 1993; Mattei et al., 2014; Ott et al., 2003; Ott et al., 2009; Yu et al., 1998).

1.2 Role of Protease and Maturation

1.2.1 Role of Protease in the HIV-1 Life Cycle

Gag itself is created as a polyprotein that drives assembly, but there is a maturation step that must occur in order for HIV-1 to become infectious. That maturation step involves the cleavage of both Gag and GagPol into their component parts so that each domain can perform its function within the mature virus. Matrix helps to coordinate the external envelope protein that is responsible for entry into new host cells (Dorfman, et al., 1994), capsid is restructured and forms a shell which protects the HIV-1 RNA upon entry into a new host cell (Gamble et al., 1997), and nucleocapsid helps condense the RNA within the particle (Dorfman et al., 1993). From Pol specifically, reverse transcriptase and integrase are freed by the protease to convert the HIV-1 RNA to DNA and then integrate that DNA into the genome of the infected cell.

The independent functions of SP1, SP2 and p6 after cleavage remain less clear. The p6 domain is necessary during assembly to recruit the ESCRT proteins and package Vpr into particles but does not seem to perform any clear function aside from its one during assembly (Jenkins et al., 2001; Kondo and Gottlinger, 1996; Morita et al., 2011). Some research suggests that cleaved p6 is a substrate for the host insulin-degrading protein (IDE), but this is still an area of active investigation (Hahn et al., 2016; Schmalen et al., 2018). SP1 acts as a molecular switch for CA lattice rearrangement (Mattei et al., 2018; Schur et al., 2016). When SP1 is cleaved from CA by protease, the immature CA lattice formed as a part of assembly begins to change into its mature conical structure. Finally, SP2 itself appears to be dispensable, but its cleavage from p6 is necessary for successful maturation (de Marco et al., 2012).

1.2.2 Structure and Function of Protease

The active form of the protease is a dimer where each 99-amino acid monomer contains half the active site (Figure 1.4). The HIV-1 protease is an aspartyl protease and has the Asp-Thr-Gly triad sequence (Kohl et al., 1988; Toh et al., 1985). In addition to the active site, other structural features of the protease include the flap, flap elbow, fulcrum, cantilever, and interface (Harte Jr. et al., 1990; Perryman et al., 2003). There are two distinct crystal structures of protease, and the major difference between them is in the flap domain which is opposite the catalytic site and helps define the substrate binding pocket. One crystal shows the flaps in a closed state with substrate bound and one crystal shows the flaps in a semi-open state without substrate (Hornak et al., 2006). A fully open state of protease is thought to occur but has not yet been crystalized.

The HIV-1 protease does not appear to have a consensus sequence, but the enzyme is still highly specific and has preference for a combination of hydrophobic and polar residues (Ghosh et al., 2016). Without a specific consensus sequence to follow, Gag and GagPol cleavage sites all have different amino acids that make up their cleavage sites. One advantage to each site having its own sequence is that each site

also has its own rate of cleavage which leads to sequential processing of Gag (Tritch et al., 1991). The initial cleavage within Gag is the SP1/NC cleavage site followed by the MA/CA and SP2/p6 cleavage sites which both show 10-fold slower processing than SP1/NC (Pettit et al., 1994). The CA/SP1 and NC/SP2 are the slowest cleavages with each being measured at 400-fold slower than SP1/NC (Pettit et al., 1994). Additionally, the speed of cleavage of the different sites within Gag was found to be dependent on where within Gag they were placed (Lee et al., 2012; Pettit et al., 2005). The PR/RT and RT/IN cleavage sites were cleaved at a consistent rate no matter which context they were placed in (Lee et al., 2012).

Since the activity of protease is indispensable for HIV-1 infectivity (Kohl et al., 1988), many inhibitors of protease activity have been created (Ghosh et al., 2016). Many protease inhibitors mimic the substrate transition state. By mimicking this state, the inhibitors shut down the HIV-1 protease active site. Unfortunately, the protease is quite flexible in its amino acid and active site composition, and resistance mutations are quite common. Treatment with more than one inhibitor of protease or other antiretroviral drugs can limit resistance mutations and effectively treat HIV-1 infection. The protease inhibitors used in Chapter 2 are Darunavir and Atazanavir which are both active site inhibitors.

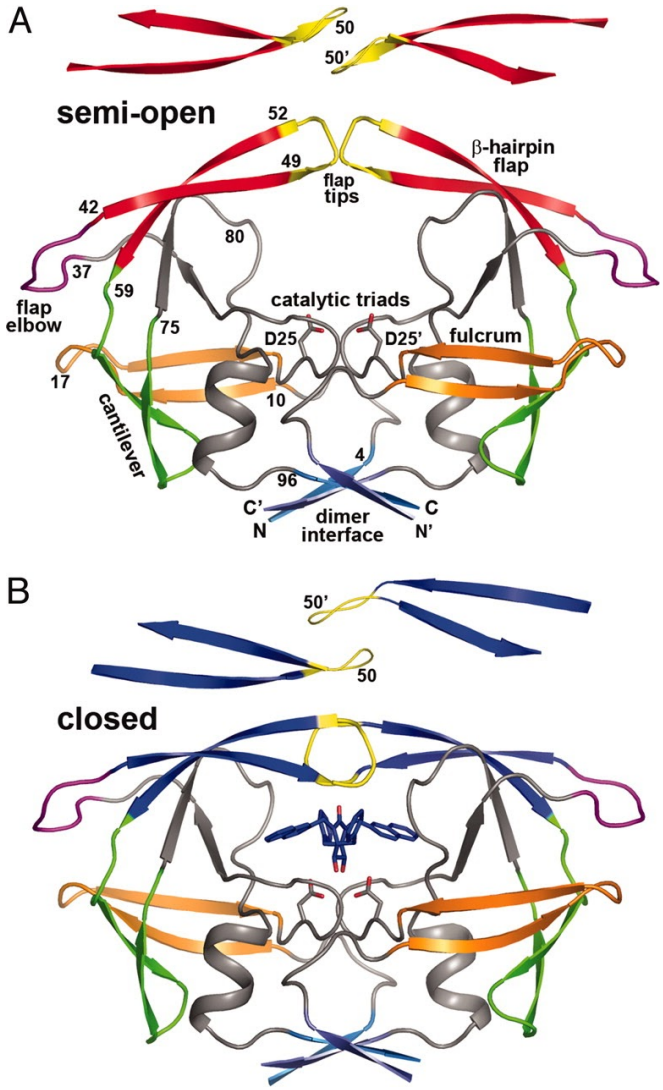

Figure 1.4 Crystal structure of HIV-1 protease
This figure and legend are reproduced from Hornak et al., 2006. The two experimentally determined conformations of HIV-PR. **A** Free HIV-PR with semi-open conformation of flaps (PDB ID code 1HHP). **B** Inhibitor-bound HIV-PR with closed flaps (PDB ID code 1HVR). Importantly, the handedness of the flaps changes in the two forms and is depicted above each structure. Color indicates distinct regions. Flaps: residues 43–58 and 43′-58′, red for free and blue for bound; flap tips: residues 49–52, yellow; flap elbow: residues 37–42, magenta; cantilever: residues 59–75, green; fulcrum: residues 10–23, orange; and interleaved β-strand motif forming the dimer interface: residues 1–4 and 96–99, blue/cyan.

1.2.3 Regulation of Protease

The timing of protease activity is important to the success of HIV-1 particle production (Karacostas et al., 1993; Mattei et al., 2014; Yu et al., 1998). If the protease becomes active too soon, Gag is processed before it is able to form into virions. If the protease doesn't become active, the particles can't take their mature form and are noninfectious. There are several steps that protease must take in order for it to become active, and it is unclear which of these is the rate limiting step. The protease must be packaged into particles, must dimerize, and must be cleaved out of GagPol. Previous work suggests that the initial cleavage that removes protease from its attachment to the rest of GagPol is an intramolecular one (Pettit et al., 2004), but there is currently no work that can place when this intramolecular cleavage occurs relative to protease dimerization or packaging. In Chapter 2 of this thesis, I shed light on the timing of protease activation and cleavage of Gag while imaging live assemblies. This work is not able to distinguish when protease dimerizes, when the initial intramolecular cleavage occurs, and when packaging of protease occurs relative to one another, but it does give us previously unknown information about when protease cleavage occurs relative to the rest of the assembly of Gag.

Previous research has established that proper timing of protease activation is critical for the formation of virions (Karacostas et al., 1993; Mattei et al., 2014; Yu et al., 1998). Mutations which delay the time course of assembly such as mutations in NC or in the ESCRT recruitment motifs in p6 often show a loss of Pol proteins back into the cell, suggesting that protease activation does not wait for scission from the cell before becoming active (Bendjennat and Saffarian, 2016; Huang et al., 1995; Ott et al., 2003; Ott et al., 2009). Mutations in the Pol coding region have also been shown to induce protease activation problems (Abram and Parniak, 2005; Chiang et al., 2010; Mohammed et al., 2011; Yu et al., 1998). Particle production in these mutant cases can be rescued by genetic inactivation of the protease, but this can't rescue infectivity without an active protease present.

1.3 retroCHMP3

Chapter 3 of this thesis will discuss a protein called retroCHMP3 which was found in originally in squirrel monkeys, but also later in mice. My work on retroCHMP3 is an active collaboration with Lara Rheinemann, Diane Miller Downhour, Wes Sundquist, and Nels Elde at the University of Utah. The retroCHMP3 protein is a truncated and mutated version of the ESCRT-III protein CHMP3 which was created through a duplication via LINE elements. ESCRT-III proteins contain an autoinhibitory domain which binds to the N-terminal alpha helices in the protein preventing polymerization. The retroCHMP3 protein is missing both the autoinhibitory domain and also its VPS4 recruitment domain which is C-terminal to the autoinhibitory domain (Figure 1.5). Although all new world monkeys have the duplication of CHMP3, not all of them have the additional stop codon that produces the retroCHMP3 version we are studying. Expression of retroCHMP3 in both mice and squirrel monkeys is in the testes and could

be maintained to protect against LINE element insertion during spermatogenesis, although the Elde lab does not currently see any positive selection for the retroCHMP3 gene. Given the results which I will present in Chapter 3 which show that retroCHMP3 inhibits the budding of HIV-1, retroCHMP3 may also play a role in preventing viral infection of the next generation.

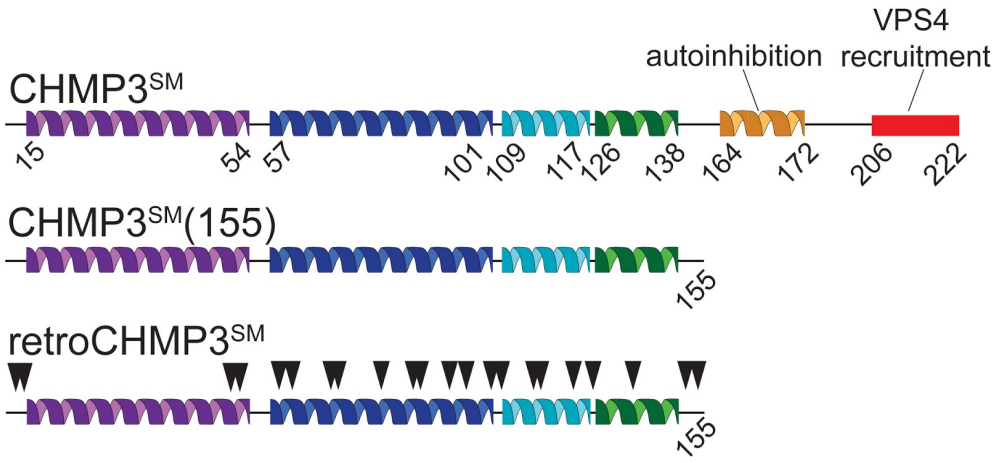

Figure 1.5 Schematic of CHMP3 variants
Schematic of full length, truncated, and retro CHMP3 variants. CHMP3^{SM} shows the full-length squirrel monkey version of CHMP3 complete with autoinhibition and VPS4 recruitment domains. CHMP3^{SM}(155) shows a truncation at aa155 of the squirrel monkey CHMP3. retroCHMP3^{SM} shows the same truncation as CHMP3^{SM}(155), but the arrows indicate additional mutations in the sequence. Both CHMP3^{SM}(155) and retroCHMP3^{SM} are missing the autoinhibition and VPS4 recruitment domains. This figure was created by Lara Rheinemann at the University of Utah.

Previous research on full length CHMP3 has shown that truncation of the C-terminus of human CHMP3 can inhibit viral budding (Zamborlini et al., 2006). As the C-terminus of retroCHMP3 is also truncated, we wanted to see if the same anti-viral phenotype was present in cells with retroCHMP3 (Figure 1.5). If the same antiviral effect was seen, we also wanted to determine the mechanism of the effect. In Chapter 3, I will present work from Lara and Diane on the inhibition of viral budding via retroCHMP3. I will also present my imaging data from cells expressing retroCHMP3 and various ESCRT components. These data together suggest that retroCHMP3 delays scission by interacting with the ESCRTs, leading to a loss of Gag components back into the cell due to protease activity.

1.4 TIRF Imaging

1.4.1 General TIRF Overview

All of the imaging presented in this thesis was done on our home-built total internal reflection fluorescence (TIRF) microscope (Johnson et al., 2014). When a sample is imaged using traditional epifluorescence microscopy, the excitation laser shines directly through the objective and into the sample. When a sample is imaged using TIRF microscopy, the excitation laser shines at an angle greater than the critical angle, meaning that the laser is reflected off the bottom of the coverslip. When the laser reflects off the bottom of the coverslip, a thin evanescent field is created which exponentially decays away from the coverslip. This makes TIRF microscopy an ideal way to image samples where the region of interest is close to the coverslip because excitation of background fluorophores is greatly reduced. An additional component to our home-built system is the ability to spin our excitation light using mirror galvanometers. Spinning the excitation light removes any aberrations in the field giving us an even TIRF illumination.

Since HIV-1 is an enveloped virus which assembles at the plasma membrane, TIRF microscopy is an ideal way to image the assembly of new viruses. TIRF offers the resolution required to see new viruses early in their assembly without exciting the large amount of Gag that is present in the cytosol (Jouvenet et al., 2006).

1.4.2 Polarized TIRF Overview

In addition to controlling the angle of illumination with our TIRF microscope, we are also able to control the polarization of the excitation laser. Being able to control the polarization of the excitation light allows us to know more about the fluorescent proteins in our sample than just their location. With polarization, we can gather information about the orientation and dynamics of the fluorescent proteins (Atkinson et al., 2013; Burghardt, 1984; Corrie et al., 1999; Dale et al., 1999; Kampmann et al., 2011; Mattheyses et al., 2010).

One measurement that I will be discussing in Chapter 2 of this thesis is anisotropy. To measure anisotropy, we first shine excitation light with a polarization that is parallel to the coverslip onto our sample. From there, we collect emission from the sample and split it between light that is parallel (the same as the excitation light) or light that is perpendicular to the coverslip. The anisotropy is then calculated using the equation: $(Intensity_{parallel} - Intensity_{perpendicular})/(Intensity_{parallel} - 2*Intensity_{perpendicular})$

Epifluorescence imaging is usually used for anisotropy, but I will be using anisotropy in live cells with TIRF. For this study, I will be using mEGFP as my fluorescent protein as it is well characterized for these types of experiments (Atkinson et al., 2013; Kampmann et al., 2011; Mattheyses et al., 2010). The mEGFP has a known dipole and the ratio of mEGFP emission when excited with light parallel versus

perpendicular to its dipole is 30:1 (Inoué et al., 2002). Anisotropy has several components that are part of the final value. The first is the orientation of the mEGFP population. If the excitation light lines up with the dipole of our population of mEGFPs, then the mEGFPs will be excited. If not, then the mEGFPs will either not be excited or will be excited to a lesser degree. The second component is the degree of freedom of the population. If the mEGFPs are free to tumble versus being fixed in a certain orientation, the anisotropy can change. The third component is specific to anisotropy measurements in TIRF and that is distance from the coverslip. The TIRF field decays with distance from the coverslip, so mEGFPs that are closer to the coverslip will have a higher chance of getting excited than those further from the coverslip. These three components make up the majority of what influences anisotropy although other smaller factors can play a role. In Chapter 2, I will show how I have used anisotropy to measure the activation of HIV-1 protease and the cleavage of Gag during assembly.

1.5 Summarizing Scientific Work

Every scientific paper is a story, but it can sometimes be a challenge to access those stories. Many papers are hidden behind subscription fees that make access prohibitive. But even if the reader gets behind the paywall, scientific stories are often written in a dense and jargon-laden fashion. This kind of style may not be limiting for experts in the field, but for those outside of that field, it can ensure that the story is not heard. This has led to a recent incorporation of different kinds of summaries with the goal of making science more accessible. In Chapter 4 of this thesis, I will present my work on evaluating the effectiveness of these science summaries.

In a recent 3M survey of 14,025 people, 88% of them thought that scientists should be sharing their results in easy to understand language (3M, 2019). Many journals have recognized this need, and they create a variety of summaries including videos, graphics, and plain language summaries in addition to the abstracts that come with every scientific paper. While all of these summaries tell the same story, they tell it using different media styles.

Having different ways to summarize published research could increase accessibility, but video abstracts, plain language summaries, and graphical abstracts all take time to make. Video abstracts can take over 20 hours to complete and graphical abstracts aren't far behind. They also require specialized equipment and skills to be effective (Newman and Schwarz, 2018; Rodríguez Estrada and Davis, 2015). While plain language summaries might seem the easiest to produce, even eLife, a noted proponent of plain language summaries, found that they were publishing too many papers for each one to have its own plain language summary, and in 2016 they scaled back the number of plain language summaries they publish (Rodgers, 2017).

Summaries are necessary for sharing scientific findings quickly with peers and the public. Unfortunately, only a small portion of journals create even one kind of

summary for their papers. To encourage more journals to summarize the research they publish, it would help to know what the most effective summaries are for different audiences. There is little data on the relative efficacy of reaching people with different kinds of summaries. We also don't know if adults with science, science-related, and non-science careers all enjoy and comprehend the same kinds of summaries.

In Chapter 4, I will present survey research which was designed to gather data on the effectiveness of different summary types for people with different careers. The survey presented participants with a video abstract, graphical abstract, plain language summary, or published abstract from two papers in the same subject area, and it collected responses on comprehension, perceived understanding, enjoyment, and whether the participants wanted to see more summaries of that type. The combination of these four measurements was used to determine which summary method is most effective. I will also present data which compared summary efficacy across career types and reported learning preferences to see what role they play.

Chapter 2
Measuring Protease Activation and Gag Cleavage

In this chapter, I will show three ways that I have tried to measure protease activation and Gag cleavage. In section 2.1 I will cover two past, unsuccessful attempts to measure Gag cleavage either by changes in FRET or by an assay with a cleavage-sensitive reporter. In the end, both the FRET and cleavage-sensitive reporters did not offer a clean enough signal and a large enough dynamic range to measure Gag cleavage in live cells during viral assembly

After discussing these past attempts to measure Gag cleavage, I will talk about my successful attempt to measure Gag cleavage with anisotropy in section 2.2. This work was done in collaboration with Joan Pulupa who provided the analysis code and intellectual contributions regarding the interpretation of the anisotropy results. This section is split into three subsections. In subsection 2.2.1, I will show data which characterizes the relationship between anisotropy and TIRF. Anisotropy is typically a measurement done using epifluorescence, but I will discuss how I applied this technique to HIV-1 assembly in live cells in TIRF.

In subsection 2.2.2, I will discuss the constructs I made to measure Gag cleavage with anisotropy and steps I took to characterize those constructs. In this thesis, the phrase “construct” refers to a plasmid which has been engineered via cloning. I will then show data on the anisotropy of collected VLPs. This data suggests that anisotropy can detect changes due to HIV-1 protease activity.

Finally, in subsection 2.2.3, I will show data from assemblies that have an active wild-type protease, a protease that has been genetically inactivated with a single point mutation, and a protease which has been inhibited via a cocktail of the protease inhibitors Darunavir and Atazanavir. This data suggests that protease activation and Gag cleavage occurs prior to ESCRT recruitment and scission from the cell.

2.1 Past attempts to measure protease activation and Gag cleavage

2.1.1 FRET

I initially attempted to measure protease activation and cleavage of Gag with Förster resonance energy transfer (FRET). FRET occurs when one fluorescent protein (the donor) is excited and, instead of emitting a photon of light, transfers the energy to another fluorescent protein (the acceptor) via nonradiative dipole-dipole coupling. The acceptor fluorescent protein is then excited, and emits light, even though it has not been directly excited. The efficiency of the energy transfer from the donor to the acceptor is inversely proportional to the sixth power of the distance between the two, making FRET an efficient sensor of distance. For fluorescent proteins, FRET typically occurs when the fluorophores are within 10 nm of each other.

I tested several possible FRET pairs to determine which pair would give the highest FRET efficiency, while having limited spectral overlap for clarity of signal. I tested only red/green pairs as they typically exhibit a higher dynamic range than other FRET pairings such as CFP/YFP (Bajar and Wang et al., 2016B).

The green fluorescent protein donors tested were mEGFP, Clover, Clover2, and Clover3. The red fluorescent protein acceptors tested were mCherry, Ruby2, and Ruby3. The Clover and Ruby variants were designed by the Lin lab to have higher FRET efficiencies than the standard mEGFP/mCherry pairing (Bajar and Wang et al., 2016A; Lam et al., 2012). I inserted each of these possible FRET proteins after p6 within a version of HIV-1 Gag called Syngag. Syngag is a mammalian-codon optimized Gag that has a number of benefits including Rev-independent export of Gag RNA from the nucleus and easier genetic manipulation to clone constructs because of the lack of long stretches of adenine and thymine which make cloning more challenging (Deml et al., 2001). Syngag has been shown to be infectious and assemble like wild-type Gag (Deml et al., 2001).

When I measured FRET efficiency with a variety of Syngag-XFP pairings side-by-side in collected virus-like particles (VLPs), the Clover/mCherry and mEGFP/mCherry pairs had the highest FRET efficiencies (Figure 2.1). For my work, the mEGFP/mCherry pair was chosen over the Clover/mCherry pair. The mEGFP/mCherry pair was chosen because the Clover/mCherry pair had spectra that overlapped more than the mEGFP/mCherry pair, which would have led to more challenges during imaging.

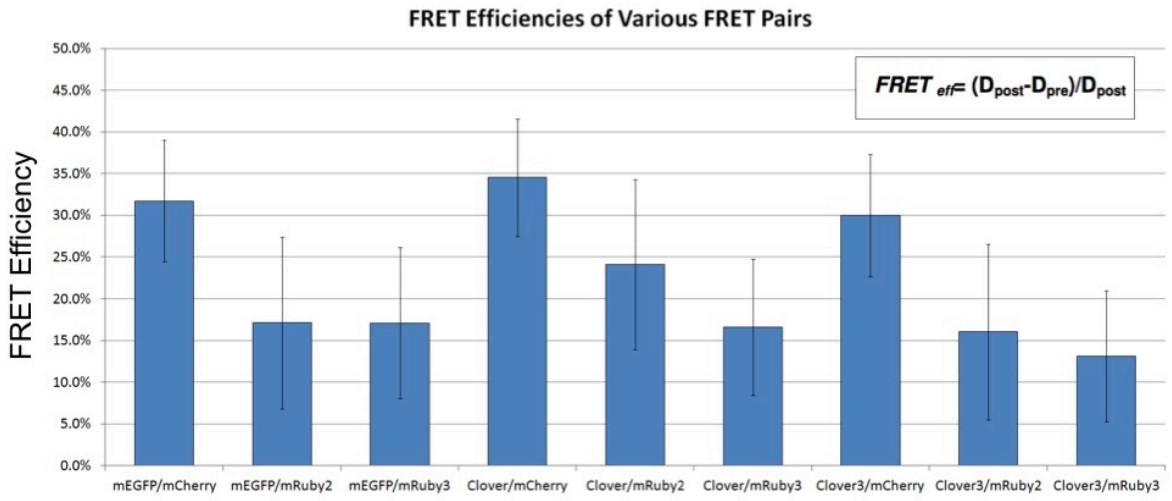

Figure 2.1 FRET Efficiencies of different pairings
FRET efficiencies as measured by acceptor bleaching in collected VLPs (n=100). All fluorescent proteins are after p6 in Syngag. Calculation of FRET efficiency is shown in the top right. D stands for Donor intensity, post is post acceptor bleach, and pre is pre acceptor bleach. Error bars represent the standard deviation.

After confirming mEGFP and mCherry as my FRET pair of choice, I created several constructs containing mEGFP and mCherry to work as reporters for protease activation and Gag cleavage. I expected these reporters to either show a gain of FRET or a loss of FRET upon protease activation. I also constructed a positive control for FRET which should not change. In this thesis, the phrase “construct” refers to a plasmid which has been engineered via cloning. The construct sets I built were the following:

A. Positive Control: Syngag-MA(mEGFP) & Syngag-MA(mCherry)
In this set, the FRET pairs were placed on different molecules, so the FRET that occurred was intermolecular. The two fluorophores were fused to different copies of Gag. Both had the fluorescent protein between MA and CA and maintained the attachment to MA (Figure 2.2A).

B. Loss of FRET: Syngag-p6-mEGFP & Syngag-p6-mCherry
My second set of constructs had the mEGFP and the mCherry after p6 (Figure 2.2B). The FRET occurring in this set of constructs was designed to be intermolecular and was designed to have a higher level of FRET prior to cleavage and a lower level of FRET after protease activation and Gag cleavage.

C. Gain of FRET: Syngag-MA(mEGFP)-mCherry or Syngag-MA(mCherry)-mEGFP
The final two constructs were each intramolecular FRET constructs, and we expect to see a gain of FRET (Figure 2.2C). These two constructs were designed to work alone and only one was transfected into cells at once. In these constructs, one member of the FRET pair would be between MA and CA and the other member of the pair would be after p6. These constructs would have the pairs held apart via the CA crystalline lattice until proteolytic cleavage occurred. After cleavage, the mEGFP and mCherry would be

free to interact within the virus-like particle (VLP). The only difference between the two constructs was whether the mEGFP was in the MA position and the mCherry in the p6 location or vice versa (Figure 2.2C).

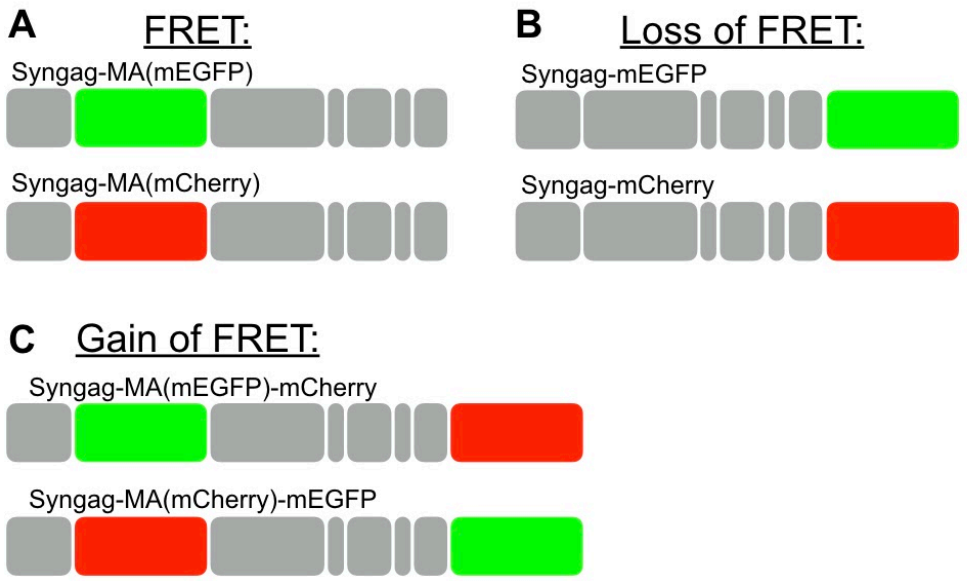

Figure 2.2 Schematic of FRET Constructs
A Positive control FRET constructs. These constructs have the MA/CA cleavage site after the XFP and require both constructs to be a FRET sensor. **B** Loss of FRET constructs. These constructs have the XFP stay attached to p6 after cleavage and require both constructs shown to be a FRET sensor. C Gain of FRET, intramolecular constructs. Each one of these constructs functions on its own as a FRET sensor. The XFP between MA/CA stays attached to MA after cleavage and the XFP after p6 stays attached to p6 after cleavage.

To test the feasibility of using these Syngag intramolecular and intermolecular FRET constructs to measure protease activation and Gag cleavage, I first tested if the protease was able to cleave Syngag when it was fused to fluorescent proteins. To determine whether the protein encoded by the construct was cleaved, I transiently transfected Hek293T cells with these constructs and then 16-48 hours later collected VLPs (Chapter 6, section 6.2). The VLPs were solubilized and then probed with a Western blot with an antibody to capsid to assay the extent of proteolytic cleavage. After initial testing, the most promising construct, based on the extent of cleavage as assayed by Western blot, was the two-color Syngag-MA(mEGFP)-mCherry construct (Figure 2.3). This construct was a gain of FRET construct where the mEGFP would be held apart from the mCherry via the CA crystalline lattice until cleavage occurred and they had the possibility to FRET (Figure 2.2C). The control constructs also showed successful cleavage (Figure 2.2A). Constructs where mEGFP or mCherry was after p6 did not cleave to completion.

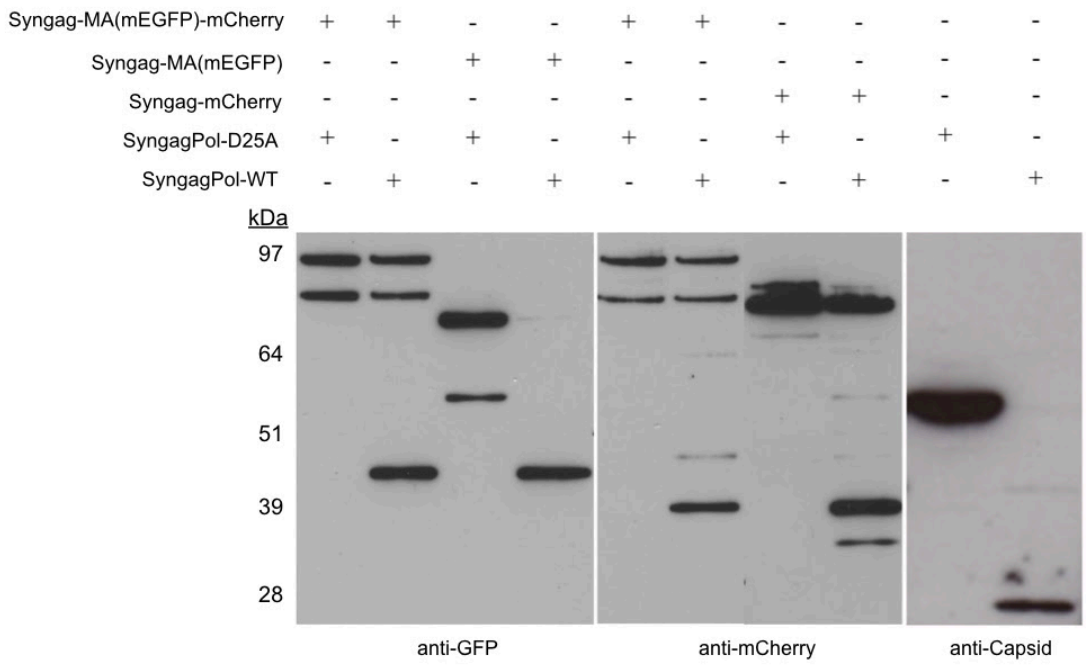

Figure 2.3 Western Blot of VLPs with FRET Constructs
Western of collected VLPs showing cleavage of FRET constructs. Constructs with a p6 tag show less complete cleavage than those with a MA tag. SyngagPol-D25A is an inactive protease and SyngagPol-A contains an active protease.

After confirming cleavage, I measured FRET in VLPs from both the intramolecular and intermolecular constructs. I collected VLPs to image by transiently transfecting Hek293T cells with a 1:5 ratio of tagged to untagged Syngag 24 hours prior to imaging. To test whether the VLPs were showing the FRET expected from the design of the constructs, I used an assay referred to as acceptor bleaching. This method is a one-time measurement and cannot be done to monitor FRET over time, but it is a reliable way to assay FRET. Acceptor bleaching works by bleaching the acceptor of the FRET pair with a strong laser pulse. By bleaching the acceptor, you prevent the donor from transferring its energy to the acceptor. If FRET is occurring, then the fluorescence of the donor increases after the acceptor is bleached. I performed acceptor bleaching with both the intramolecular and the intermolecular constructs and none of them showed a clear enough difference between VLPs with active protease and VLPs with a genetically inactivated protease to consider moving forward (Figure 2.4).

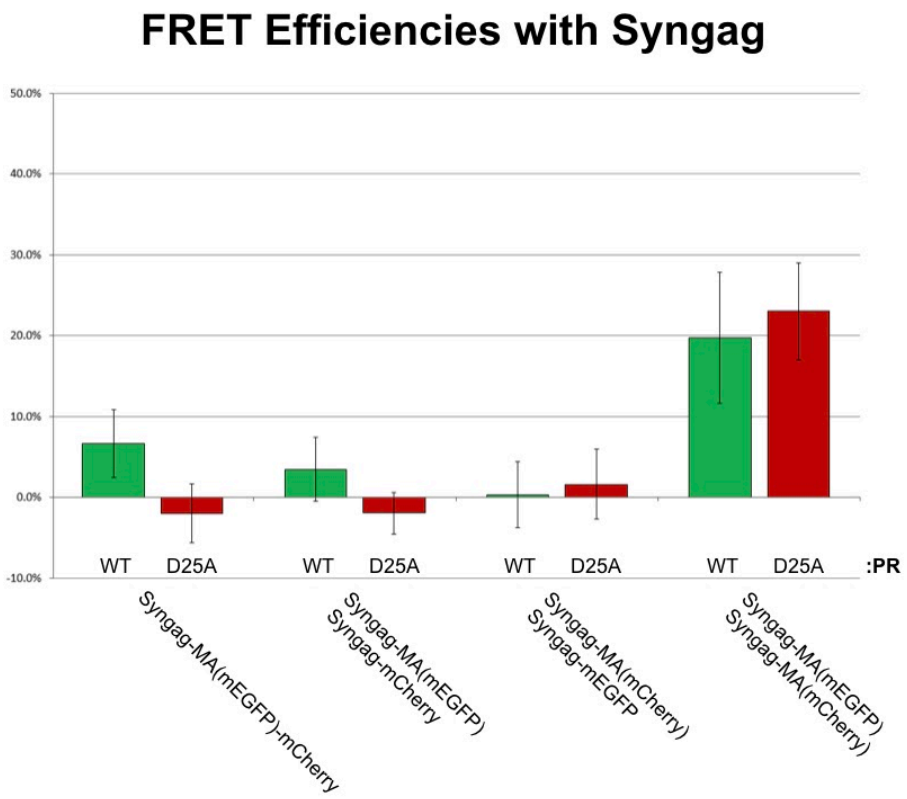

Figure 2.4 FRET Efficiencies of Syngag Constructs
Bar graph of FRET efficiencies measured by acceptor bleaching in collected VLPs. Green bars labelled WT are VLPs with an active protease. Red bars labelled D25A are VLPs with a genetically inactivated protease. Error bars are standard deviations (n=100).

2.1.2 Cleavage-sensitive reporters

I believe that the main problem with my FRET constructs was their ability to cleave to completion as assayed by western blot, so I temporarily moved away from FRET and tagging Gag. Instead, I tried new fluorescent assays. The most promising new assays were a series of fluorescent cleavage-sensitive reporters.

Reporters that fluoresce upon cleavage often work in two ways. The first method uses a fluorescent protein followed by a quencher peptide, expressed in tandem. The quencher peptide quenches the fluorescent protein until it is cleaved off. The second method uses a split fluorescent protein. With the split fluorescent protein, two pieces of a fluorescent protein are prevented from coming together by a cleavable piece of protein.

Both of these methods have caveats that can make them less effective for certain applications. The fluorescent protein paired with a quencher often has a high background because the fluorescent protein is fully intact prior to cleavage and is not always efficiently quenched. The reporters with a split fluorescent protein have a much

lower background since the fluorescent protein is unable to fluoresce until cleavage has occurred, but it is a slower reporter system since two cleavage events have to occur and then the newly free piece of the fluorescent protein must come together. Despite these disadvantages, both types of reporters have the advantage that they gain signal upon cleavage rather than lose it.

In addition to reporters that fluoresce after cleavage, there are also reporters whose fluorescence is altered upon cleavage. One example of this type of reporter is the fluorescent protein exchange system (FPX) (Ding et al., 2015). FPX was created as an alternative to FRET. It relies on two different proteins, a red and a green protein that are termed A proteins. These A proteins can only fluoresce when paired with a B protein. The same B protein works with both the red and green A proteins. This allows for a switch of color by changing which A protein is paired with the B protein through cleavage (Ding et al., 2015) (Figure 1C). This reporter has the advantage that the cell is fluorescent at all times and that the color of fluorescence changes.

I used three different cleavage-sensitive reporters to maximize my chance of finding one that worked for measuring protease activation. For reporters that fluoresce upon cleavage, I used the zipGFP system (To et al., 2016) and the VC3AI system (Zhang et al., 2013) (Figure 2.5 A,B). Both are based on the split fluorescent protein model which limits the background seen without cleavage. For reporters that change their fluorescence upon cleavage, I used the FPX system (Ding et al., 2015) (Figure 2.5 C).

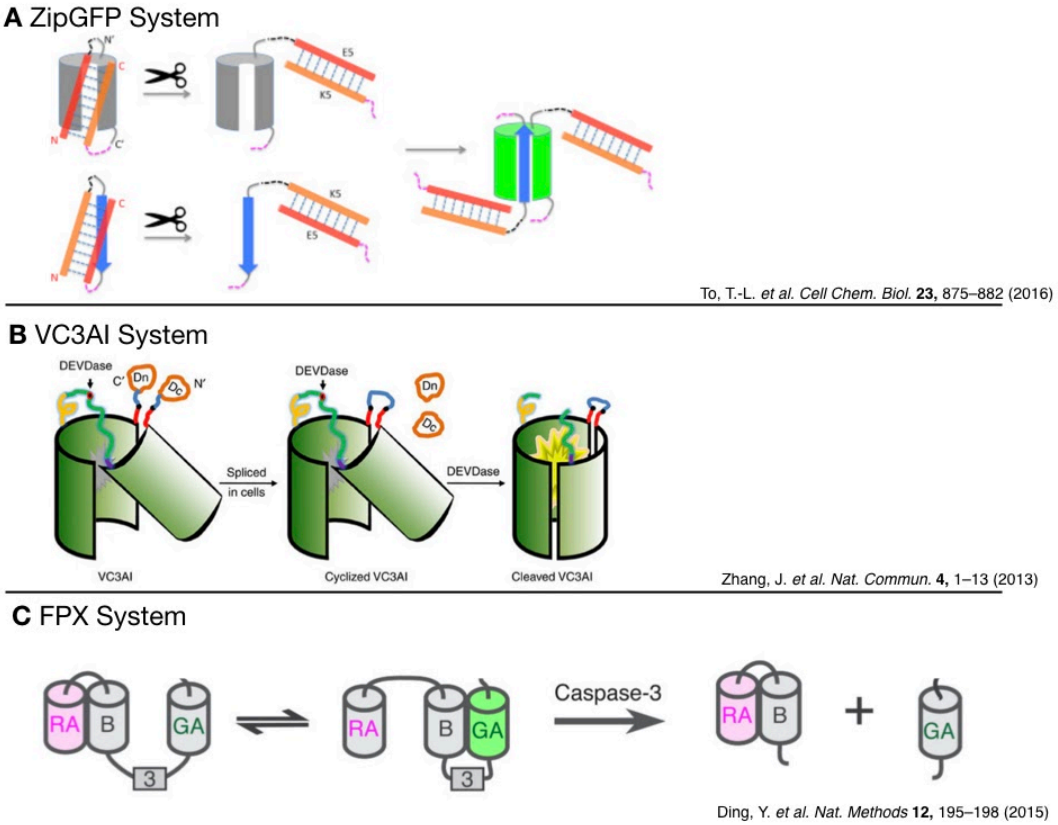

Figure 2.5 Schematic of Cleavage-Sensitive Reporters
Cleavage sensitive reporters are shown. The two pieces of the ZipGFP system (ZipGFP1-10 and ZipGFP-11) are shown in **A**. The single VC3AI component is shown in **B**. A construct containing all three pieces of the FPX system linked together to show an increase in red fluorescence after cleavage is shown in **C**.

The ZipGFP, VC3AI, and FPX systems were all transfected into cells to see if I could quickly replicate their activity before any modifications were made. The ZipGFP system was received with a TEV protease cleavage site and couldn't readily be tested with the materials I had on hand. The VC3AI and FPX systems arrived with a caspase-3 cleavage site. To test those two, I transfected both systems into cells then treated the cells with staurosporine. Initial imaging seemed promising since fluorescence was detected upon addition of staurosporine.

After initial testing, all three of the fluorescent reporters were engineered to create protease sensitive versions. One version was created with the RT/IN cleavage site and one with the MA/CA cleavage site. These two cleavage sites were chosen because the RT/IN site is reported to be context independent and the MA/CA site is reported to cleave fairly early in the gag cleavage order (Lee et al., 2012; Pettit et al., 1994). Using one Pol cleavage site and one Gag site increased my chances of accurately measuring protease activity.

The cleavage of the MA/CA versions of the fluorescent reporters were tested via western blot. I created a “fixed frame” version of GagPol (GagPol-FF) where the slippage site was mutated to create primarily GagPol rather than Gag. GagPol-FF was used as a positive control since this construct was previously reported to show early activation of the protease (Karacostas et al., 1993). The ZipGFP and the FPX systems showed the most robust response to the GagPol-FF positive control, so they were selected to move to the next step (Figure 2.6 and 2.7). As a negative control, I made a GagPol-D25A construct that has a protease with an inactivating D25A point mutation and should show no fluorescence. The ZIPGFP-MA/CA and FPX-MA/CA versions were transiently transfected into cells along with either GagPol-D25A or GagPol-FF. The GagPol-FF construct should have its protease become active early and the cells should be maximally fluorescent. By using both the GagPol-D25A and GagPol-FF, I was able to determine the extent of the dynamic range I would have with each cleavage-sensitive reporter.

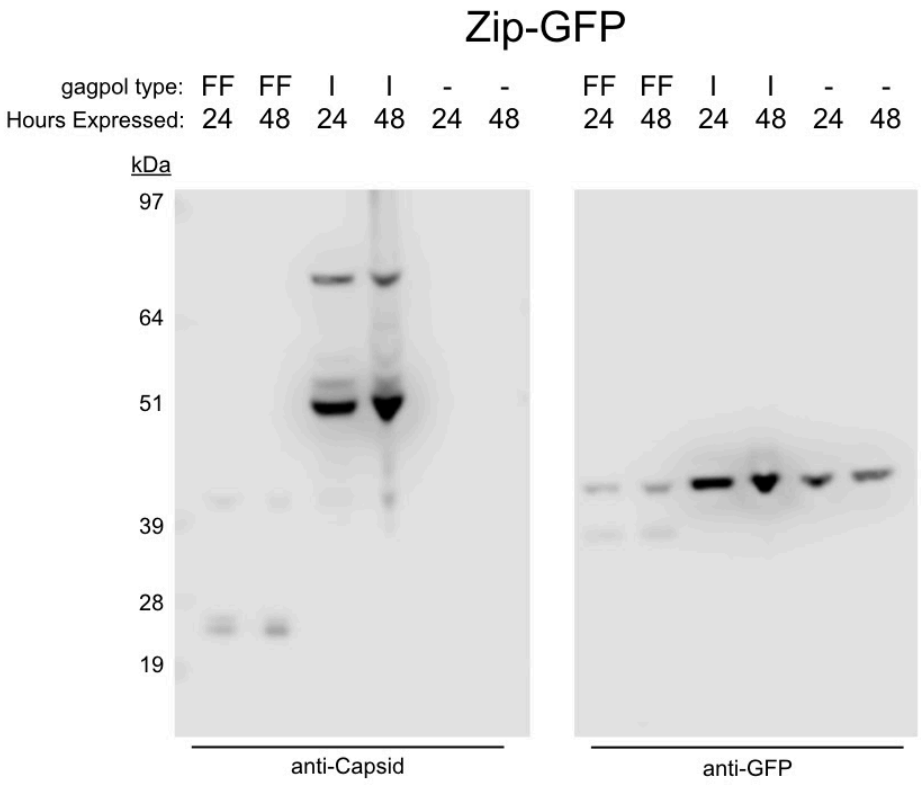

Figure 2.6 Western Blot of ZipGFP Cleavage
Western on cell lysates collected either 24 or 48 hours post-transfection. GagPol types include the positive-control GagPol-FF (FF), the protease inactive negative control GagPol-D25A (I), and no GagPol (-). The anti-Capsid antibody detects GagPol and the anti-GFP detects the ZipGFP1-10.

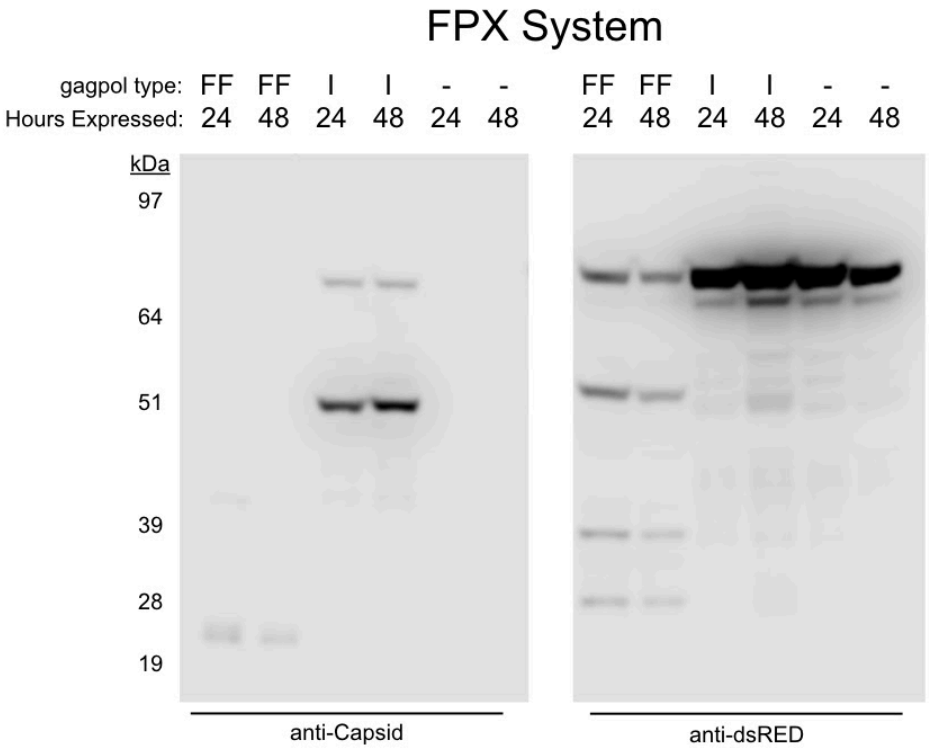

Figure 2.7 Western Blot of FPX System Cleavage
Western on cell lysates collected either 24 or 48 hours post-transfection. GagPol types include the positive-control GagPol-FF (FF), the protease inactive negative control GagPol-D25A (I), and no GagPol (-). The anti-Capsid antibody detects GagPol and the anti-dsRED detects each member of the FPX system.

To get a robust signal from the fluorescent reporters that report cleavage, they must be expressed for longer than 24 hours, preferably around 48 hours. Unfortunately, expressing GagPol for 48 hours causes the majority of cells to die and leads to images that are full of bits of broken cells leading to a high background. For the best GagPol assembly and expression, expression for 6-10 hours is better.

I attempted to overcome this by a two-step transfection where the fluorescent reporter was transfected 48 hours prior to imaging and the GagPol was transfected the evening before. This was not an effective solution as most cells expressed either the fluorescent reporter or GagPol rather than both.

Besides the expression issues, the constructs were also challenging to work with due to the fact that before protease activation, several of the reporters were not fluorescent. This made it challenging to confirm that cells were expressing the reporter to the appropriate levels to be able to detect any possible protease activation. Due to these issues, the cleavage sensitive reporters were set aside.

2.2 Measuring Gag cleavage with Anisotropy

2.2.1 Anisotropy is compatible with TIRF Imaging

In order to be confident in our use of anisotropy for measuring protease activity, we first needed to characterize anisotropy measurements on our TIRF microscope. The polarization of our laser is calibrated to be ideal within TIRF angles of 62.7-66.3 degrees (where 61.2 degrees is the critical angle), so varying the angle outside that range does have an effect on how even the polarization of the field is. To get illumination of the cytosol in order to relate our values to previously published values for mEGFP, we used an angle of 56.6 degrees.

The constructs we used to calibrate our anisotropy values are cytosolic mEGFP, palmitoylated mEGFP (palm-mEGFP), and mEGFP attached to the matrix domain of HIV-1 Gag (MA-mEGFP). For cytosolic mEGFP and palm-mEGFP, the values we obtain should be close to the reported cytosolic value of mEGFP which is 0.32 (Clayton et al., 2002; Rocheleau et al., 2003; Swaminathan et al., 1997). The palm-mEGFP construct was used to show that localizing mEGFP to the membrane alone does not change the anisotropy since the palm-mEGFP is free to rotate about the palmitoylation site (Atkinson et al., 2013). Due to our microscope calibrations and the angle used for these measurements, the value we obtained for mEGFP and palm-mEGFP were both approximately 0.3 with palm-mEGFP having a lower anisotropy than cytosolic mEGFP ($p=.005712$) (Figure 2.8). Both of these values are closer to the expected 0.32.

For MA-mEGFP, we obtained values closer to 0.39 (Figure 2.8). This increase in anisotropy corresponds to decreased tumble time experienced by the mEGFP because it is attached to the mystrioylated MA domain. When mEGFP is fixed in a random orientation, values of approximately 0.4 are expected, so our MA-mEGFP value is in line with previous work.

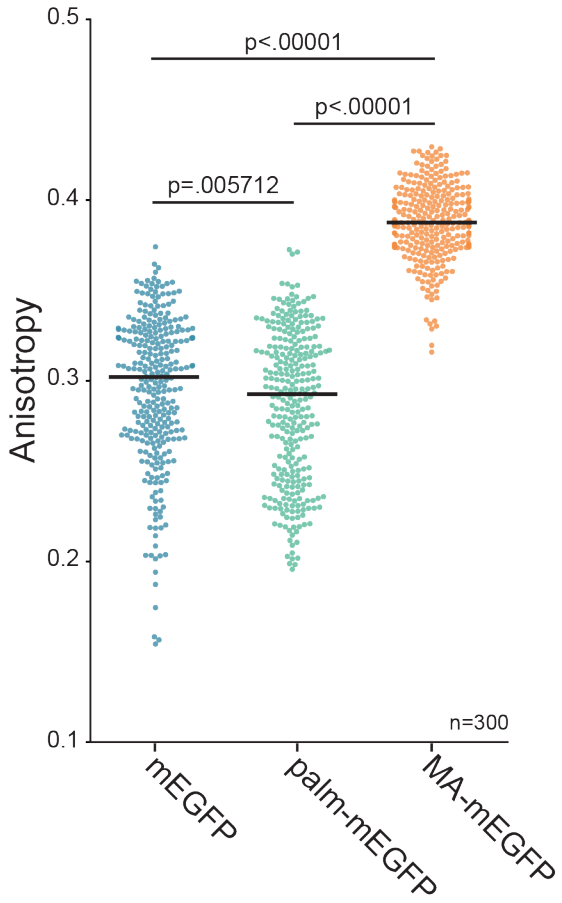

Figure 2.8 Anisotropy for Control Constructs
Anisotropy values obtained from HeLa cells expressing either mEGFP (blue), palm-mEGFP (green), or MA-mEGFP (orange) for 24 hours. Each data point corresponds to a single region on a cell (n=300 regions, 6 cells). Black bars indicate the median of the data. The dotted line is placed at 0.32 which is the published value for cytosolic mEGFP imaged with epifluorescence. Anisotropy means showed a statistically significant difference as determined by one-way ANOVA ($F(2,897)=732.24573=<.00001$), further comparison was done via two-tailed T-test. The p-values from the T-test are displayed on the plot.

Because we are using anisotropy with TIRF, we wanted to characterize the effect that increasing the TIRF angle, thereby decreasing the depth of the evanescent field, had on anisotropy values. We measured the same cells as above with varying angles of TIRF going from a deeper field of illumination to a narrower field with increasing angle values. Again, the polarization of our laser is calibrated to be ideal within TIRF angles of 62.7-66.3 degrees, so varying the angle outside that range does have an effect on how even the polarization of the field is. Despite this limitation, we were still able to see that increasing the TIRF angle decreased the anisotropy values of all constructs tested. This decrease in anisotropy was uniform across all constructs, so the differences between constructs stayed the same despite the changing angles (Figure 2.9).

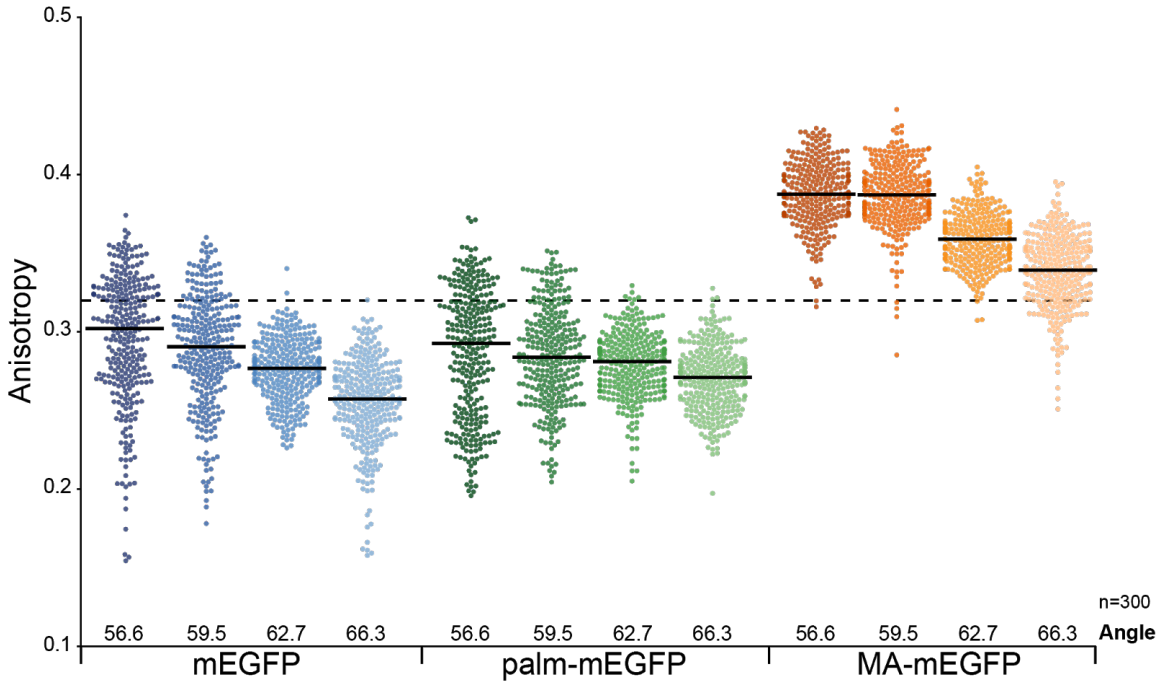

Figure 2.9 Anisotropy at different TIRF angles with Control Constructs
Anisotropy values obtained from HeLa cells expressing either mEGFP (blue), palm-mEGFP (green), or MA-mEGFP (orange) for 24 hours. TIRF angles are at the bottom of the plot. The TIRF critical angle is 61.2 degrees. Each data point corresponds to a single region on a cell (n=300 regions, 6 cells). The regions are the same within each condition. Black bars indicate the median of the data. The dotted line is placed at 0.32 which is the published value for cytosolic mEGFP imaged with epifluorescence.

Given that we were able to obtain anisotropy values for cells that are close to previously reported values (Clayton et al., 2002; Rocheleau et al., 2003; Swaminathan et al., 1997), and our control mEGFP constructs behaved in the expected matter, we felt confident moving forward with measuring the anisotropy of HIV-1 particles.

2.2.2 Anisotropy can detect structural differences in HIV-1 VLPs

To see whether the anisotropy values reflected the structural differences within HIV-1 particles due to maturation, we collected VLPs from HEK293T cells transiently transfected with either GagPol containing an active protease (WT), GagPol containing a genetically inactivated protease (D25A), or GagPol containing an active protease treated with a protease inhibitor cocktail (PI-WT). The GagPol used in these experiments was an NL4.3 HIV-1 packaging vector which was a gift from the Bieniasz lab. To maximize the possibility of detecting a difference in anisotropy with Gag, we created two versions of tagged GagPol. One version (GagPol-mEGFP-DC) was designed to have a change in anisotropy from Gag cleavage and the other (GagPol-mEGFP-MA) is a negative control construct that shouldn't show a shift in anisotropy.

Our version that should change (GagPol-mEGFP-DC) has mEGFP inserted between MA and CA with the MA/CA protease cleavage site on either side of the mEGFP (Figure 2.10A). The anisotropy of our VLPs is a function of three factors: (1) the orientation of the mEGFP within the VLPs, (2) the freedom of movement of mEGFP within the VLPs, and (3) the distance of the VLPs from the coverslip. With the GagPol-mEGFP-DC construct, all three of those factors will change when the construct is cleaved by the protease.

The second version of GagPol (GagPol-mEGFP-MA) is a negative control. This construct has the mEGFP inserted between MA and CA, but it only has a cleavage site on the CA side (Figure 2.10B). This construct will have the mEGFP remain attached to MA, and therefore to the membrane of the VLP, after cleavage. With this construct, we are eliminating the change in distance from the coverslip experienced by our mEGFP population because it remains attached to MA. We are also limiting the changes to orientation and freedom of the population because the mEGFP stays attached to MA and is not free to diffuse throughout the particle.

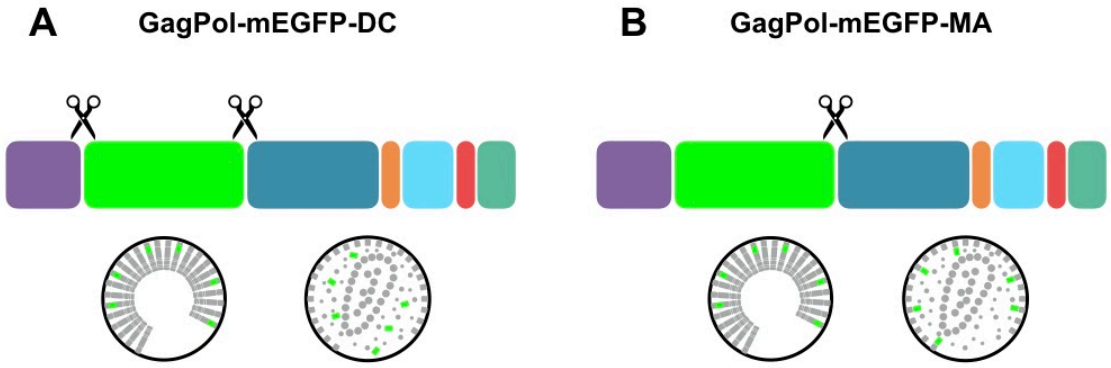

Figure 2.10 Schematic of GagPol Anisotropy Constructs
A Schematic of GagPol-mEGFP-DC which contains an mEGFP between MA and CA with a cleavage site on either side. **B** Schematic of GagPol-mEGFP-MA which contains an mEGFP between MA and CA with a cleavage site only on the CA side. Diagrams of VLPs in either an immature (left) or mature (right) state can be seen below each construct. Both constructs do have the full GagPol sequence complete with the slippage site, so they do slip to create the Pol proteins 5% of the time.

In order to be sure that the tag does not affect the packaging or cleavage of Gag, we performed western blot on collected populations of VLPs. These blots confirmed that our constructs were successfully incorporated into VLPs and could be cleaved by the protease (Figure 2.11). We also confirmed that our protease inhibitor cocktail effectively prevented particle maturation (Figure 2.11).

Once we confirmed that our constructs behaved as expected via western blot, we imaged collected VLPs and measured the anisotropy. With the GagPol-mEGFP-DC construct, the anisotropy values of the VLPs with a WT protease showed a distinct shift compared to those with either a D25A protease ($p<.00001$) or those treated with PI-WT

(p<.00001) (Figure 2.12). When we imaged collected VLPs with the GagPol-mEGFP-MA negative control, the anisotropy values with a WT, PI-WT, and D25A protease no longer showed a shift in anisotropy (p=.680174) (Figure 2.12). We also measured the anisotropy at different TIRF angles and saw that increasing TIRF angles decreased the anisotropy, which was what we had seen previously in cells expressing cytosolic mEGFP, palm-mEGFP, and MA-mEGFP (Figure 2.13 and Figure 2.14). Similar to those constructs, the VLPs still showed the same shift between WT and D25A protease regardless of angle. When we plotted the intensities of the collected VLPs, we saw that there was a relationship between anisotropy and intensity, as we would expect given that intensity and distance from the coverslip are components of anisotropy, but intensity does not seem to be the only determinant of anisotropy (Figures 2.12, 2.13, 2.14). To aid in comparison, all intensity plots in this chapter of the thesis have been rescaled such that the maximum intensity is one and the minimum intensity is zero. They were rescaled using the equation $(I-I_{min})/(I_{max}-I_{min})$ where I is intensity.

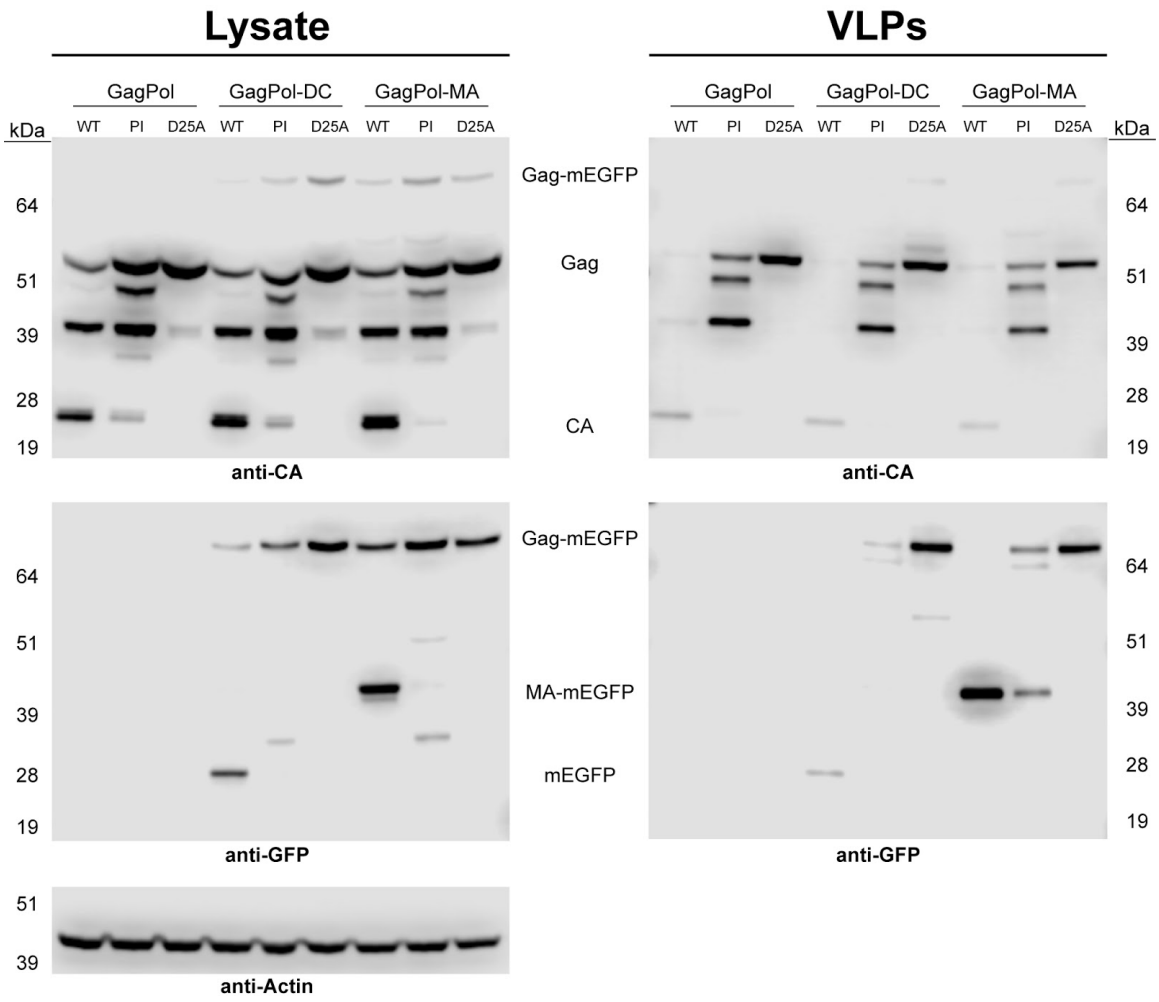

Figure 2.11 Westerns of GagPol Anisotropy Constructs
Western blots on cell lysate (left) and collected VLPs (right) from untagged GagPol, GagPol-mEGFP-DC (GagPol-DC), and GagPol-mEGFP-MA (GagPol-MA). Each construct has either WT, PI-WT (PI), or D25A protease. Blots are probing against CA (top), GFP (middle), and actin (bottom).

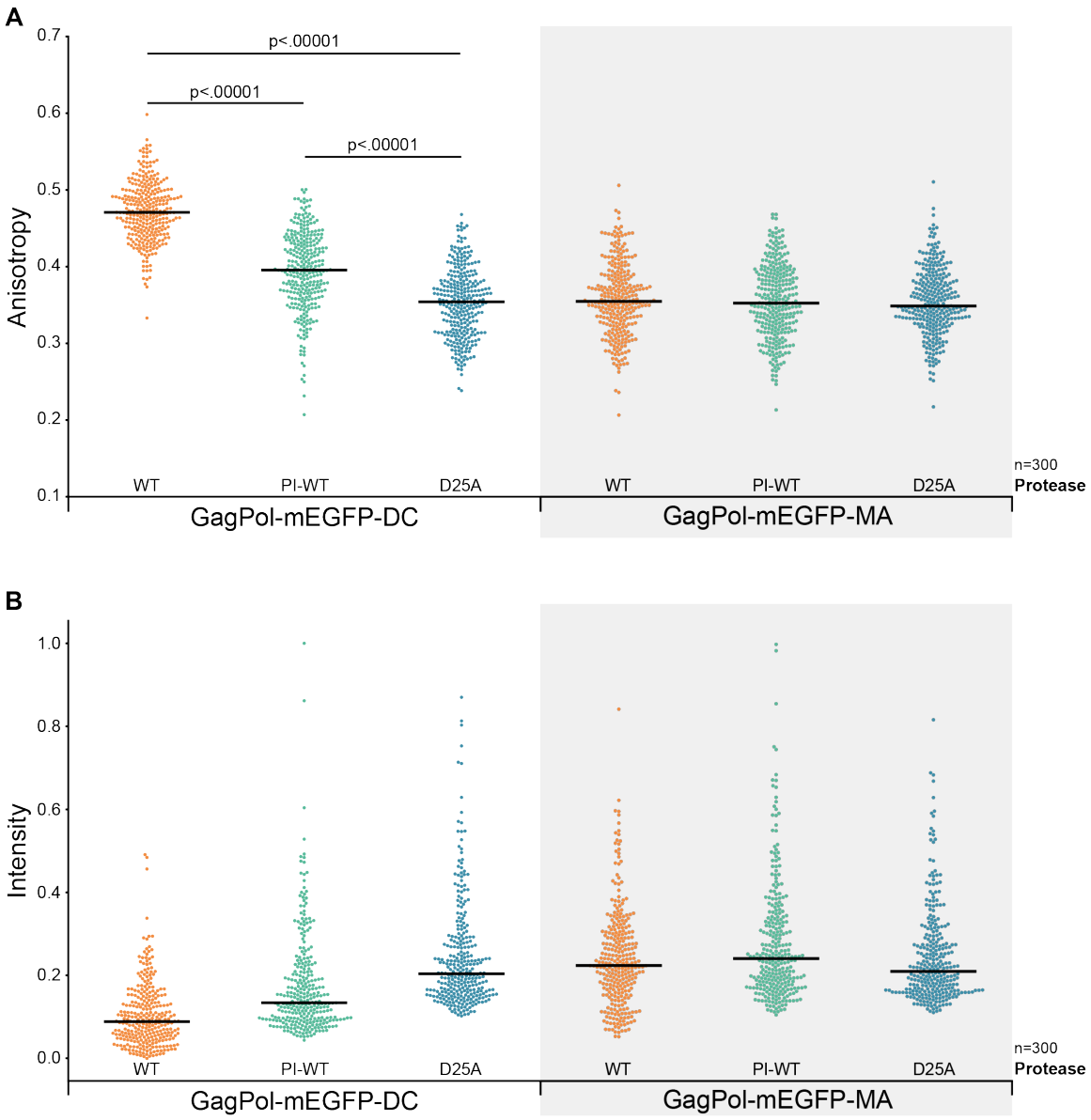

Figure 2.12 Anisotropy of VLPs
A Anisotropy of collected VLPs from both GagPol-mEGFP-DC and GagPol-mEGFP-MA. GagPol-mEGFP-DC shows data from WT (orange), PI-WT (green), and D25A (blue) protease. GagPol-mEGFP-MA shows data from WT, PI-WT, and D25A. Black bars are the median of the plotted values (n=300). GagPol-mEGFP-DC anisotropy means showed a statistically significant difference as determined by one-way ANOVA ($F(2,897)=481.60323=<.00001$), further comparison was done via two-tailed T-test. The p-values from the T-test are displayed on the plot. GagPol-mEGFP-MA anisotropy means did not show a statistically significant difference as determined via one-way ANOVA ($F(2,897)=0.38557=.680174$). **B** Rescaled intensity of the VLPs from **A**. Intensities were rescaled to be on a 0-1 axis via $(I-I_{min})/(I_{max}-I_{min})$ prior to plotting.

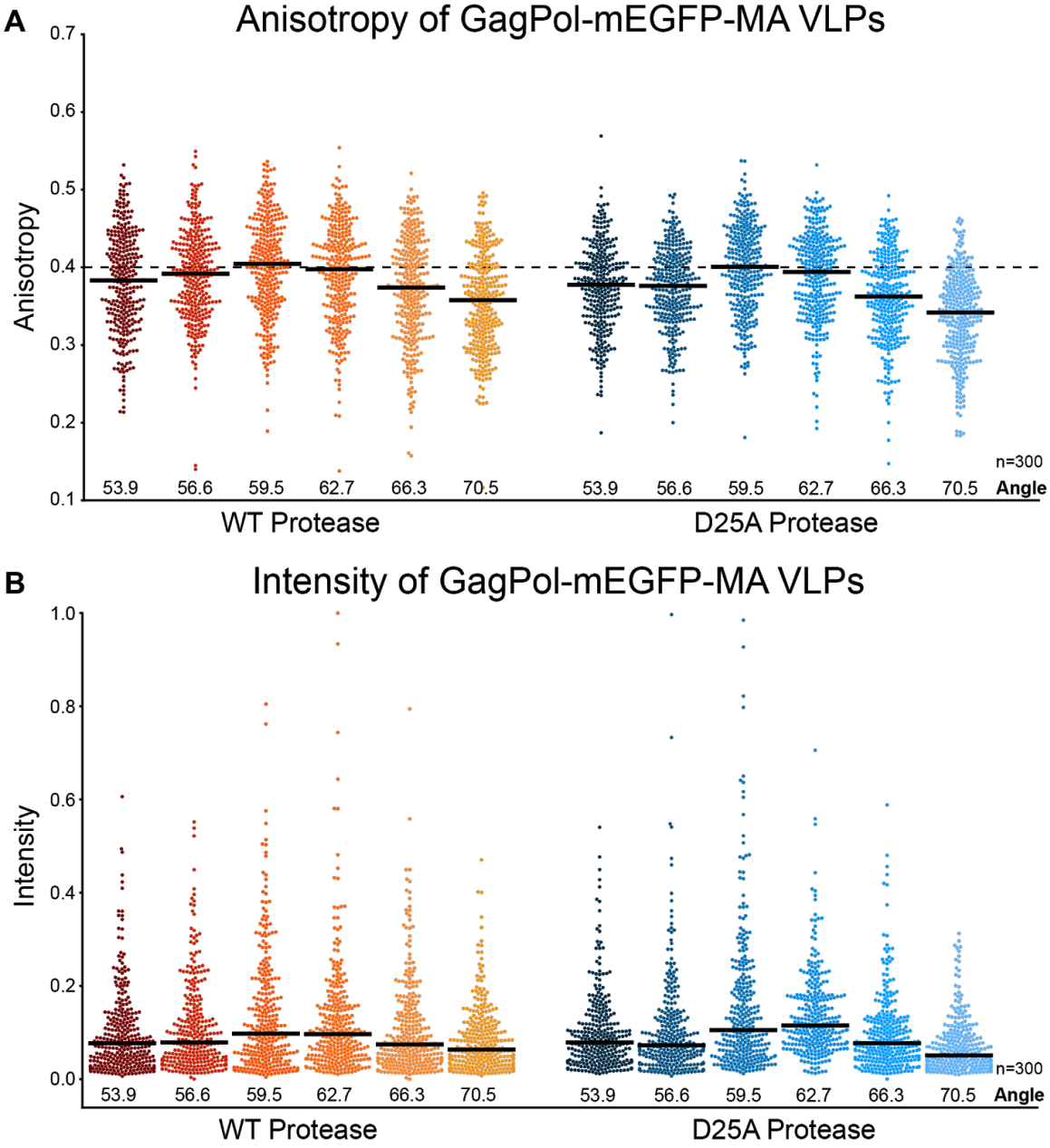

Figure 2.13 Intensity and Anisotropy of GagPol-mEGFP-MA VLPs with different TIRF angles

A Anisotropy of GagPol-mEGFP-DC VLPs with both active WT protease (reds) and D25A protease (blues). TIRF angles go from 53.9 to 70.5 degrees as shown below each plot. The TIRF critical angle is 61.2 degrees. **B** Rescaled intensity of the VLPs from **A**. Intensities were rescaled to be on a 0-1 axis via $(I-I_{min})/(I_{max}-I_{min})$ prior to plotting.

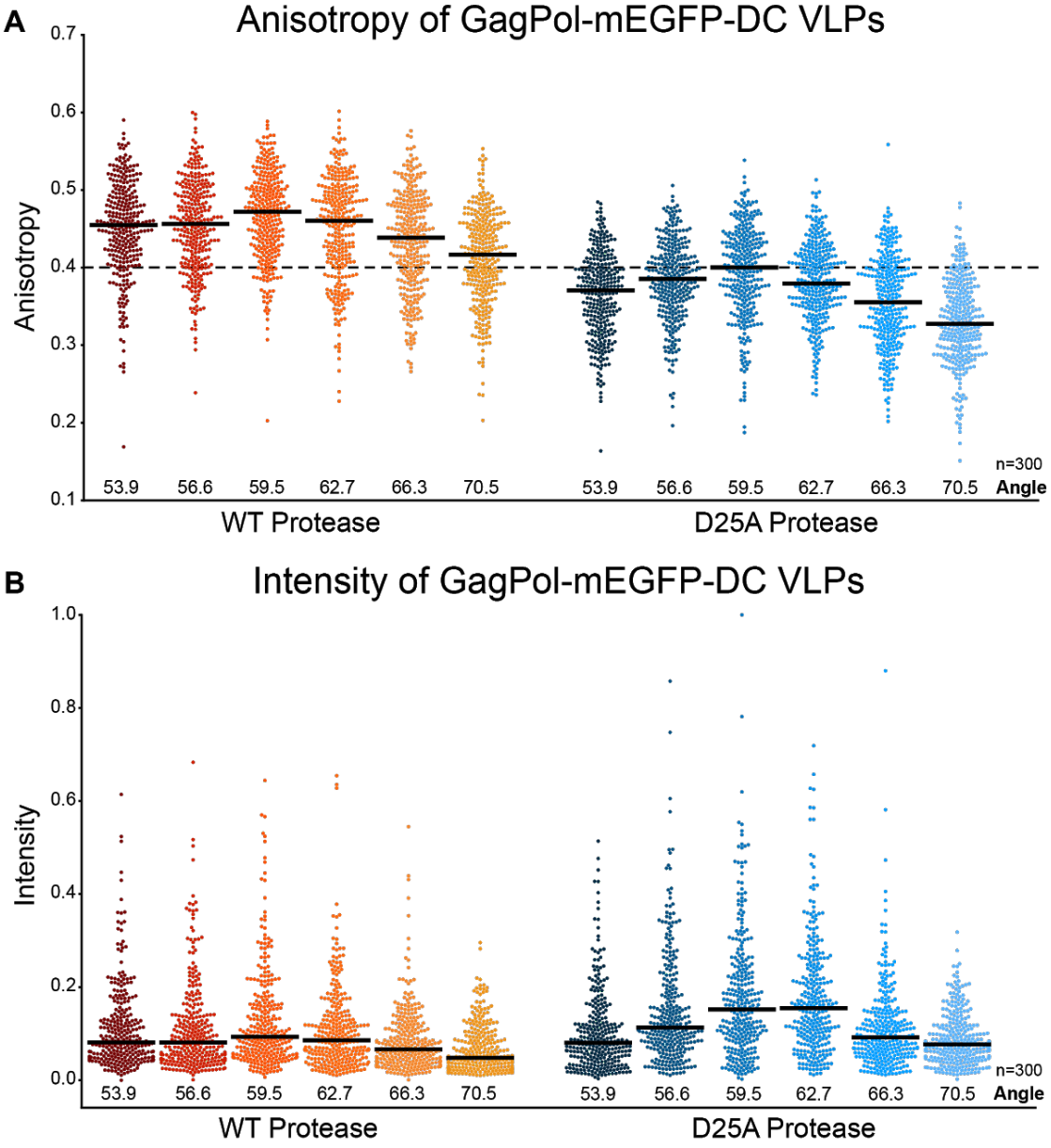

Figure 2.14 Intensity and Anisotropy of GagPol-mEGFP-DC VLPs with different TIRF angles

A Anisotropy of GagPol-mEGFP-DC VLPs with both active WT protease (reds) and D25A protease (blues). TIRF angles go from 53.9 to 70.5 degrees as shown below each plot. The TIRF critical angle is 61.2 degrees. **B** Rescaled intensity of the VLPs from **A**. Intensities were rescaled to be on a 0-1 axis via $(I-I_{min})/(I_{max}-I_{min})$ prior to plotting.

In an attempt to further characterize the relationship between TIRF angle, intensity, and the three-dimensional structure of the VLP, we imaged VLPs with a variety of TIRF angles and looked at the intensity ratio for higher and lower TIRF angles. When we imaged the GagPol-mEGFP-DC construct using standard spinning TIRF, the 66.3/59.5 intensity ratio showed a statistically significant shift between WT and D25A protease (p=.0077); however, the difference in the 66.3/59.5 intensity ratio showed a larger shift between WT and D25A protease when we used the GagPol-mEGFP-MA construct (p<.00001) (Figure 2.15). The direction of the shift in the GagPol-mEGFP-MA constructs shows that mEGFP is easier to excite when released from the CA crystalline lattice. The lack of shift in the GagPol-mEGFP-DC case indicates that although mEGFP becomes easier to excite when the CA lattice is cleaved, the mEGFP population with the GagPol-mEGFP-DC construct moves further away from the coverslip and is excited less. Essentially, the ease of mEGFP excitation is countered by the increased distance of the mEGFP from the coverslip. This finding gives us a clearer view of the relationship between TIRF, intensity, and the VLP structure. It also convinces us that the anisotropy values we are obtaining from our VLPs are not solely a function of intensity.

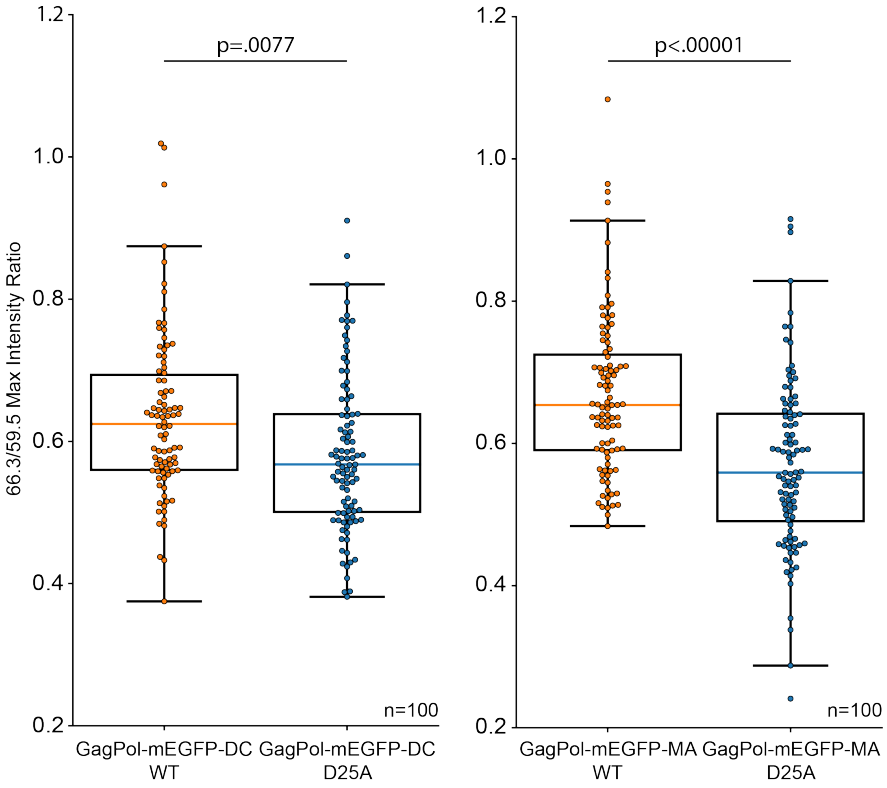

Figure 2.15 66.3/59.5 degree intensity ratio of VLPs
Box plots of the maximum intensity of VLPs with a TIRF angle of 66.3 degrees over max intensity at an angle of 59.5 degrees. The TIRF critical angle is 61.2 degrees. GagPol-mEGFP-DC is shown in the left plot and GagPol-mEGFP-MA is in the right. Both have WT (orange) and D25A (blue) protease plotted (n=100). The p-values displayed are from a two-tailed T-test.

2.2.3 HIV-1 Protease activation occurs during assembly of new particles

After confirming that we were able to see a shift in anisotropy with the GagPol-mEGFP-DC construct and that we saw little to no shift in anisotropy with the GagPol-mEGFP-MA construct in VLPs, we wanted to look at assemblies in live cells to determine when Gag cleavage was occurring. We imaged assembly in HeLa cells transfected with our GagPol-mEGFP-MA negative control construct either with WT or D25A protease using an angle of 66.3 degrees. Analysis of 25 assemblies showed that the assembly intensity and kinetics did not differ between the WT and D25A protease and also that the anisotropy values obtained were not significantly different between the two (Figure 2.16A,B). There are slight differences at the earliest timepoints in assembly, but they converge on the same values after the plateau is reached. We analyzed assemblies with a PI-WT protease to confirm that protease inhibitors would not change the anisotropy. Assemblies with the PI-WT protease show a slight difference in assembly kinetics compared to WT and D25A protease (Figure 2.16A). Assemblies in cells with PI-WT protease tend to assemble faster, but they show the same accumulation followed by a plateau. Assemblies with a PI-WT protease also show a slight shift in anisotropy (Figure 2.16B). Unfortunately, cells treated with protease inhibitors tend to die early in the imaging process. This means that most of our PI-WT protease assemblies do not reach 20 minutes in length. Repeat imaging and analysis of longer assemblies may correct this shift as the 95% confidence intervals for PI-WT protease overlap with those for WT protease (Figure 2.16B).

When we imaged GagPol-mEGFP-DC with either a WT or a D25A protease, we again saw that there was no difference in assembly intensity or kinetics; however, the anisotropy of WT protease was shifted relative to D25A protease (Figure 2.17A,B). This shift was in the same direction that was seen with the VLPs. To confirm that this shift was not due to any differences that the D25A mutation might have on the GagPol structure, we analyzed assemblies with a PI-WT protease. Similar to GagPol-mEGFP-MA assemblies with a PI-WT protease, assemblies with the PI-WT protease with GagPol-mEGFP-DC also showed a difference in assembly kinetics compared to WT and D25A protease (Figure 2.17A). Assemblies with PI-WT seem to assemble faster and reach the plateau sooner, but the shape of the assembly curve remains the same. When we looked at the anisotropy values for PI-WT protease traces, we saw that they showed the same anisotropy over time as the D25A protease except for very early in assembly where they show an intermediate phenotype (Figure 2.17B). We were able to repeat the PI-WT protease imaging enough times that the majority of our traces for GagPol-mEGFP-DC are at least 20 minutes in length, as opposed to the GagPol-mEGFP-MA PI-WT protease assemblies.

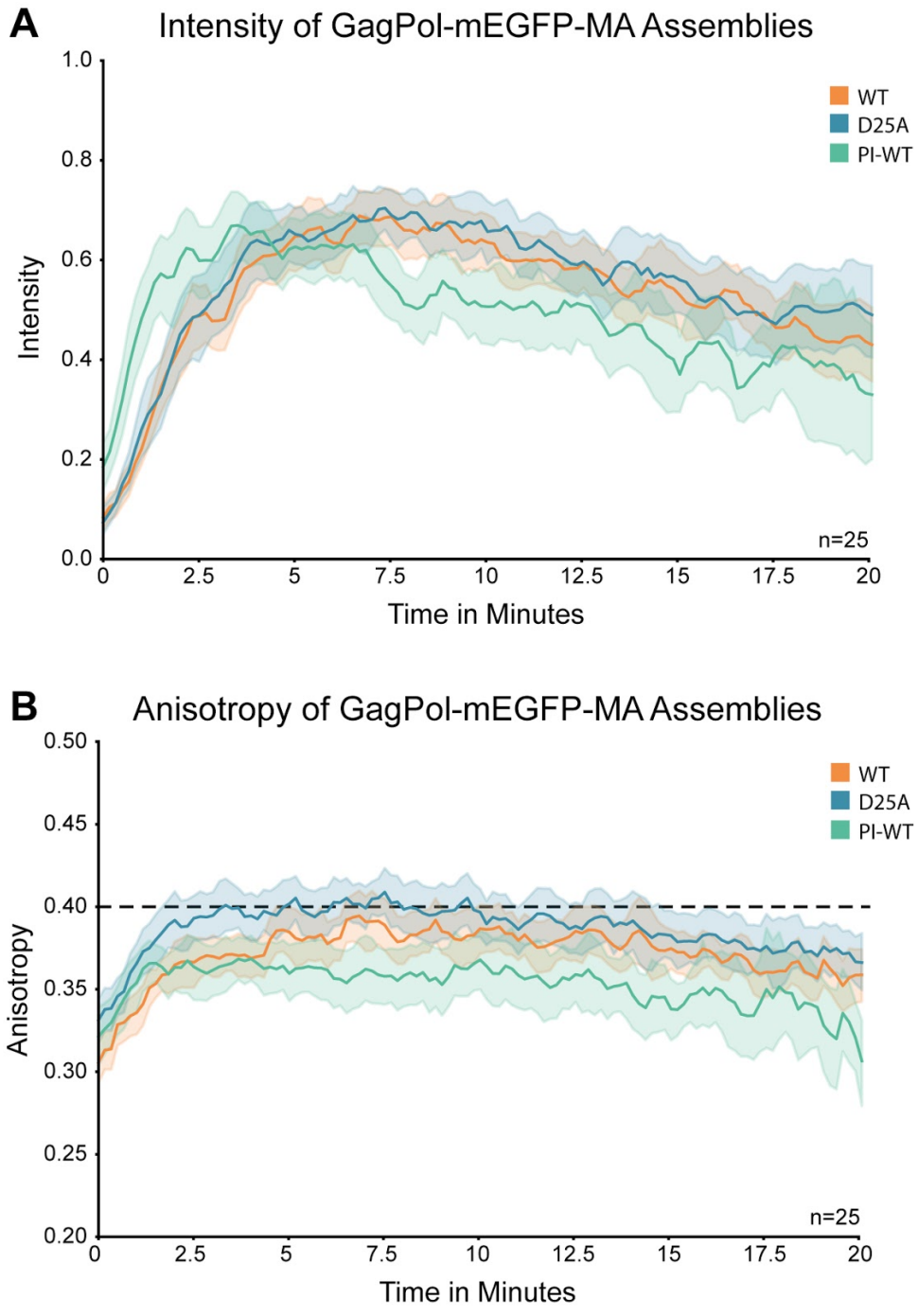

Figure 2.16 Intensity and Anisotropy of GagPol-mEGFP-MA during Assembly
A Intensity of GagPol-mEGFP-MA assembly over time with WT (orange), D25A (blue), and PI-WT (green) protease. Each assembly was rescaled to be on a 0-1 axis via $(I-I_{min})/(I_{max}-I_{min})$ prior to plotting. **B** Anisotropy over time of the same traces shown in A. Dotted line is at 0.4. **A,B** Solid lines show the average and shaded regions show the 95% confidence interval (n=25).

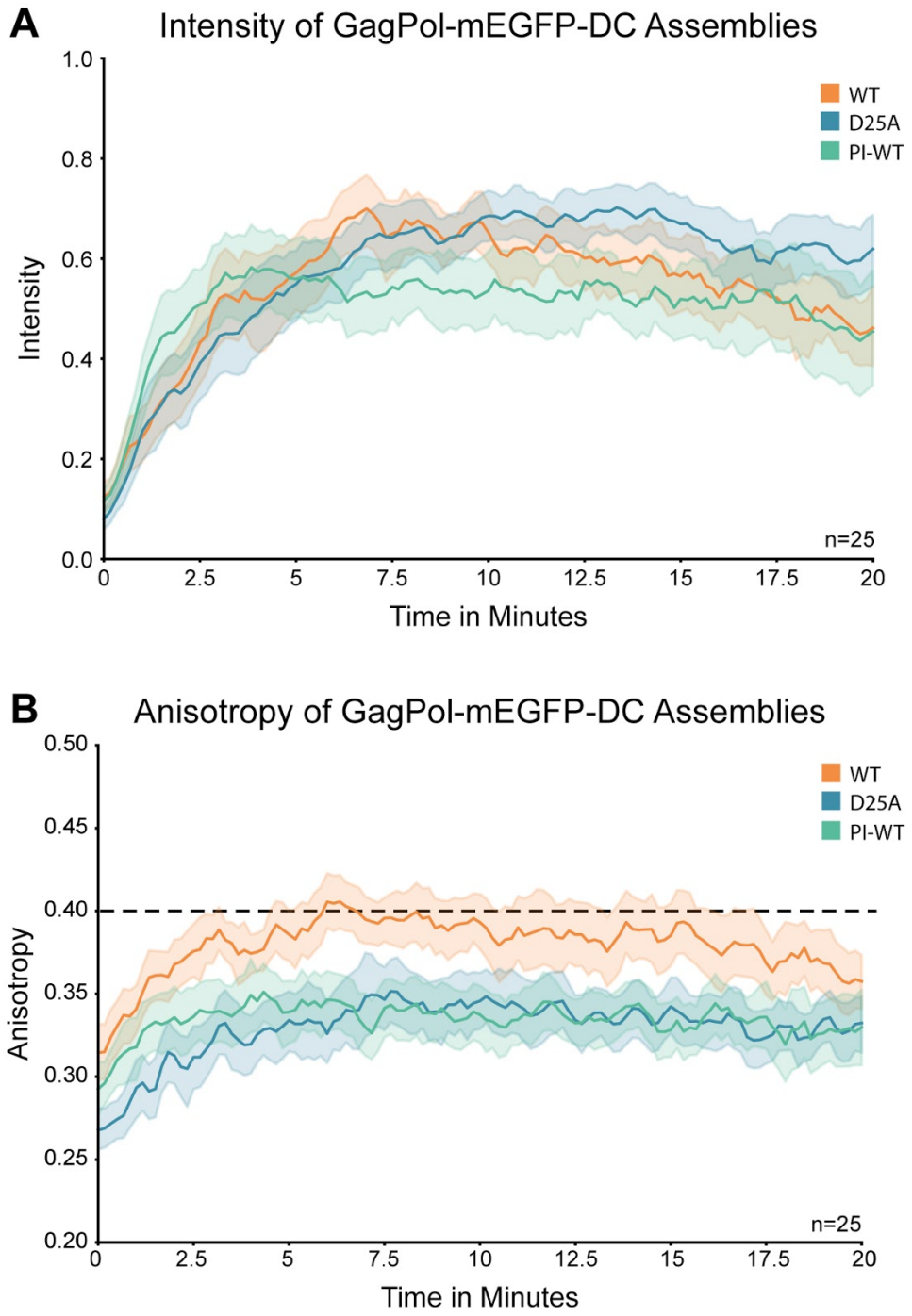

Figure 2.17 Intensity and Anisotropy of GagPol-mEGFP-DC during Assembly
A Intensity of GagPol-mEGFP-DC assembly over time with WT (orange), D25A (blue), and PI-WT (green) protease. Each assembly was rescaled to be on a 0-1 axis via $(I-I_{min})/(I_{max}-I_{min})$ prior to plotting. **B** Anisotropy over time of the same traces shown in A. Dotted line is at 0.4. **A,B** Solid lines show the average and shaded regions show the 95% confidence interval (n=25).

Chapter 3
Further Characterization of Events during Assembly

In this chapter, I will show data from two assembly-related events. In section 3.1, I will show data regarding the antiviral activity of retroCHMP3. The retroCHMP3 protein is found in both mice and squirrel monkeys, but the data in this Chapter will only feature the squirrel monkey version of retroCHMP3. I will present data in this section from Lara Rheinemann and Diane Miller Downhour in the Sundquist Lab that show that retroCHMP3 has antiviral activity. I will also present my data that suggest that retroCHMP3 acts as an antiviral protein by interacting with the host ESCRT protein CHMP4B at sites of HIV-1 assembly. We believe that the delay in scission caused by retroCHMP3 allows for the cell to endocytose assembling HIV-1 particles and also allows for components of Gag to be lost back to the cytosol due to protease activation.

In section 3.2, I will show data regarding the HIV-1 accessory protein Vpr. Vpr is a HIV-1 accessory protein that is recruited to sites of HIV-1 assembly via interaction with the LXXLF motif on the p6 domain of Gag. I will present data that compares the kinetics of this recruitment to Gag recruitment. My findings show that Vpr co-assembles with a four to six-minute delay compared to Gag. The data suggest that there may be turnover and possible interactions between the members of the ESCRT pathway that bind p6 and Vpr.

3.1 retroCHMP3 interacts with ESCRTs during assembly

3.1.1 retroCHMP3 has antiviral activity without cellular toxicity

Previous research has shown that truncated human CHMP3 has an antiviral effect (Zamborlini et al., 2006). Since retroCHMP3 is also C-terminally truncated, we wanted to see if retroCHMP3 would show a similar effect on viral budding. When we expressed increasing amounts of retroCHMP3 in HEK293T cells, which were also expressing HIV-1, we saw that the release of virus was diminished (Figure 3.1A). We also measured the infectivity of the virus released and found that the infectivity decreased with increasing amounts of retroCHMP3 (Figure 3.1A). This effect was not seen when full-length CHMP3 was expressed instead of retroCHMP3. TEM images of cells expressing HIV-1 and retroCHMP3 together showed the previously seen lollipop assemblies that are characteristic of defects in ESCRT recruitment (Figure 3.1B). In addition to inhibiting HIV-1 budding, retroCHMP3 also inhibited the budding of EIAV, Ebola, MLV, and PIV5, which are all dependent on ESCRTs for scission.

Truncated CHMP3(155) is a potent antiviral protein, but it is also toxic to cells. The removal of the autoinhibitory domain produced large aggregates of ESCRT proteins in the cell that prevented cells from successfully dividing (Figure 3.2A). When truncated squirrel monkey CHMP3(155) was expressed in cells, the cell viability dropped to 35% and the percent of cells with midbodies in culture went from 10% to over 60% (Figure 3.2 B, C). We wanted to see whether retroCHMP3 also created these issues in cells or whether the mutations within retroCHMP3 detoxified it. When we expressed retroCHMP3 in HEK293T cells and performed immunofluorescence, the retroCHMP3 had a similar appearance to the full length CHMP3 rather than the punctate appearance of the truncated CHMP3(155) (Figure 3.2A). When we measured the cell viability, cells expressing retroCHMP3 had an 86% survival rate which was similar to cells expressing full length CHMP3 that had a 93% survival rate (Figure 3.2B). Cells expressing retroCHMP3 also had fewer midbodies than those expressing truncated CHMP3(155) (19% with retroCHMP3, 60% with CHMP3(155)) (Figure 3.2C). The cells expressing retroCHMP3 did have a slightly higher percentage of cells with a midbody than cells expressing the full length CHMP3 (6% with CHMP3, 19% with retroCHMP3) (Figure 3.2C). However, the retroCHMP3 midbody counts are much closer to the full length CHMP3 midbody counts.

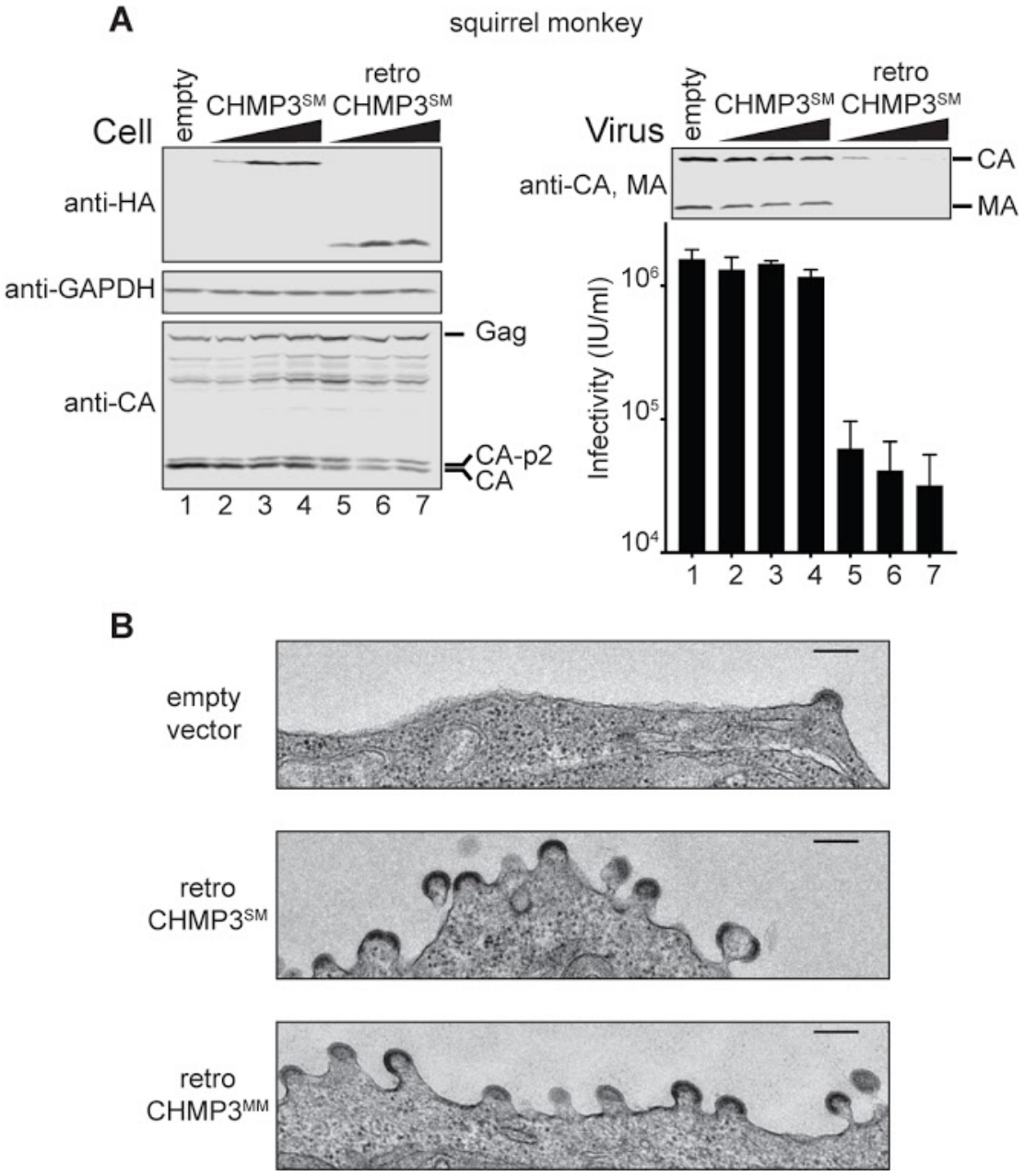

Figure 3.1 retroCHMP3 affects viral budding
A Western blots on cell lysate (left) and collected HIV-1 virus (right) for cells with either an empty vector, full length CHMP3, or retroCHMP3. Bar graph shows infectivity for collected virus. **B** TEM of HEK293T cells expressing HIV-1 and either empty vector (top) or retroCHMP3 (bottom). Data in this figure are from Lara Rheinemann.

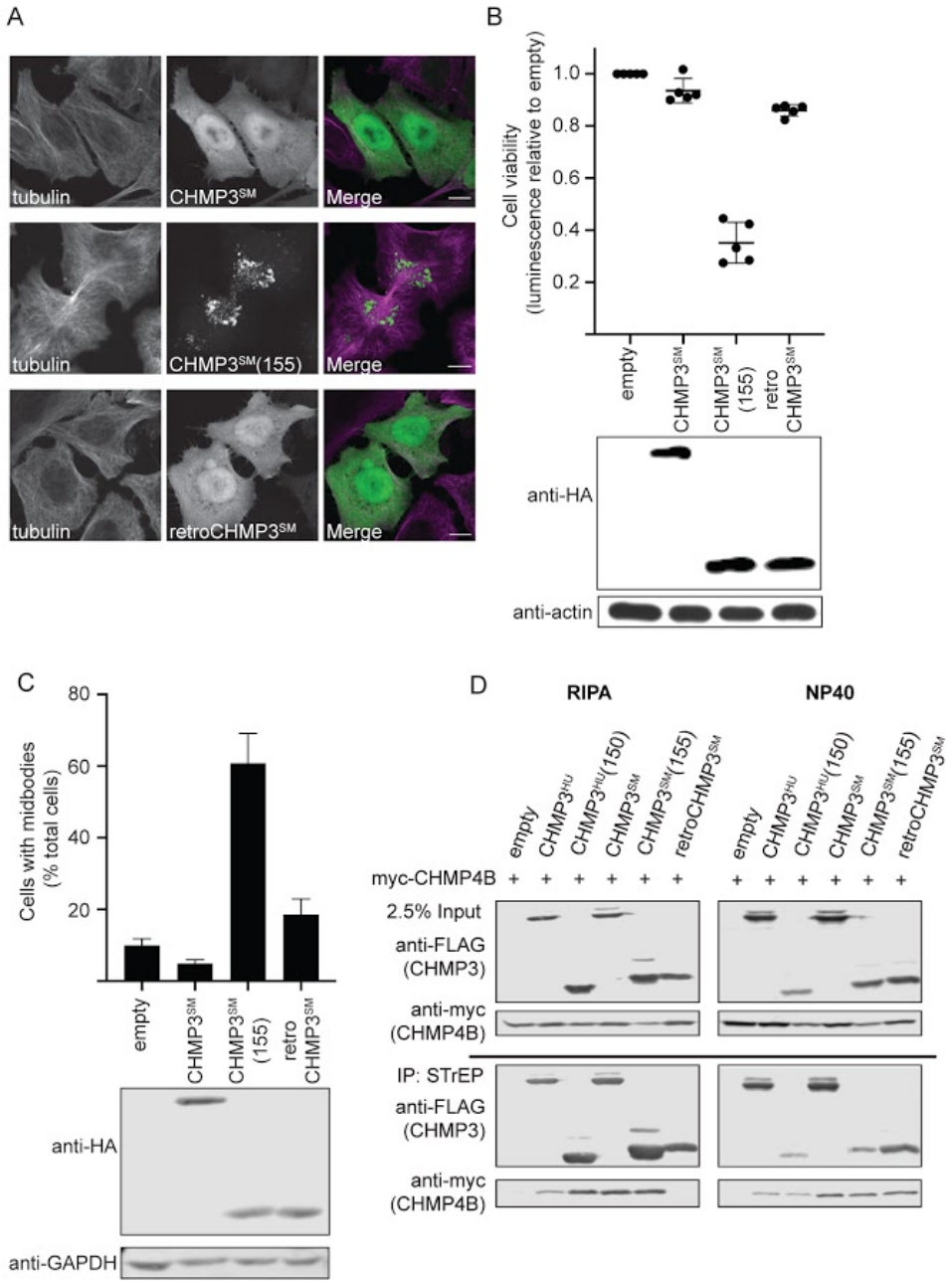

Figure 3.2 retroCHMP3 is non-toxic
A Immunofluorescence of cells expressing full length CHMP3 (top), truncated CHMP3 (155) (middle), or retroCHMP3 (bottom). **B** Plot of cell viability with either empty, CHMP3, CHMP3(155), or retroCHMP3. Western blot of cell lysate is shown below the plot. **C** Bar plot of number of cells with midbodies (n=900). Western blot of cell lysate is shown below the plot. **D** Western blot of pulldown using strep-tag on CHMP3 variants with either RIPA (left) or NP40 (right). For both RIPA and NP40, lane one is an empty vector, lanes 2 and 3 are human CHMP3 variants, and lanes 4-6 are squirrel monkey CHMP3 variants. Immunofluorescence and cytotoxicity data in this figure are from Diane Miller Downhour. The remaining data in this figure are from Lara Rheinemann

3.1.2 retroCHMP3 affects the recruitment of ESCRT proteins to HIV-1 assembly sites

After confirming that retroCHMP3 had an antiviral effect without the toxicity seen with truncated CHMP3, we wanted to determine the mechanism of activity. Pulldowns of CHMP4B using either full length CHMP3, truncated CHMP3(155), or retroCHMP3 showed that the interactions between retroCHMP3 and CHMP4B were weaker than they were with full length CHMP3 and CHMP4B (Figure 3.2D).

In order to get a more nuanced view of the interactions between retroCHMP3 and CHMP4B, we decided to move into live cell imaging of HIV-1 assembly. Unfortunately, attempts to tag retroCHMP3 with a fluorescent protein were not successful. RetroCHMP3 did not show the same inhibition of budding when attached either N- or C-terminally to a fluorescent protein. As we needed confirmation that cells were expressing retroCHMP3 in order to be confident that any changes in ESCRT recruitment were due to retroCHMP3 interference, I created a construct that would express retroCHMP3 followed sequentially by a T2A peptide and an H2B-tagBFP. The T2A peptide is a special sequence that causes the translating ribosome to release the peptide already synthesized while still translating the rest of the sequence. The construct I created would have the retroCHMP3 translated and released followed by an H2B-tagBFP. The H2B-tagBFP localizes to the nuclei of cells expressing this retroCHMP3 allowing for the imaging of blue nuclei to be a marker of confidence of the presence of retroCHMP3. When tested, this construct behaved the same as an untagged retroCHMP3, so we moved forward and imaged cells expressing retroCHMP3-T2A-H2B-tagBFP.

In order to see any effects on ESCRT recruitment, we chose to image CHMP4B and VPS4A. Our pulldown experiments suggested that CHMP4B binding is weakened with retroCHMP3, and we know that CHMP4B and VPS4A have well defined interactions and recruitment kinetics (Bleck et al., 2014). To see if retroCHMP3 affected recruitment of CHMP4B or VPS4A, we transiently transfected HIV-1 GagPol-mEGFP along with either mCherry-CHMP4B or mCherry-VPS4A. We then imaged cells that showed both colors of fluorescence for one hour taking mCherry images every five seconds and mEGFP images every twenty seconds. To look for ESCRT recruitment, we selected every GagPol-mEGFP assembly that took place on the cell during the one-hour imaging time course with circular regions that encompassed the entire assembling particle. We then applied those regions to the corresponding mCherry images and looked for mCherry puncta with a Gaussian distribution that correlated with the GagPol-mEGFP puncta. For cells expressing retroCHMP3-T2A-H2B-tagBFP, we confirmed that the cells had blue nuclei in addition to the mEGFP and mCherry fluorescence prior to imaging. All other analysis was identical to cells without retroCHMP3.

When we imaged cells expressing HIV-1 GagPol-mEGFP along with mCherry-CHMP4B, we recorded that 71% of HIV-1 assemblies recruited CHMP4B one time, 17% recruited CHMP4B twice (Figure 3.3C). None of the assemblies recruited CHMP4B more than four times. When we expressed the retroCHMP3-T2A-H2B-tagBFP, the

percentage of cells recruiting CHMP4B one time dropped to 37%, two recruitments increased to 33%, and 11% of the assemblies analyzed had seven or more CHMP4B recruitments (p=.000979) (Figure 3.3C). We additionally looked at the length of time that CHMP4B remained at the sites of assembly once it was recruited. For cells expressing GagPol-mEGFP and mCherry-CHMP4B, the average length of time that CHMP4B remained was 23 seconds (Figure 3.3D). When we looked at cells expressing GagPol-mEGFP, mCherry-CHMP4B, and retroCHMP3-T2A-H2B-tagBFP together, the average length of time that CHMP4B remained was increased to 41 seconds (p=.000409) (Figure 3.3D).

After determining that retroCHMP3 had an effect on the recruitment of CHMP4B to sites of assembly, we wanted to look downstream of CHMP4B recruitment to see if VPS4A recruitment was also affected in the same way. When we looked at cells expressing GagPol-mEGFP and mCherry-VPS4A, we saw that 79% of assemblies analyzed recruited VPS4A one time and 19% recruited VPS4A twice (Figure 3.4C). When we added retroCHMP3-T2A-H2B-tagBFP to the cells in addition to GagPol-mEGFP and mCherry-VPS4A, we did not see a significant difference in the number of times that VPS4A was recruited. In cells with retroCHMP3, VPS4A was recruited once 76% of the time and twice 14% of the time (Figure 3.4C). Although the number of recruitments did not appear to change, the length of each recruitment changed between cells with and without retroCHMP3. In cells without retroCHMP3, VPS4A remained at assembly sites for an average of 17 seconds. With retroCHMP3, the length of recruitment dropped to 11.5 seconds (p=.002163) (Figure 3.4D).

Figure 3.3 CHMP4B recruitment with and without retroCHMP3
A,B Average recruitment of GagPol-mEGFP to an assembling VLP (top) and recruitment of mCherry-CHMP4B (bottom). Cells were transfected with GagPol-mEGFP and mCherry-CHMP4B, and in **B** the cells are also transfected with retroCHMP3-T2A-H2B-tagBFP. The solid line for recruitment of Gag (top) is the average (n=3) and the shaded overlay represents the 95% confidence interval. Gag intensities were rescaled to be on a 0-1 axis. For recruitment of CHMP4B (bottom) in **A** and **B**, each number shaded region highlights a recruitment and the corresponding sequence of images from that recruitment. The width of each image is 1.27μm. **C** Histogram of number of times that CHMP4B was recruited to sites of assembly with (n=46) and without (n=41) retroCHMP3 ($p<0.001$). **D** The duration for each CHMP4B recruitment with (n=126 recruitments from 46 assemblies) and without (n=59 recruitments from 41 assemblies) retroCHMP3 ($p<0.0005$). For both **C** and **D**, data without retroCHMP3 are in blue and data with retroCHMP3 are in red.

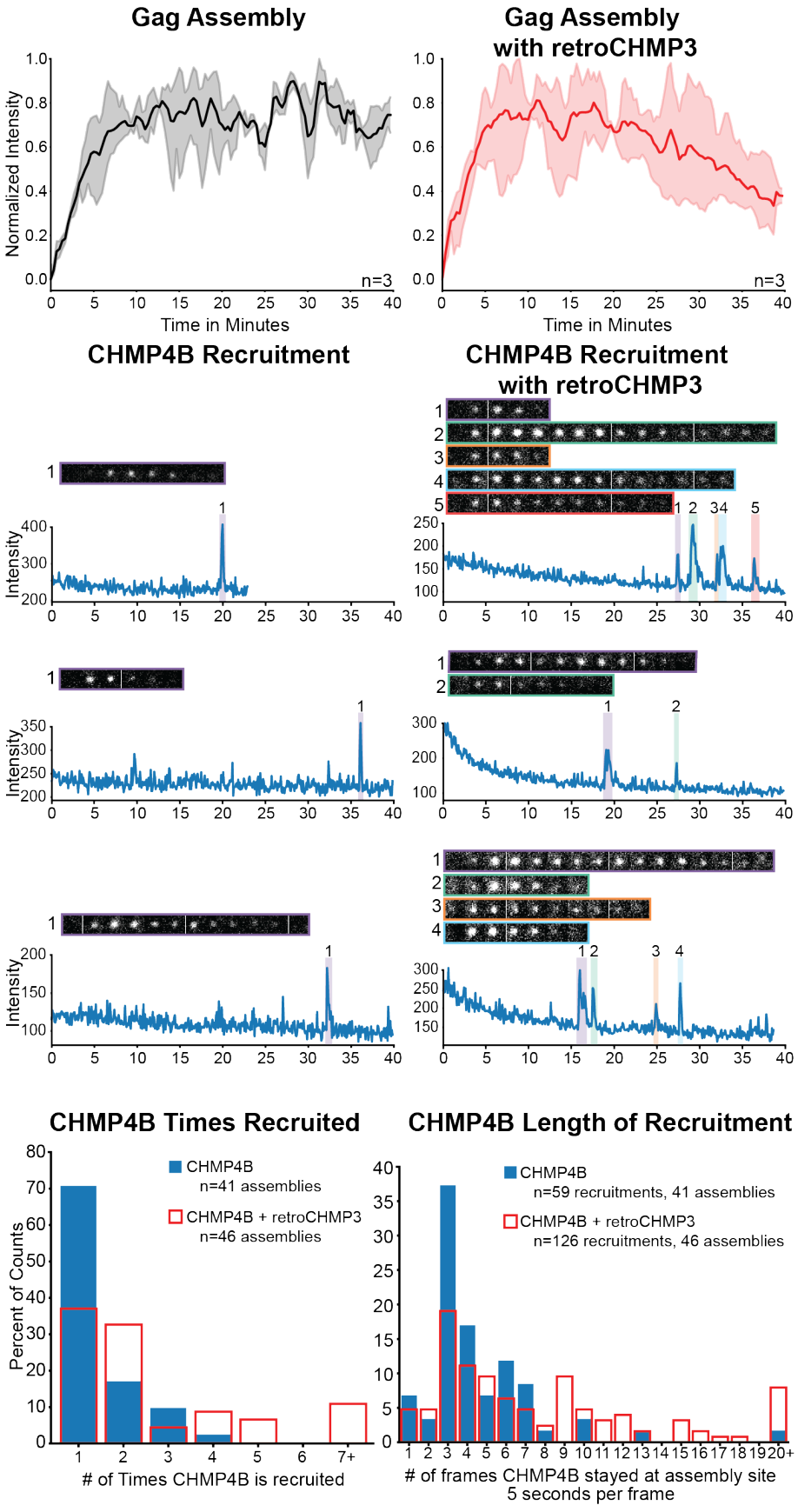
Gag Assembly
Gag Assembly with retroCHMP3
Normalized Intensity
Time in Minutes
n=3
CHMP4B Recruitment
CHMP4B Recruitment with retroCHMP3
Intensity
CHMP4B Times Recruited
CHMP4B Length of Recruitment
CHMP4B
n=41 assemblies
CHMP4B + retroCHMP3
n=46 assemblies
Percent of Counts
# of Times CHMP4B is recruited
CHMP4B
n=59 recruitments, 41 assemblies
CHMP4B + retroCHMP3
n=126 recruitments, 46 assemblies
# of frames CHMP4B stayed at assembly site
5 seconds per frame

Figure 3.4 VPS4A recruitment with and without retroCHMP3
A,B Average recruitment of GagPol-mEGFP (top) with mCherry-VPS4A recruitment plotted below. Cells were transfected with GagPol-mEGFP and mCherry-VPS4A, and in **B** the cells were additionally transfected with retroCHMP3-T2A-H2B-tagBFP. The solid line for recruitment of Gag (top) is the average (n=3) and the shaded overlay represents the 95% confidence interval. Gag intensities were rescaled to be on a 0-1 axis. For VPS4A recruitments (bottom) in **A** and **B**, each shaded region highlights a recruitment and the corresponding sequence of images from that recruitment. The width of each image is 1.27μm. **C** Histogram of the number of times that VPS4A was recruited to sites of assembly with (n=42) and without (n=48) retroCHMP3 (no significance).
D The duration of recruitment for each VPS4A recruitment with (n=59 recruitments from 42 assemblies) and without (n=62 recruitments from 48 assemblies) retroCHMP3 ($p<0.0022$). For both **C** and **D**, data without retroCHMP3 are in orange and data with retroCHMP3 are in red.

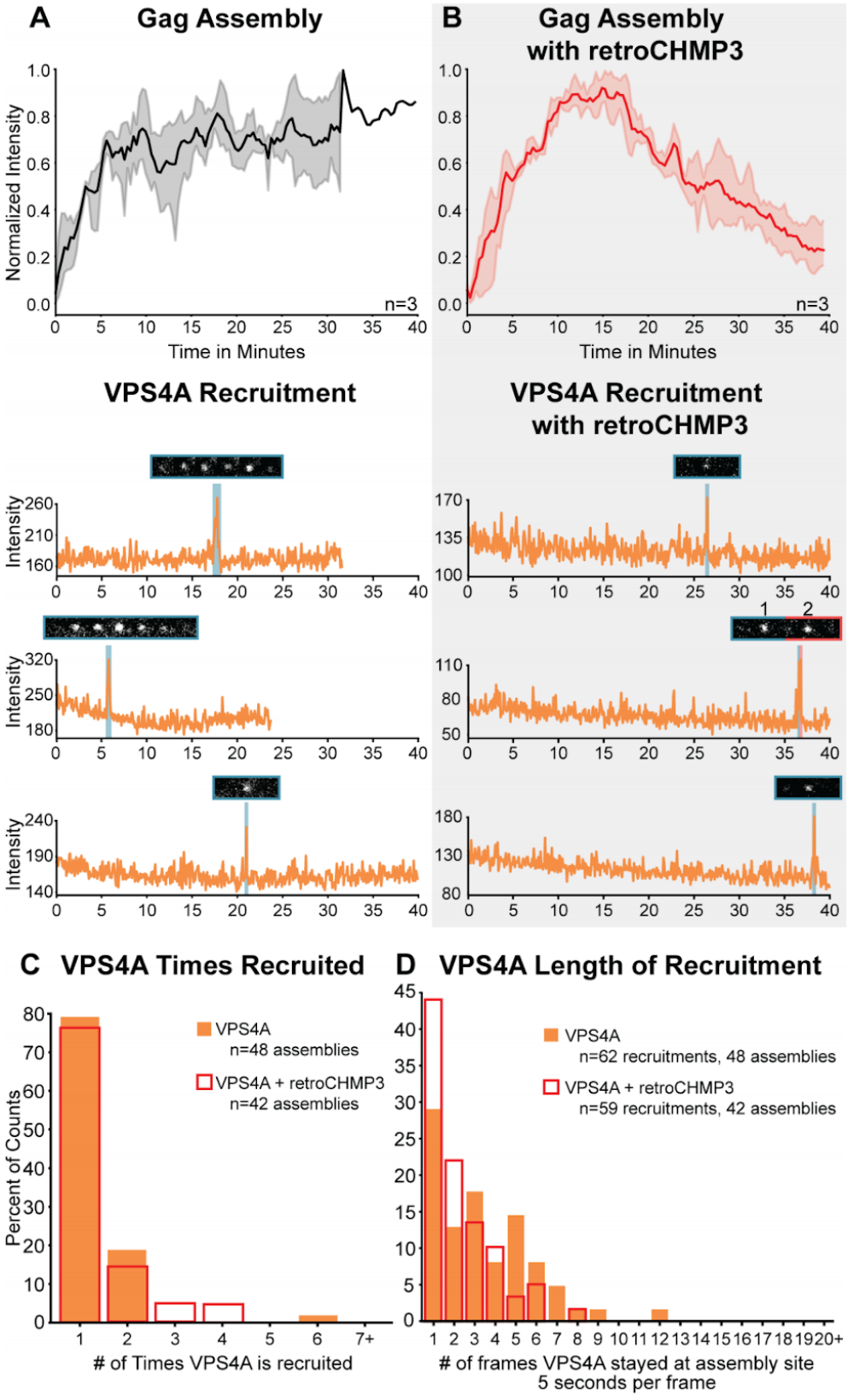
A
Gag Assembly
Normalized Intensity
Time in Minutes
n=3
B
Gag Assembly
with retroCHMP3
Time in Minutes
n=3
VPS4A Recruitment
VPS4A Recruitment
with retroCHMP3
Intensity
1
2
C
VPS4A Times Recruited
VPS4A
n=48 assemblies
VPS4A + retroCHMP3
n=42 assemblies
Percent of Counts
# of Times VPS4A is recruited
D
VPS4A Length of Recruitment
VPS4A
n=62 recruitments, 48 assemblies
VPS4A + retroCHMP3
n=59 recruitments, 42 assemblies
# of frames VPS4A stayed at assembly site
5 seconds per frame

Issues with properly recruiting ESCRTs to sites of assembly have a detrimental effect not only because the viruses don't properly scission from the cell, but also because the viruses can lose crucial viral components back into the cell due to protease activity. We wanted to see whether this was happening as a result of retroCHMP3 interacting with ESCRTs. The GagPol-mEGFP construct that we are using in this work is one where the mEGFP is inserted between the MA and CA domains with the MA/CA cleavage site on either side of the mEGFP. This means that if protease cleavage occurs and if retroCHMP3 affects the process of scission such that the VLPs are still attached to the cell, the mEGFP will be free to diffuse out of the particle and back into the cell. This means that we should see a decrease in fluorescence over time in cells with assemblies that have retroCHMP3 present and a maintenance of fluorescence with assemblies lacking retroCHMP3.

When we looked at 26 assemblies that recruited CHMP4B without retroCHMP3 expressed and compared them to 26 assemblies with retroCHMP3 expressed, we saw that traces with retroCHMP3 present tended to end with lower fluorescence than those without retroCHMP3 (Figure 3.5A). When we plotted an average of all 26 traces, we saw that traces with retroCHMP3 tended to have a decay in fluorescence after reaching the assembly peak whereas assemblies without retroCHMP3 had their fluorescence remain steady after reaching the peak (Figure 3.5B). To be sure that this loss of fluorescence in assemblies on cells expressing retroCHMP3 was specifically due to protease activity, we imaged cells with a GagPol-mEGFP that contained the protease inactivating D25A mutation. In cells expressing the GagPol-mEGFP(D25A), mCherry-CHMP4B, and retroCHMP3-T2A-H2B-tagBFP together, the loss of fluorescence seen previously with retroCHMP3 present was rescued (Figure 3.5B,E). Inactivation of the protease allowed for maintenance of the fluorescence after reaching the peak, despite the fact that retroCHMP3 was expressed.

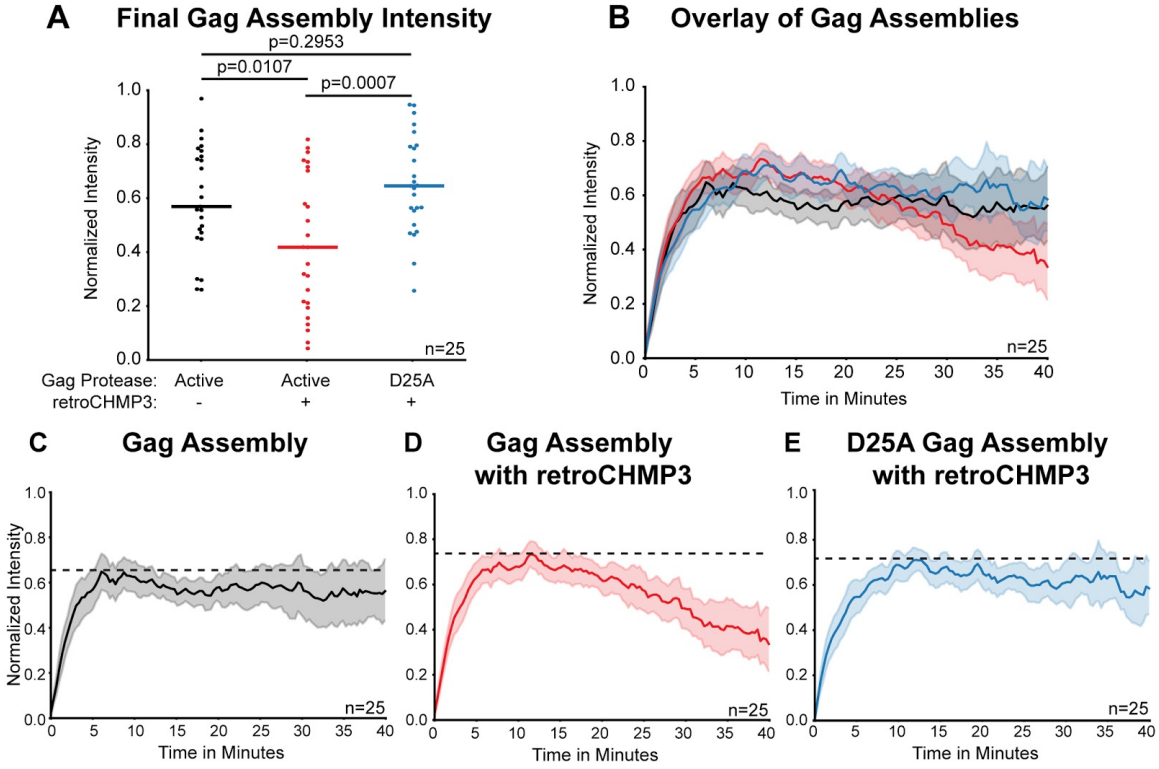

Figure 3.5 Fluorescence is lost in assemblies with retroCHMP3
A Plot of average final intensity for each trace which visibly recruited mCherry-CHMP4B for GagPol-mEGFP without retroCHMP3 (black), GagPol-mEGFP with retroCHMP3 (red), and GagPol-mEGFP-D25A with retroCHMP3 (blue) (n=25). GagPol-mEGFP-D25A contains an inactivated protease. Colored bars indicate the median of the data. **B** Plot of average Gag recruitment for GagPol-mEGFP with (black) and without (red) retroCHMP3 and GagPol-mEGFP-D25A with retroCHMP3 (blue). **C-E** Individual plots of each condition seen in **B**. Dotted lines indicate the peak of the assembly trace. Gag intensities were rescaled to be on a 0-1 axis. The solid line for recruitment of Gag in **B-E** is the average and the shaded overlay represents the 95% confidence interval.

3.2 Vpr co-assembles with Gag

3.2.1 Vpr is incorporated into VLPs

To determine the kinetics of Vpr recruitment, we wanted to be able to image Vpr using fluorescence. Thus, we first had to confirm that fluorescently tagged Vpr was packaged specifically into our VLPs. We created an mEGFP-Vpr construct and co-expressed it with an NL4.3-GagPol packaging vector with an mCherry inserted after the matrix domain of Gag (GagPol-mCherry) (Figure 3.6). This latter construct will mostly make Gag-mCherry, but also GagPol-mCherry when slippage occurs. The expression and packing of the mEGFP-Vpr into VLPs was confirmed by Western blots (Figure 3.7A). To confirm that Vpr was specifically being recruited to sites of assembly via the LXXLF motif, we introduced a stop codon into the LXXLF motif of Gag which removed the last 9AA of p6 while leaving the Alix and TSG101 recruitment motifs intact (GagPol-mCherry-LXXLF) (Figure 3.6). This mutation also leaves the Pol amino acid sequence fully intact. When we co-expressed mEGFP-Vpr with GagPol-mCherry-LXXLF, we were able to collect VLPs that were positive for capsid and mCherry, albeit at reduced levels, but mEGFP-Vpr was not detectable (Figure 3.7A).

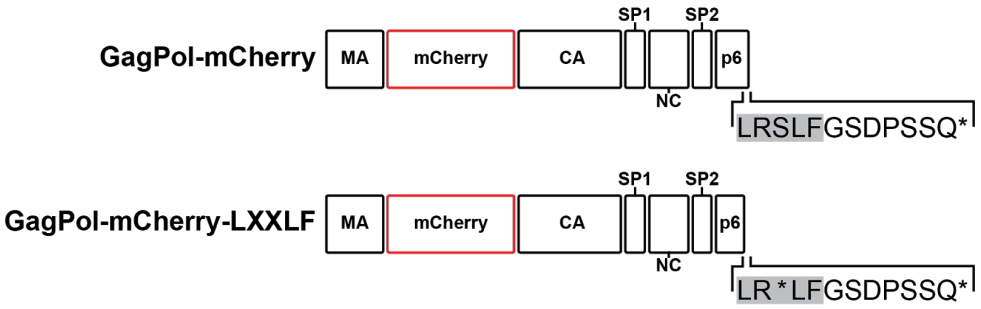

Figure 3.6 Schematic of GagPol Plasmids
Both GagPol-mCherry and GagPol-mCherry-LXXLF are NL4.3 sequences with the slippage site intact. The mCherry in both is inserted without a linker within the matrix domain prior to the Matrix/Capsid cleavage site. GagPol-mCherry-LXXLF has a stop codon introduced in the middle of the LXXLF Vpr recruitment motif which removes the last 9 amino acids from Gag but leaves the Pol coding sequence intact.

To further test the assembly of mEGFP-Vpr into VLPs, we co-transfected it together with GagPol-mCherry and collected supernatant after 24 hours. There are some caveats with this approach. First, VLPs are created via transient transfection, which means that the VLPs come from a population of cells with different amounts of plasmid and expressing differing levels of each protein. Further, the collection of VLPs includes small pieces of cell debris that go through the filter. For this reason, quantifying the relative levels of proteins VLPs collected from a mixed population of cells has potential limitations for quantifying the packaging of Vpr. Additionally, VLPs with GagPol-mCherry can be excited at 488 nm. While they will not be as efficiently excited as a GFP, at a high concentration VLPs with GagPol-mCherry excited at 488nm may falsely be recorded as positives for mEGFP-Vpr. To limit any false positives, we imaged

VLPs (n=100) with GagPol-mCherry and GagPol-mCherry-LXXLF in the absence mEGFP-Vpr to quantify the cross-channel contamination so the mCherry excited by the 488nm laser could be subtracted from the mEGFP images.

Despite the stringent subtraction of the mCherry signal from the GFP channel and the inherent problems with collecting VLPs from transient transfection, 51% of all GagPol-mCherry VLPs also contained detectable mEGFP-Vpr (Fig 3.7B). When we analyzed VLPs made with GagPol-mCherry-LXXLF, which is missing the Vpr recruitment domain, the percent of GagPol-mCherry VLPs with mEGFP-Vpr dropped to 9% (Fig 3.7B).

To test if mEGFP-Vpr was only found in VLPs and not found in other cell debris or in puncta without Gag, we checked mEGFP-Vpr positive puncta (n=100) and found that 77% of them were also GagPol-mCherry positive (Fig 3.7C). When we transfected cells with GagPol encoding an embedded fluorescent protein, we co-transfected them with a plasmid with GagPol without a tag. This avoided morphological problems in VLPs that occurred when all of the copies of GagPol are expressed as fusion proteins (Larson et al., 2005). The ratio we used is a 1:4 ratio of tagged/untagged GagPol. We believe that the percentage of mEGFP-Vpr puncta that also contain GagPol-mCherry was not 100% due to a proportion of cells that were only transfected with untagged GagPol and mEGFP-Vpr without tagged GagPol. The results from Western blots and imaging were consistent with mEGFP-Vpr being packaged specifically into VLPs. We also confirmed that the LXXLF motif is necessary for that recruitment.

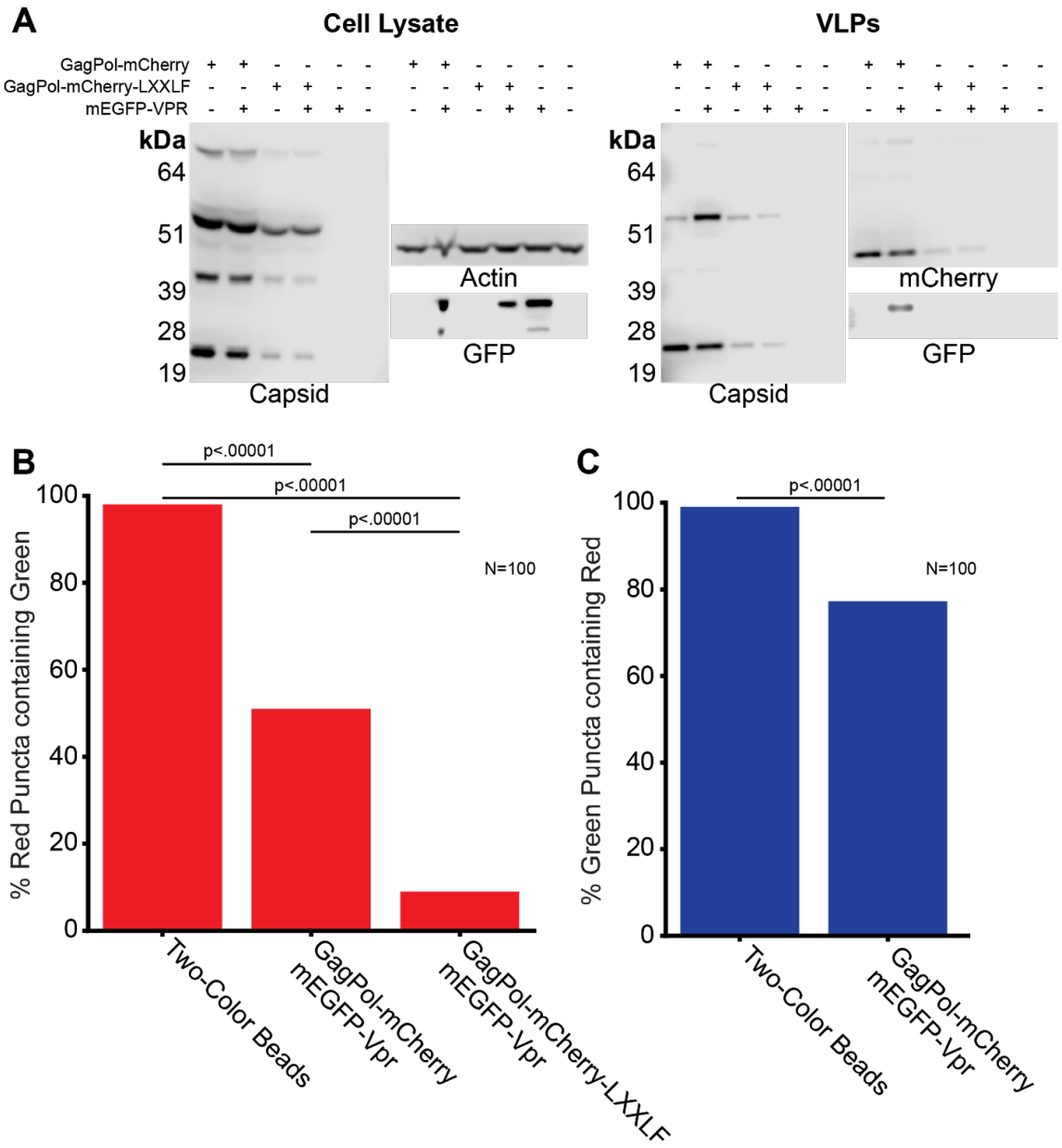

Figure 3.7 Vpr is packaged specifically into VLPs
A Cell lysate (left) and VLPs (right) collected from Hek293T cells 48 hours after transfection. Cell lysate was probed with anti-capsid, anti-actin, and anti-GFP antibodies. Western blots were probed with anti-capsid, anti-mCherry, and anti-GFP antibodies. **B** shows the quantification of the percent of red puncta that were also green (n=100). **C** shows the quantification of the percent of green puncta that were also red (n=100).

3.2.2 Vpr co-assembles with GagPol

We next examined the recruitment of mEGFP-Vpr in cells expressing either GagPol-mCherry or GagPol-mCherry-LXXLF. Single frames from cells with GagPol-mCherry and mEGFP-Vpr six hours after transfection showed puncta in both red and green that co-aligned. In contrast, when we co-transfected the GagPol-mCherry-LXXLF with the mEGFP-Vpr, cells assembled VLPs, but mEGFP-Vpr was not detected at sites of GagPol (Fig 3.8A). Quantification of VLPs in the single frames showed that 78% of the selected GagPol-mCherry puncta on the cell were also mEGFP-Vpr positive, but only 5% of GagPol-mCherry-LXXLF puncta were mEGFP-VPR positive (Fig 3.8B). The percentage of GagPol-mCherry puncta that were positive for mEGFP-Vpr on the surface of cells was higher than from isolated VLPs. This substantiates the conclusion that a contributing factor to the lower level of colocalization in the VLPs were cells expressing GagPol-mCherry but not mEGFP-Vpr.

To determine the kinetics of recruitment of Vpr to VLPs, we imaged mEGFP-Vpr in live cells. When we did a time-lapse imaging of mEGFP-Vpr together with GagPol-mCherry in HeLa cells, we saw that mEGFP-Vpr co-localized with GagPol (Fig 3.9A). The intensity of the fluorescence from mEGFP-Vpr reached a plateau, indicating the end of net recruitment, similar to the plateau reached by GagPol assembly. Vpr did show a delay of four to six minutes in reaching its plateau when compared to GagPol. The kinetics or recruitment we observed for the mEGFP-Vpr was the same whether we used only untagged GagPol or a mixture with untagged and tagged GagPol-mCherry (Fig 3.9B).

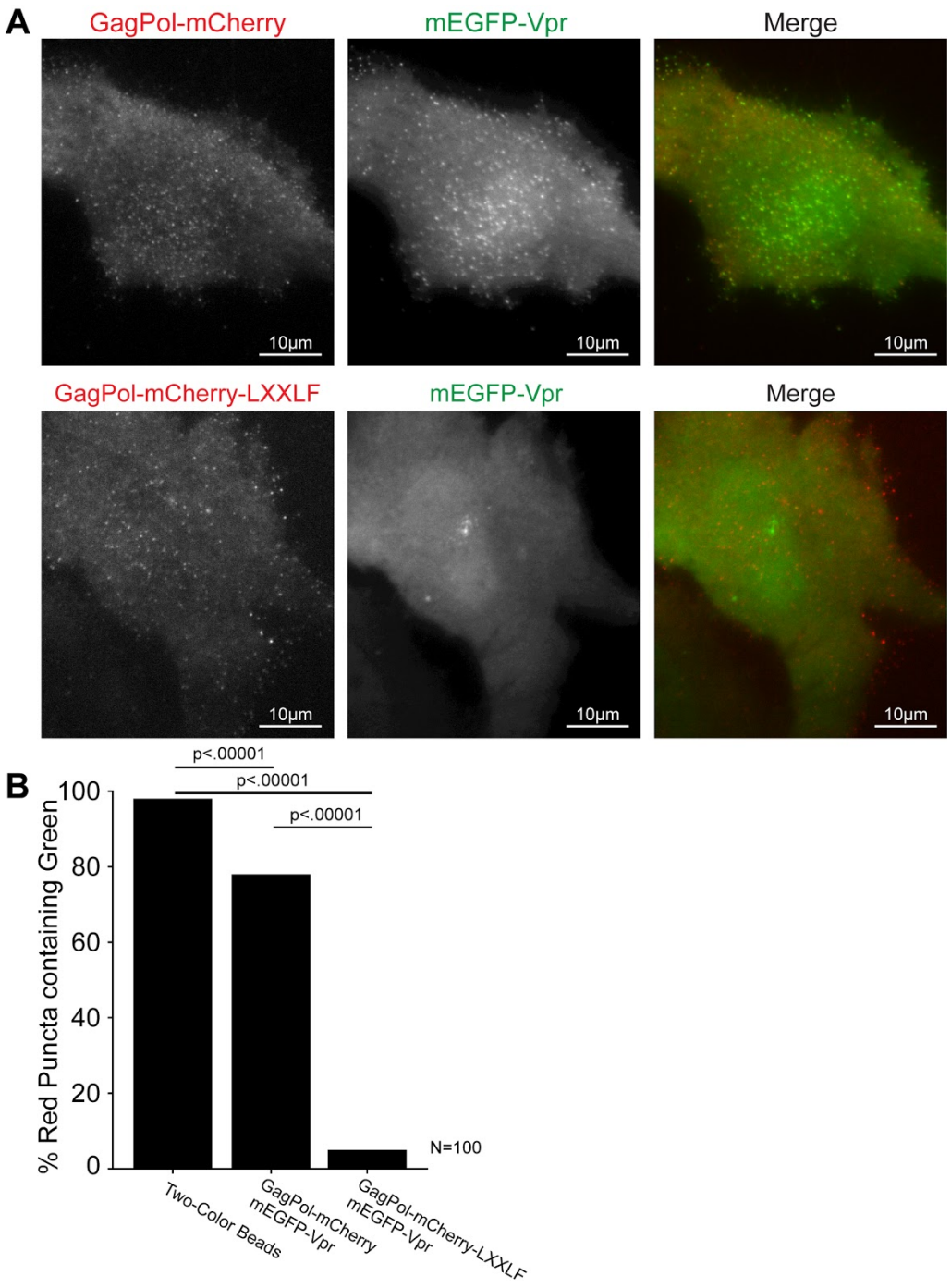

Figure 3.8 GagPol with or without the LXXLF mutation
Single frames from a sequence of HeLa cells actively assembling new particles (**A**). The top row of images is from cells transiently expressing GagPol-mCherry and mEGFP-Vpr. The bottom row is from cells transiently expressing GagPol-mCherry-LXXLF and mEGFP-Vpr. The first column is GagPol in red, the second is Vpr in green, and the final column is a merge of the first two. All scale bars are 10μm. Quantification of puncta from two-color beads and GagPol-mCherry or GagPol-mCherry-LXXLF puncta on from cells (n=100).

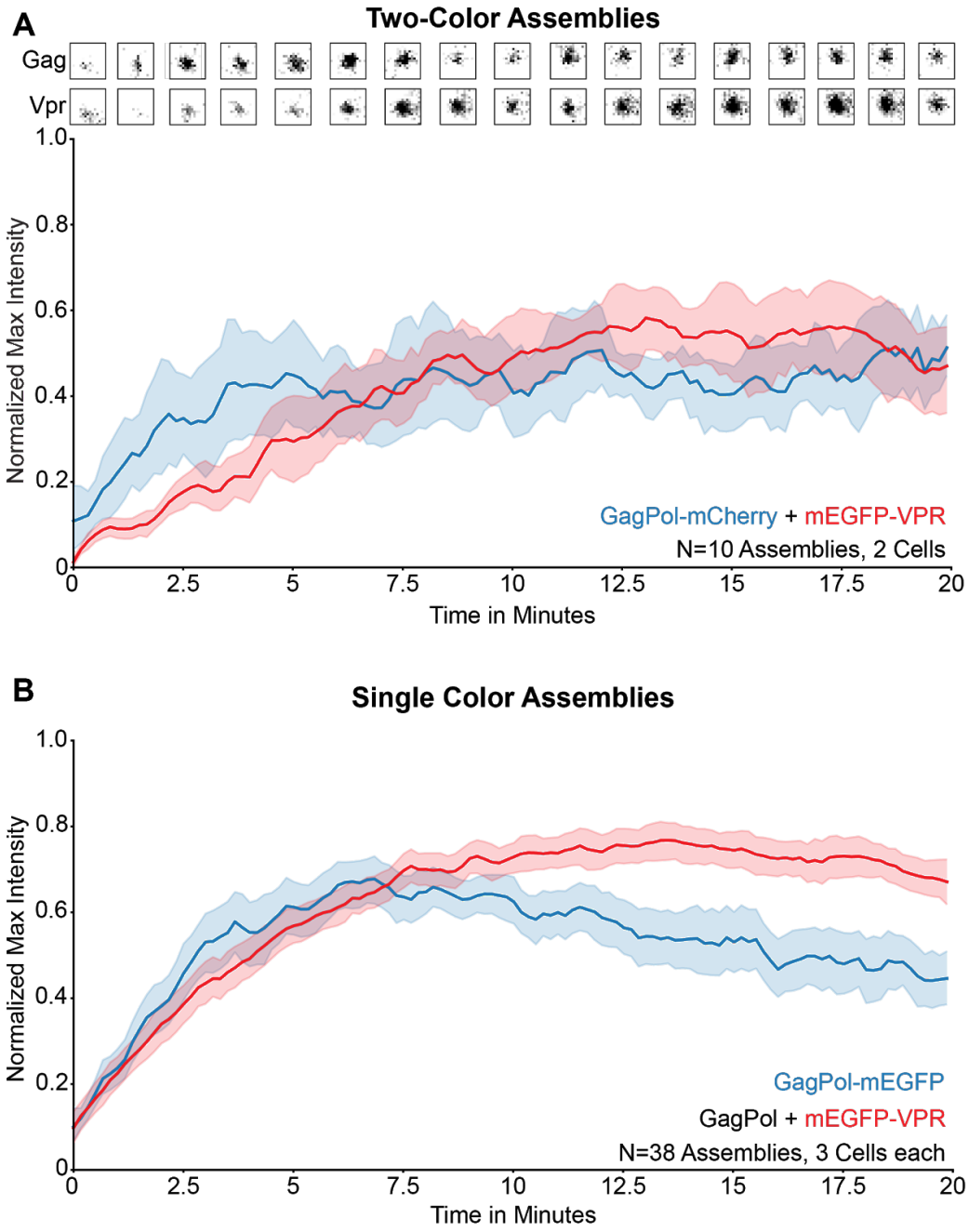

Figure 3.9 Assembly traces of GagPol and Vpr
A Assembly of Vpr and Gag-Pol. Select images from assembly (top) and the fluorescence intensity of the recruitment of mEGFP-Vpr and Gag-Pol-mCherry (average of 10 assemblies) (bottom). **B** Traces for assembly traces for 38 VLPs where Vpr and GagPol were imaged separately in different cells. GagPol-mEGFP was imaged without Vpr. mEGFP-Vpr was imaged with untagged GagPol. The solid line in the graphs in both **A** and **B** shows the average while the shaded region surrounding the solid line shows the 95% confidence interval. Each assembly was rescaled to be on a 0-1 axis via $(I-I_{min})/(I_{max}-I_{min})$.

Chapter 4
How to summarize a graduate career studying HIV-1

This chapter will present my survey work on the most effective way to summarize scientific research. It is adapted from my publication in PLoS ONE (Bredbenner and Simon, 2019). This research analyzed the effectiveness of video abstracts, graphical abstracts, and plain languages summaries as compared to original academic abstracts. The purpose of this research was to help scientists and journal editors decide how best to present their research and make it accessible for more people.

I will start this chapter with section 4.1 which is a brief methods section for the study. The full methods for this work can be seen in Chapter 6, section 6.8.

In section 4.2, I will give an overview of the participants of the survey and some information collected about the participants prior to them seeing any of the summaries. Section 4.3 will discuss the data on which summary was the most effective.

Sections 4.4 and 4.5 will delve further into the collected data and talk about correlations within the results. Section 4.4 will discuss correlations between what the participants said they preferred versus the scores they gave the science summaries, and section 4.5 will discuss correlations between the understanding and comprehension scores.

4.1 Brief Methods for Study

To study which science summary was most effective, two papers within the HIV-1 field from Rockefeller labs with Rockefeller graduate student first authors both published in the Nature journal family were chosen. The first was *Clonal CD4+ T cells in the HIV-1 latent reservoir display a distinct gene profile upon reactivation* from Cohn *et al.* published in Nature Medicine on April 23, 2018 (Cohn et al., 2018). The second paper was *CG dinucleotide suppression enables antiviral defence targeting non-self RNA* from Takata *et al.* published in Nature on September 27, 2017 (Takata et al., 2017).

After choosing both papers, a video abstract, graphical abstract, and plain language summary was created for each paper. These summaries along with the original published abstracts for each paper were then displayed to survey participants from a variety of backgrounds including scientists, adults with science-related careers, and adults with non-science careers. Participants were asked a series of questions about the research itself and about how much the participants enjoyed and understood the summaries.

Each survey participant only saw one type of summary whether that was the graphical abstract, video abstract, plain language summary, or original published abstract. The same questions were asked regardless of which science summary the participants saw.

The full methods for this research can be found in Chapter 6, section 6.8. The results of the survey are presented in the rest of this chapter.

4.2 Survey Participants and Preferences

Participation in the survey was fairly even across careers. The Cohn et al. data set contained 201 science, 156 science-related, and 181 non-science participants (Table 3). The Takata et al. data set contained fewer science related (n=112) and non-science (n=133) participants due to a Google Form error that was corrected shortly after the survey was first publicized (Fig 4.1 and Table 4.1). Of the 538 total participants, 505 reported having a binary gender. The female/male split of those 505 participants was fairly even with the science and non-science participants having approximately a 60:40 split and the science-related participants having a 70:30 split. The 70:30 female/male split in science-related participants is representative of the number of women in outreach and other science-related careers as compared to men in those same careers (NSF, 2019).

Table 4.1 Participant numbers for Cohn et al. and Takata et al.

Participant Numbers for Cohn et al.					
Career	**Video**	**Graphic**	**Plain Language**	**Abstract**	**Total**
Science	42	49	49	61	**201**
Non-Science	44	47	47	43	**181**
Science-related	26	42	39	49	**156**
Total	**112**	**138**	**135**	**153**	**538**
Participant Numbers for Takata et al.					
Career	**Video**	**Graphic**	**Plain Language**	**Abstract**	**Total**
Science	42	49	49	61	**201**
Non-Science	35	31	38	29	**133**
Science-Related	18	29	30	35	**112**
Total	**95**	**109**	**117**	**125**	**446**

Numbers of participants separated by paper, by career, and by summary type.

The number of participants who viewed each type of summary is also fairly even. Only science-related video participants are lagging in number of participants (n=26 for Cohn et al., n=18 for Takata et al.) compared to the other summary and career types (n>39 for Cohn et al., n>29 for Takata et al.).

Before showing participants a science summary, our survey asked participants to report their preference for getting scientific information via written summaries, graphics/infographics, videos, audio sources like podcasts, and reading the original research paper. We gathered this information to see how much prior preferences affect

the comprehension, enjoyment, understanding, and desire for updates of the different summary types. Participants from all careers had the same hierarchy of reported learning preferences with the exception of research papers (Fig 4.1). Written summaries were by far the most preferred learning type followed by graphics/infographics, videos, and then audio/podcasts (Fig 4.1). For research papers, non-science participants preferred them the least, science-related participants preferred them second only to written summaries, and science participants preferred them the most.

We also wanted to know how scientists like to receive updates inside versus outside of their field so we could learn how that might affect their view of the different science summaries. We gathered information by asking participants with science careers how much they preferred getting research updates via scientific journals, newspaper articles, social media, recommendations from colleagues, or by PubMed alert. Recommendations from scientific journals, recommendations from friends and colleagues, and PubMed/Other Alerts are the most preferred update mechanisms inside the scientists' field of study (Fig 4.1B). When asked about their preferences outside their field, recommendations from friends and colleagues were the most preferred followed by social media, then newspaper articles and recommendations from scientific journals (Fig 4.1B).

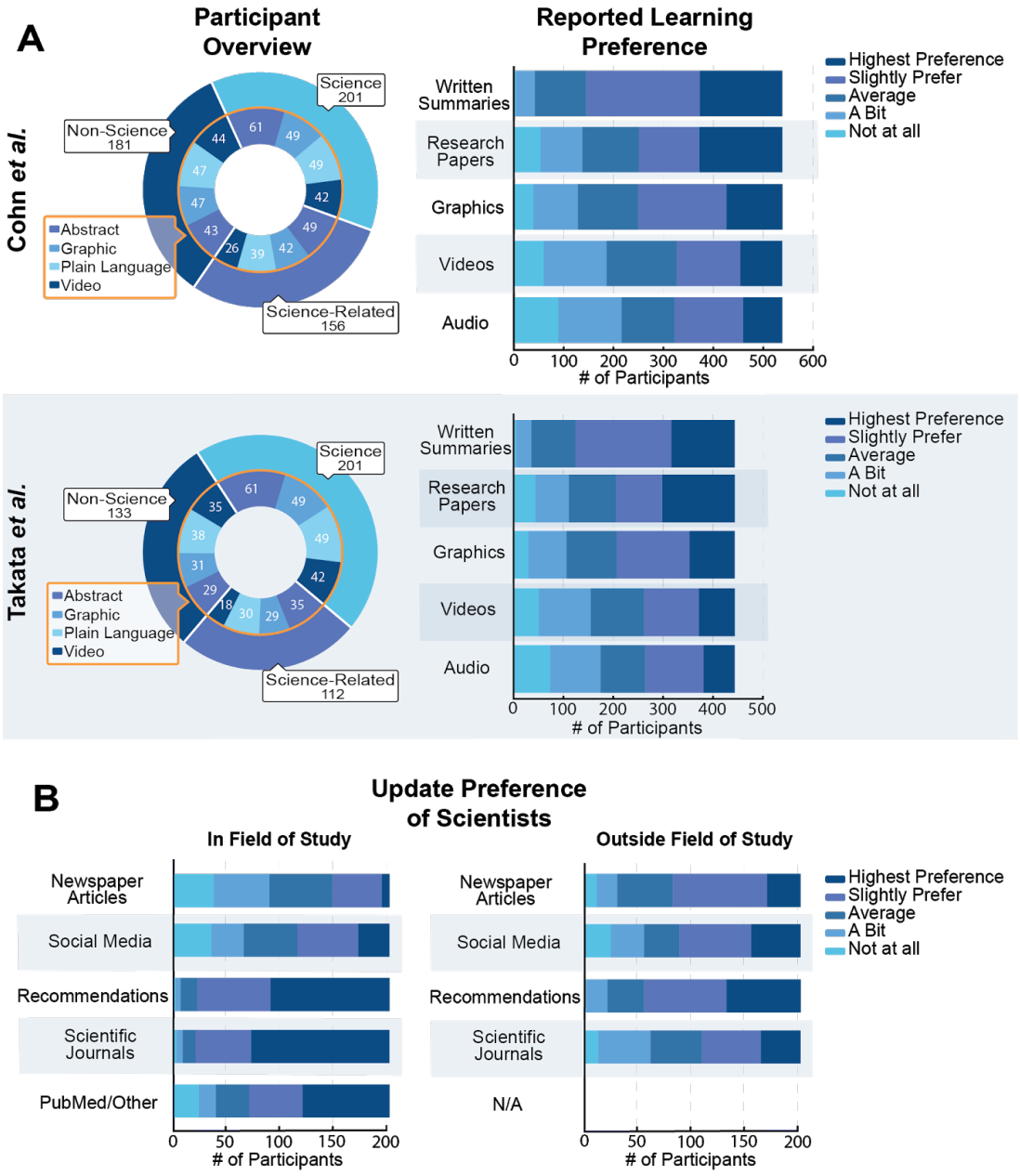

Figure 4.1 Participant reported preferences
Reported learning preferences for all participants and update preferences of participants with science careers. (**A)** shows data of all participants that answered the Cohn et al. paper and the Takata et al. paper. The bar charts show the reported preference of the participants for different ways to hear about science. (**B)** shows the update preferences of science participants both in their field of study and outside of it. The graph on the left shows preferences for research inside the scientist's field of study and the right shows preferences for research outside the field of study.

4.3 Video and Plain Language Summaries are the most effective regardless of Career

Given the clear reported preference for written forms of communication (Fig 4.1A), it was expected that the plain language summaries and perhaps the published abstracts would be the most effective summaries when tested. Contrary to our expectations, videos had the highest scores for comprehension, understanding, enjoyment, and desired updates (Median(M)>4 of 6, M>3 of 4, M>3 of 4, M>2 of 4 for videos respectively) (Fig 4.2). Plain language summaries often had equal scores to videos (M>4 of 6, M>2 of 4, M>2 of 4, M>2 of 4 for plain language respectively), but videos were either as effective or more effective than plain language summaries in all cases except comprehension of science-related participants for the Cohn et al. paper where plain language summaries had a higher average score (M=4 of 6 for video, M=5 of 6 for plain language) (Fig 4.2).

The differences in comprehension were generally small across summary types and careers. These small differences indicated that people are able to get the main takeaways of the paper no matter what type of summary they are shown. When statistically significant differences did occur, they indicated that video and plain language summaries produced higher comprehension scores (Fig 4.2).

Video and plain language summaries had higher reported understanding scores than published abstracts and graphical abstracts (Fig 4.2). This was true of participants from all careers and was true for both papers tested. In some cases, video even outperformed plain language summaries (Fig 4.2), which is surprising given that the majority of participants ranked written summaries as their highest preference for getting new scientific information (Fig 4.1A).

Videos and plain language summaries had the highest enjoyment scores, but there were some differences between careers. Participants with science careers enjoyed videos the most (M=4 of 4 for Cohn et al. and Takata et al., $p<0.00001$) followed by plain language summaries (M=2 of 4 for Cohn et al., M=3 of 4 for Takata et al., $p<0.00001$). Participants with non-science careers enjoyed videos the most as well (M=3 of 4 for Cohn et al. and Takata et al., $p<0.00001$). Participants with science-related careers liked the videos and plain language summaries equally (M=3 of 4 for video and plain language for Cohn et al. and Takata et al.). Published abstracts and graphical abstracts were enjoyed the least by all careers (all $p<0.0027$) with the exception of non-science participants who enjoyed abstracts the least (M=1 of 4 for Cohn et al., M=0 of 4 for Takata et al.), but enjoyed graphical abstracts and plain language summaries equally (M=2 of 4 for graphic, M=2 of 4 for plain language for Cohn et al.; M=1 of 4 for graphic, M=2 of 4 for plain language for Takata et al.) (Fig 4.2).

Figure 4.2 All data from all summaries
Histograms of the comprehension, understanding, enjoyment, and desire for more updates data for all survey types and all career types. **A** shows data for the Cohn et al. paper participants. **B** shows data for the Takata et al. participants. Each histogram shows the data as a percentage of participants. Comprehension histograms are plotted from 1-6, and understanding, enjoyment, and want updates plots are plotted from 0-4. Comprehension scores are from a series of questions asked in the survey (table 2, S6 File). Understanding, enjoyment, and want updates scores are numerical representations of responses where 0 was “not at all” and 4 was “very much” (table 2, S6 File). Statistical significance is shown above each plot where $p<0.01$ using the Mann-Whitney U-Test. Specifically, the asterisks represent the following p-values: $p<0.00001$(****), $p<0.0001$(***), $p<0.001$(**), $p<0.01$(*).

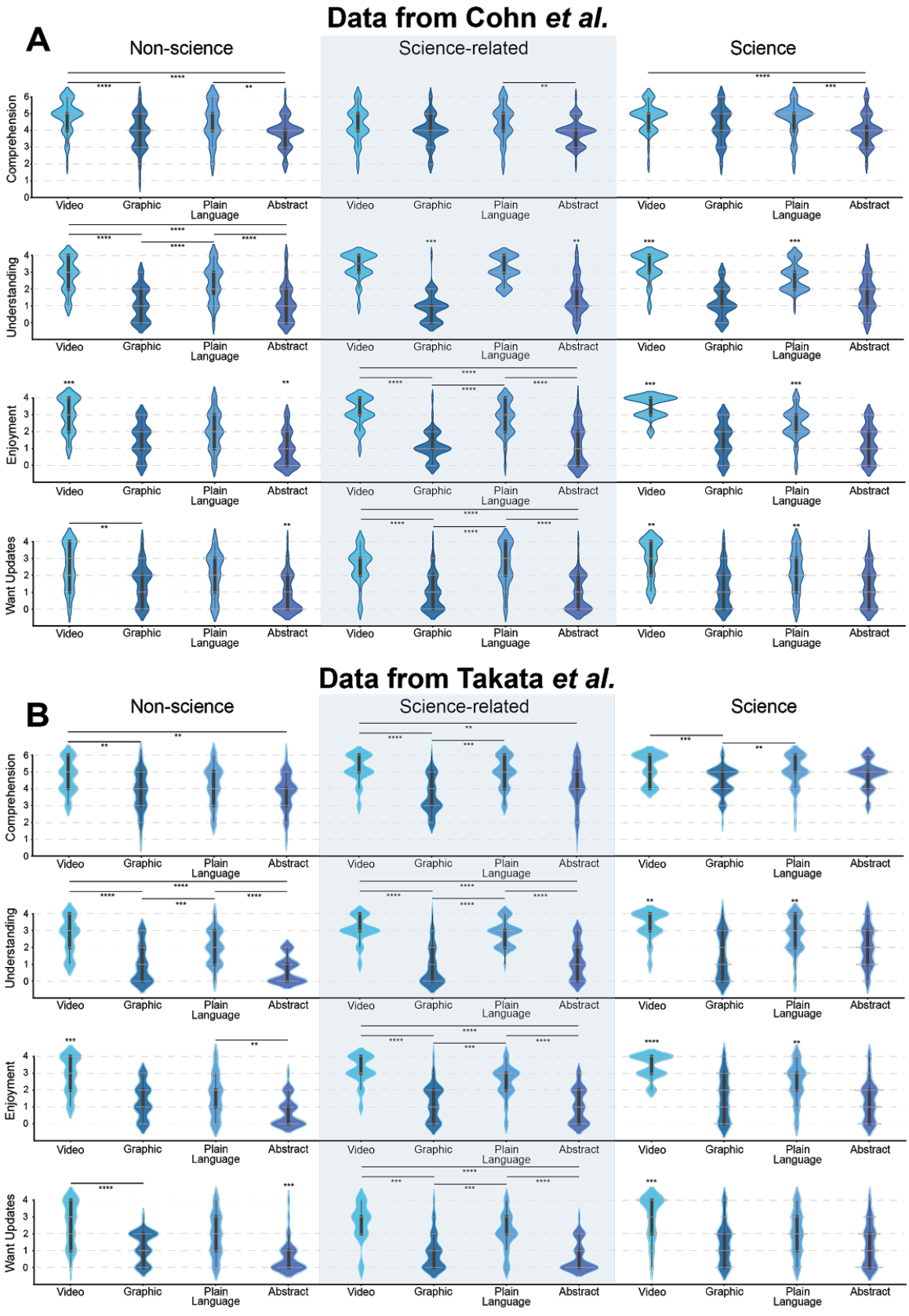
Data from Cohn et al.
A
Non-science
Science-related
Science
Comprehension
Understanding
Enjoyment
Want Updates
Video
Graphic
Plain Language
Abstract
Data from Takata et al.
B
Non-science
Science-related
Science
Comprehension
Understanding
Enjoyment
Want Updates
Video
Graphic
Plain Language
Abstract

When asked if they wanted to get more updates in the form of the summary they saw, participants rated videos or plain language summaries the highest, independent of career (all $p<0.00148$ for video, all $p<0.01$ for plain language summaries) (Fig 4.2). Published abstracts and graphical abstracts had the lowest update scores (all $p<0.00148$) with the exception of non-science participants who scored published abstracts the lowest ($M=0$ for Cohn et al. and Takata et al.), but scored graphics and plain language summaries equally ($M=2$ of 4 for Cohn et al.; $M=1$ of 4 for graphic, $M=2$ of 4 for plain language for Takata et al.) (Fig 4.2).

Overall, video abstracts and plain language summaries produced the highest comprehension, understanding, enjoyment, and desire for more updates. This led us to the conclusion that video abstracts and plain language summaries are the most effective summary formats regardless of career.

4.4 Strong correlations exist between reported learning preferences and summary ranks

Generally, participants from all careers felt similarly about the summaries. All participants scored the video and plain language summaries the highest and the graphical abstracts and published abstracts the lowest in all categories. We thought that if we sorted the participants by their reported preferences rather than by their careers, we might see strong correlations between reported preference and comprehension, understanding, enjoyment, or desire for updates.

To see whether reported preference was correlated with the summary scores, we looked at the comprehension, enjoyment, understanding, and update scores from participants that viewed each of the summaries and saw if those scores correlated with their reported preference for getting updates of that type. For example, to look at the published abstracts, we looked to see if the comprehension, understanding, enjoyment, and desire for updates scores correlated with the reported preference for reading the original research paper. For the video scores, we looked to see if the scores correlated with the video reported preference. For the graphical abstract scores, we looked to see if the scores correlated with the graphic/infographic preference. We could not evaluate plain language summaries because almost all of the participants marked average or higher preference for written summaries when asked how they prefer to get science updates prior to viewing any of our summaries (Fig 4.1A). This limited our ability to see any correlation, so plain language summaries were not analyzed. Videos, graphical abstracts, and published abstracts each had a wider distribution of reported preferences from lowest to highest, so they were analyzed (Fig 4.1A).

Although the comprehension, understanding, enjoyment, and update scores were similar between the Takata et al. and Cohn et al. papers when the data was separated by career, the preference correlations showed a clear difference between the two papers (Fig 4.3). In the Cohn et al. data set, comprehension score was not correlated with the reported preference in any of the summary types (Fig 4.3A). This

lack of correlation means that participants did not perform better on the comprehension test when they were paired with their preferred type of summary whether it was a video, graphic, or the original published abstract. The Takata et al. data showed similar results for the video and graphical summaries, but it showed a significant correlation between preference for reading the original research paper and the published abstract comprehension score ($r=0.29$, $p=0.0009$) (Fig 4.3B). This correlation indicates that participants which marked reading the original research paper as their highest preference performed better on the comprehension test and participants that marked reading the original research paper lower performed worse. This Takata et al. specific correlation could be due to the basic biology nature of that paper and the background knowledge required to understand their findings.

Significant correlations were also seen for published abstracts in reported understanding, enjoyment, and the desire for more updates in both papers (all $p<0.00001$). This indicates that participants which prefer reading the original research paper also score the abstracts higher in all categories, and those that do not prefer reading the original research paper score the abstracts lower in all categories. The same correlations were not seen for videos. The only significant correlation for the video summaries was a correlation between the desire for more video updates and the reported video preference ($r=0.387$, $p=0.000024$ for Cohn et al.; $r=0.33$, $p=0.0011$ for Takata et al.) (Fig 4.3). This indicates that participants who reported a preference for videos wanted to keep seeing more videos even after viewing our video abstracts. The lack of correlation between video reported preference and understanding/enjoyment highlights how effective videos were overall. Participants gave high scores to the video abstracts in the understanding and enjoyment categories regardless of whether they reported that they preferred videos as a way to get new scientific information before seeing our video abstracts.

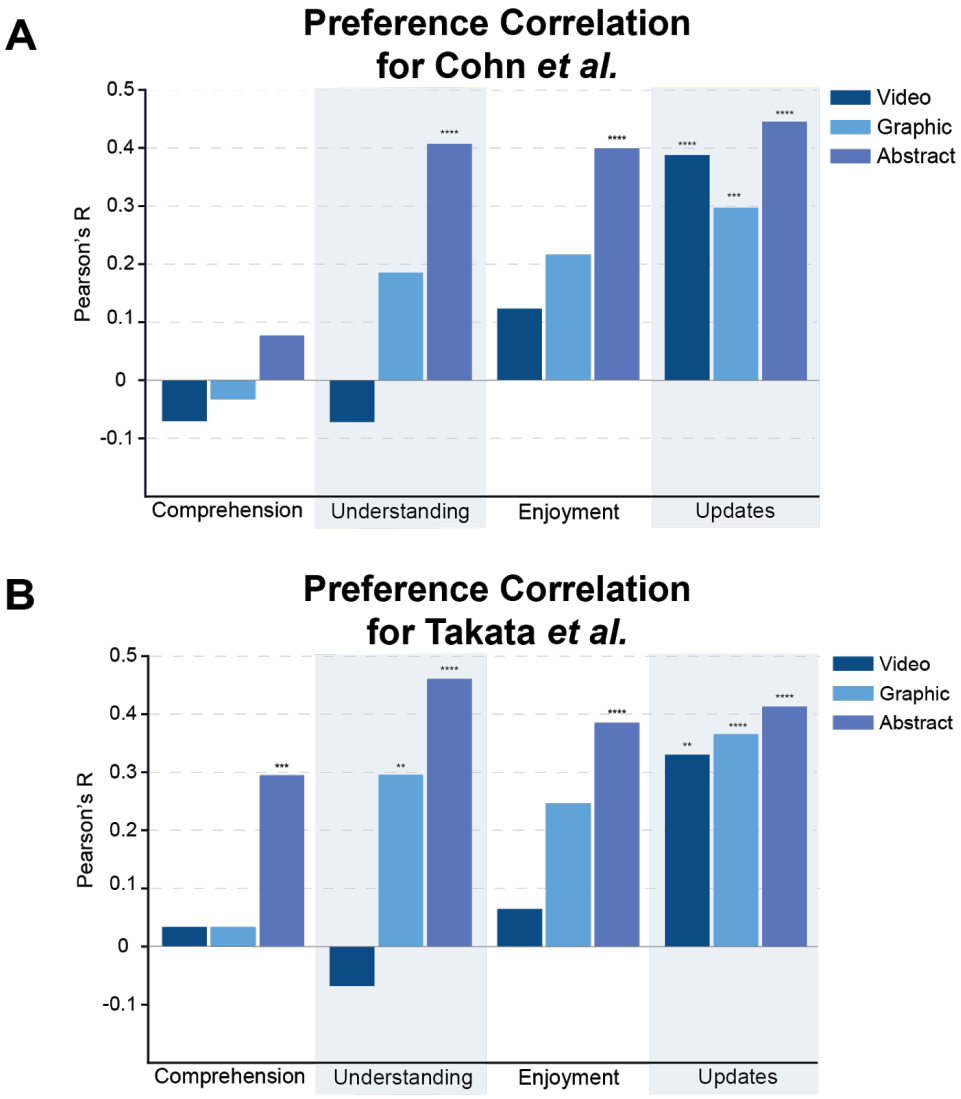

Figure 4.3 Correlations between reported preference and summary values
Bar graphs of preference correlation for Cohn et al. and Takata et al. papers. Both graphs show data for videos, graphics, and published abstracts. Analysis was not completed for plain language summaries due to the overwhelming reported preference for written summaries (see Fig 2 for reported preference data). For each summary type, the reported preference for that type was tested for correlation with the comprehension score, reported understanding, reported enjoyment, or the desire for more updates of that type using a Pearson's r correlation calculation. **A** shows the data for Cohn et al. **B** shows the data for Takata et al. Statistical significance is noted where $p<0.01$. Specifically, the asterisks represent the following p-values: $p<0.00001$(****), $p<0.0001$(***), $p<0.001$(**), $p<0.01$(*).

4.5 Reported understanding and comprehension show strong correlations for Takata et al. summaries

It might be expected that the better you perform on a quiz, the more confident you are that you understood the material covered in that quiz. When we examined the relationship between comprehension score and reported understanding, the Cohn et al. and Takata et al. papers diverged (Fig 4.4).

The Cohn et al. data showed correlations between comprehension scores and understanding scores for the video ($r=0.223$, $p=0.018$) and plain language summaries ($r=0.193$, $p=0.025$), but no correlation for the graphical abstracts or published abstracts (Fig 4.4). The correlation between understanding and comprehension scores in video and plain language summaries suggest that participants felt confident in their answers and their understanding of the Cohn et al. paper after watching the video or reading the plain language summary. It also suggests that participants did not feel as confident after reading the published abstract or viewing the graphical abstract.

Contrary to the Cohn et al. data, the Takata et al. data showed significant correlations in all summary types (all $p<0.00018$) (Fig 4.4). These correlations hint at the possibility that more background knowledge is needed to understand the findings of the Takata et al. paper as compared to the Cohn et al. paper.

Figure 4.4 Heat maps of reported understanding versus comprehension score
Heat maps of reported understanding versus comprehension score of Cohn et al. and Takata et al. separated by summary type. The larger heat maps show the summed data for all participants and the three smaller heat maps to the right show the data for each career type. Each larger heat map contains the Pearson's r correlation value for all careers. Statistical significance is noted where $p<0.05$. Specifically, the asterisks represent the following p-values: $p<0.00005$(****), $p<0.0005$(***), $p<0.005$(**), $p<0.05$(*).

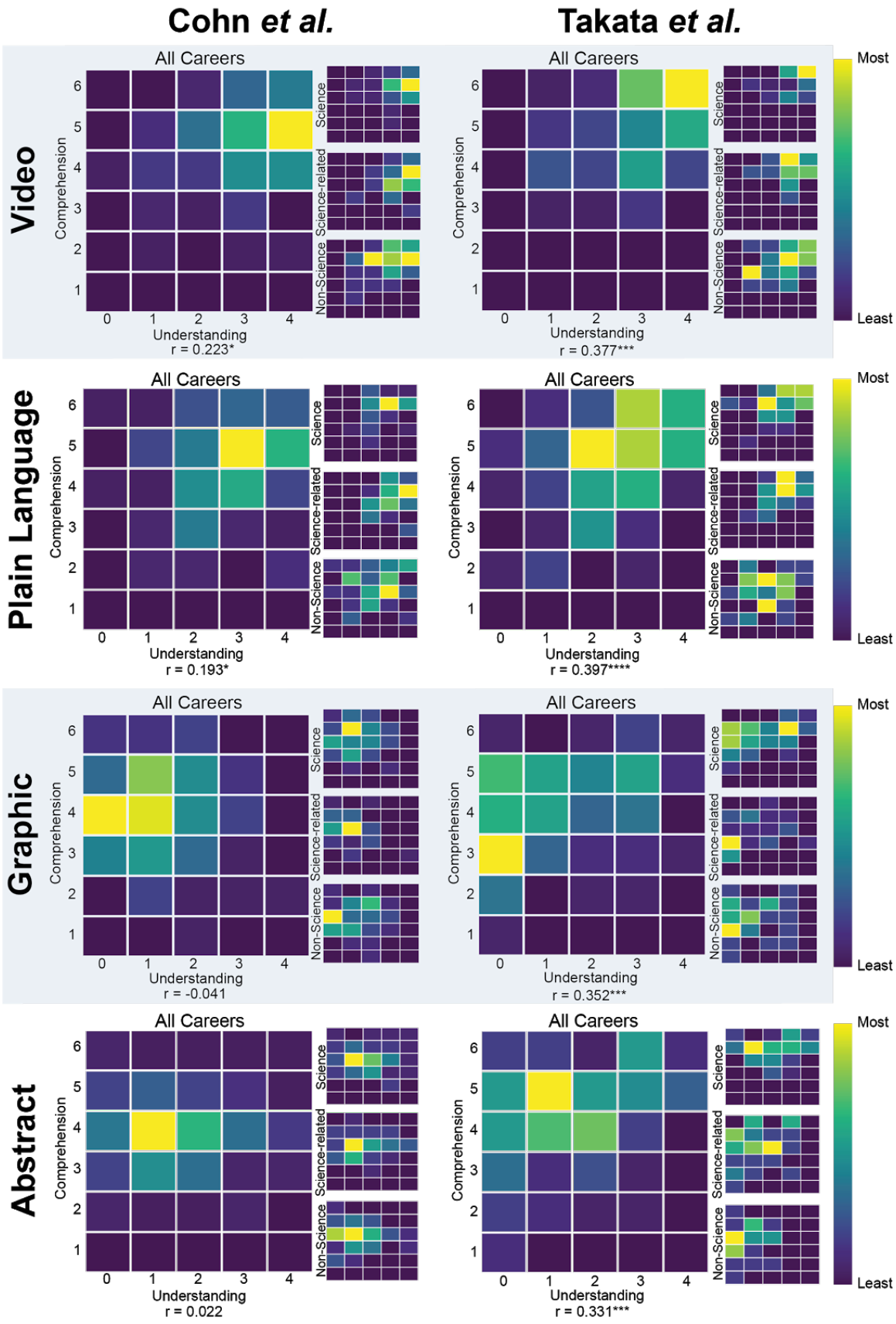
Cohn et al.
Takata et al.
Video
Plain Language
Graphic
Abstract
All Careers
Science
Science-related
Non-Science
Comprehension
Understanding
Most
Least
r = 0.223*
r = 0.377***
r = 0.193*
r = 0.397****
r = -0.041
r = 0.352***
r = 0.022
r = 0.331***

Chapter 5
Implications and Future Directions

This chapter will discuss the implications and future directions from the work presented in Chapters 2-4.

In Chapter 2, I presented my work on the HIV-1 protease. Using anisotropy, I showed that protease becomes active and cleaves Gag during the process of assembly rather than after or concurrent with scission. In section 5.1 of this chapter, I will discuss the implications of this finding on the process of HIV-1 assembly. I will also discuss the possibility of testing Gag mutations for defects in protease activity along with other future work.

In Chapter 3, I presented two projects that relate to HIV-1 assembly. The first was examining the effect of the retroCHMP3 protein on the process of assembly. The second was determining the kinetics of Vpr recruitment to assemblies. In section 5.2 of this chapter, I will discuss how retroCHMP3 acts as an antiviral protein and how we believe it works with other ESCRT components. I will also talk about future experiments involving retroCHMP3 including the possibility of tagging and following retroCHMP3 in cells. In section 5.3, I will discuss the implications of the delay in Vpr recruitment relative to Gag and possible interactions between Vpr and ESCRT recruitment.

Finally, in section 5.4 I will discuss the work presented in Chapter 4 on science summaries. I will offer suggestions on how to summarize research papers based on the data I presented. I will also suggest areas of future work including research on how the quality of the summary plays into its effectiveness and also research using other types of summaries like podcasts or infographics.

5.1 Gag Cleavage Discussion

Our results suggest that HIV-1 protease activation and cleavage of Gag happens during assembly rather than concurrently with or post scission (Figure 5.1). This finding is consistent with previous data showing that delays in assembly often lead to loss of HIV-1 proteins back into the cell. Mutations in NC, RT, and IN within GagPol have been shown to prevent viral budding and/or severely limit particle infectivity (Abram and Parniak, 2005; Chiang et al., 2010; Mohammed et al., 2011; Ott et al., 2003; Ott et al., 2009; Yu et al., 1998). Many of these mutations can be rescued with the D25A protease inactivating mutation. These findings suggest that any delay in budding leads to the dissolution of particles. Additionally, PTAP mutations or use of a dominant-negative VPS4A have been shown to delay HIV-1 scission and thus lead to a loss of Pol proteins back into the cell (Bendjennat and Saffarian, 2016). This phenotype too was rescued by inactivating the protease. This previously published work complements the work that I showed in Chapter 2, all suggesting that protease activation does not rely upon scission or ESCRT recruitment to begin cleaving Gag.

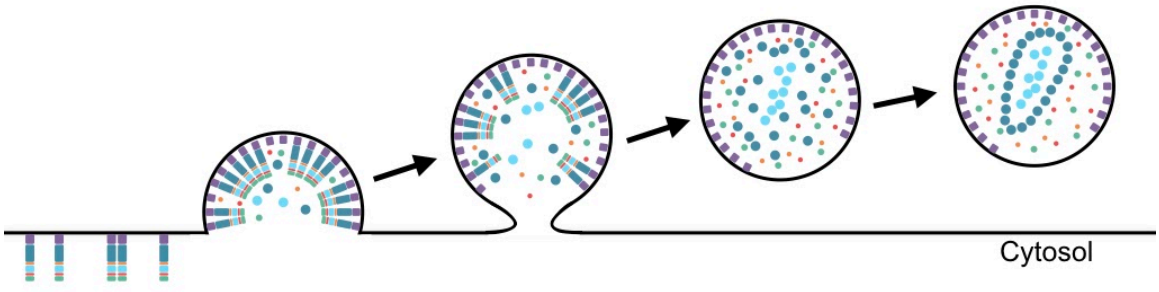

Figure 5.1 New diagram of HIV-1 protease activation
Diagram of the process of assembly with anisotropy evidence taken into account. Protease activation and cleavage of Gag begins while assembly is taking place.

In evolutionary terms, not having protease be dependent on scission or ESCRT recruitment makes for a stronger virus. Any viruses that have mutations that slow down assembly or make them less efficient are selected against due to protease activation and Gag cleavage happening and releasing key components back into the cell which produces a viral particle with fewer necessary HIV-1 proteins and lower infectivity. Having protease be independent of other assembly steps like scission or ESCRT recruitment also allows for greater flexibility of protease sequence. The most important part of the protease is its activity rather than any possible regulatory domains which allows more sequences within the protein to change.

One caveat of this work is that it was specifically done using a packaging vector containing NL4.3 HIV-1 GagPol, but the packaging vector does not contain all the viral proteins. It could be informative to perform this work using a provirus or even a full HIV-1 viral sequence to see if our results hold when the rest of the HIV-1 proteins are present. We also trimmed the traces shown in Chapter 2 to the first time we could see a

punctum and the last time we could see that same punctum. That means that our earliest time point is actually while the assembly is fairly advanced. While we don't have a reliable way to know how advanced, we suspect that it is as much as one quarter of the way complete based on fluorescence intensity. It's possible that measuring when the HIV-1 RNA arrives at the cell surface in addition to the anisotropy of Gag is another way to timestamp the overall assembly process since appearance of the RNA is the first step. Presence of the HIV-1 RNA within the particle may also have an effect on protease activation.

It would also be interesting to measure protease activity in cases where assembly is delayed either due to interference with ESCRT recruitment or with mutations in Gag itself. Previous work on PTAP and other Gag mutations or use of dominant-negative VPS4A have suggested that protease becomes active while the puncta is still attached to the cell, but it would be helpful if we could confirm those statements with our anisotropy setup. Additionally, in Chapter 3, I discussed my work on retroCHMP3 and its interaction with proteolytic cleavage of Gag, so this could be another area of experimentation.

Another current area of experimentation is a more advanced background subtraction for the live assembly data. At the earliest timepoints for our assemblies, the tagged Gag in the cytosol makes up a large percentage of the fluorescence we are measuring. Later in Gag assembly, the puncta itself is the major source of fluorescence. With a more advanced background subtraction, we could remove the tagged Gag fluorescence in the cytosol of the cell and focus only on the fluorescence coming from the assembling particle. This would help clean up our earliest time points during assembly and give us a clearer view of what is happening with protease activation during that time.

Anecdotally, we see an increase in lateral motion of the assembling VLPs with a WT protease versus those with a D25A protease. In addition to the lateral motion, we also see an increase in particles fusing and particles that assemble from the same membrane location. This increase in mobility and particle interaction could suggest that particles assembling with a WT protease are more dynamic and are capable of interaction due to their flexible structure. Immature particles may not show this dynamic phenotype because of their inflexible crystalline structure.

In addition to the information we've gathered about HIV-1 assembly, measuring protease activation and Gag cleavage with anisotropy also highlights polarization microscopy as a powerful tool for imaging events which are otherwise unmeasurable. Measuring activation of the HIV-1 protease has been possible with anisotropy as both the orientation and freedom of the mEGFP are changing with protease activity, but it is not the only cellular event that could benefit from imaging of this type. There is a large gap in the knowledge between the static, structural information provided by crystal structures and cryo-EMs of proteins versus fluorescence imaging of that protein in living cells. Polarization microscopy helps to bridge that gap by providing not only temporal and spatial information about a tagged protein, but also helps to resolve information

about its orientation and dynamics. That kind of information is helpful for proteins that are part of complexes that undergo rearrangements, conformational changes, or dilations where the kinetics of those structural changes *in vivo* are unknown.

In this thesis, I presented data on using polarization imaging to determine when Gag cleavage via the HIV-1 protease takes place. I showed that anisotropy measurements can distinguish between mature and immature particles, and I measured the cleavage of Gag via the protease during assembly events. These measurements would not have been possible without the power of polarization microscopy.

5.2 retroCHMP3 Discussion

In Chapter 3, I presented data on the mechanism of action of retroCHMP3. I presented data from Lara Rheinemann and Diane Miller Downhour in the Sundquist lab that showed that retroCHMP3 prevents HIV-1 budding, has weaker binding of CHMP4B, and does not have the toxic effect of truncated CHMP3 in cells. My data showed that at HIV-1 assembly sites in cells expressing retroCHMP3, CHMP4B is recruited to sites multiple times and stays longer each time. I also showed that VPS4A does not seem to come multiple times and that its recruitment becomes more transient. Finally, I showed that VLPs assembled in the presence of retroCHMP3 resulted in the loss of mEGFP back into the cell and that the loss of fluorescence could be rescued with genetic inactivation of the protease.

Given that cells expressing retroCHMP3 do not show the same kinds of toxic effects seen with the expression of truncated CHMP3, we have to assume that the action of retroCHMP3 is broad, but it is not strong enough to prevent ESCRT-dependent processes like cell division and membrane repair from happening. The finding that retroCHMP3 inhibits all ESCRT-dependent enveloped viruses that we tested, in addition to the finding that it inhibits LINE element insertion, adds weight to the idea that the action of retroCHMP3 is broad but not strong. Our pulldown results suggest that retroCHMP3 does interact with CHMP4B but that the interaction is weaker than with the full length CHMP3. This interaction may destabilize the CHMP4B polymers such that they fall apart prior to VPS4A recruitment. Alternatively, retroCHMP3 may interfere with the full proper recruitment of VPS4A, resulting in longer individual recruitments of CHMP4B, which then leads to multiple recruitments. A third possibility is that as a consequence of interaction with retroCHMP3, the CHMP4B polymers are less capable of being correctly remodeled to allow for scission. This model is supported by our imaging results which show CHMP4B being recruited in more subsequent rounds than usual and staying longer while VPS4A does not seem to be coming more frequently and is staying for shorter amounts of time. It is possible that VPS4A is coming to sites of assembly multiple times, but that we are unable to catch that recruitment because it is more transient or less robust than the typical recruitment. VPS4A CRISPR cell lines could be helpful in this case to increase the signal seen in cells.

We believe that viruses in particular are more susceptible to the activity of retroCHMP3 because any delay in the scission of the virus allows for protease activation and loss of viral components back into the cell. Given the results from our CHMP4B imaging in cells with retroCHMP3, we believe that the delay in scission is approximately 15 minutes though it could be shorter or longer depending on the assembly. Delay of scission also gives cells more time to endocytose or otherwise prevent the viruses from leaving to go infect another cell. Our data suggested that with retroCHMP3 present, there is a loss of fluorescence back into the cell and that this phenomenon is rescued when a mutant protease is used. This finding suggested that protease activation combined with retroCHMP3 delay prevents budding of infectious virus. At lower expression levels of retroCHMP3, we see that some virus is released

from cells but that the infectivity of that virus is greatly diminished. This is another line of evidence that suggested that any delay in scission leads to noninfectious virus.

The reason that we still see midbody resolution and a lack of cytotoxicity with retroCHMP3 expression is that retroCHMP3 does eventually allow for proper scission; it is just delayed. This delay is consequential for a virus where scission must occur quickly to allow for proper virus formation and escape from the cell. The delay does not appear to have an impact on events like cytokinesis where possible multiple failed scission attempts is not a major problem for the cell as long as scission eventually happens.

There are many aspects of retroCHMP3 involvement that we would like to follow up on experimentally. It would be ideal if we could eventually find a way to tag retroCHMP3 and confirm that it does in fact come to sites of assembly. With a tagged retroCHMP3, we could determine the kinetics of recruitment and get a clearer view of which step is affected by retroCHMP3 within the formation of ESCRT polymers. We have also imaged CHMP4B and VPS4A separately in our data, but it could provide further information on the activity of retroCHMP3 to image them together and see if there is a delay between the time of CHMP4B recruitment and the time of VPS4A recruitment. In our previous research where CHMP4B and VPS4A were imaged together, we saw that they came within a few seconds of one another but that might be altered with the presence of retroCHMP3 (Bleck et al., 2014).

With all of our data together, we feel confident in our proposed mechanism for retroCHMP3 action. We propose that retroCHMP3 inhibits HIV-1 budding by interacting with CHMP4B polymerization causing CHMP4B to fall apart or otherwise be harder to remodel into the correct spiral for scission. Other cellular processes such as midbody resolution and membrane repair can accommodate the additional instability introduced by retroCHMP3, but events like viral assembly or LINE insertion are more time sensitive and cannot accommodate retroCHMP3.

5.3 Vpr Discussion

In Chapter 3, I showed that Vpr co-assembles with Gag but with a slight delay. I also confirmed that the LXXLF motif is required for Vpr recruitment both in VLPs using Western blots and in live cells imaging assemblies.

The delay of assembly of Vpr compared to Gag suggests that Vpr might attach to Gag at the membrane rather than Vpr being attached to Gag before Gag comes to the membrane. It has been shown previously that Vpr and TSG101 can competitively bind to Gag since their recruitment sites are close together in p6 (Chutiwitoonchai et al., 2016). The competition with TSG101 may also contribute to the delay of Vpr assembly compared to Gag. Our imaging can detect overall fluorescence, but it cannot determine whether there is turnover at the LXXLF binding site. It is possible that TSG101 and Vpr might influence each other when it comes to binding Gag. This potential interaction of TSG101/Vpr might also suggest why only about 340 Vpr proteins are found in VLPs when approximately 2400 Vpr binding sites exist in a single assembled virus (Carlson et al., 2008; Muller et al., 2000).

Our findings also suggest that Vpr imaging a good protein to monitor assembly in-trans without tagging or altering Gag. Any protein fused to Vpr would arrive early in the assembly process, stay through scission, and be present in the final VLP. This contrasts with proteins like the ESCRTs that only show up in the final stages of assembly and do not make it into the final VLP (Baumgartel et al., 2011; Bleck et al., 2014; Jouvenet et al., 2011; Morita et al., 2011).

The incorporation kinetics of other accessory proteins like Vif and Nef are also unknown. It has been reported that Vif gets into particles by interactions with the viral RNA (Khan et al., 2001), and it is suspected that Nef gets into particles due to its myristoylation and interaction with membranes (Bentham et al., 2006; Bukovsky et al., 1997; Pandori et al., 1996; Welker et al., 1996; Welker et al., 1998). Imaging could reveal other aspects of the kinetics of that packaging and give a clearer picture of how the HIV-1 virion is assembled.

5.4 Discussion of how to summarize a graduate career studying HIV-1

In Chapter 4, I presented my data that videos and plain language summaries are the most effective summaries, based on comprehension, understanding, and enjoyment. This finding was independent of an individual's career type.

Based on the data I presented, we suggest that all researchers consider writing a plain language summary of their research. Those summaries can be published with their paper or published in other relevant locations including lab websites, university websites, or university newsletters. To get started with a plain language summary, it can be helpful to look at the eLife questions for researchers (Inside eLife, 2017). Also, we recommend editing the summaries at least once and getting feedback from a member of the intended audience since previous research has shown that editing and getting feedback leads to higher quality summaries (Barnfield et al., 2017; Kirkpatrick et al., 2017). Another possibility is using a jargon detection program to make sure the summary is accessible (Rakedzon et al., 2017). Summaries can be put into a readability calculator to help make sure that the summary is easy to read. However, we don't recommend depending solely on readability scores because scientific summaries must use unfamiliar words or phrases at times for accuracy, and readability calculators only report on how easy a written document is to read, not how easy it is to understand. Finally, a plain language summary can be a great way to organize a research paper as it forces researchers to focus on the take-home message, so writing plain language summaries can have benefits to both the researcher and the audience.

If the findings of their research are of public relevance, researchers could consider investing the time and money to make a video of their results. Videos had the highest ratings across the board, and they left people feeling confident and positive about the research being presented (Figure 4.2). Not all papers require a video, but it is an excellent option for certain relevant papers that should not be overlooked.

We also recommend that journals consider including plain language summaries with all of their papers as a separate section available outside the paywall, if a paywall exists for that publication. We also recommend that journals with topics of high public relevance or those that would benefit from strong interdisciplinary ties consider creating videos of their papers to share with the community.

One caveat of this work is that it was only on two papers and the summaries were of the same or similar quality because they were made by a single person. In reality, summaries are made by a variety of people with a variety of qualities. In the future, we would like to see more research into how the quality of the summary is related to the effectiveness of that summary. Video abstracts in particular would benefit from this kind of research since videos are sometimes made by professional videographers and sometimes by the researchers themselves.

Overall, our research only identifies which science summary is the most effective when a single researcher carefully creates content-identical summaries following the

rules set out by the journals that are associated with those summaries. There is still much more work to be done in order to know exactly how we should summarize our science. One type of summary that was completely omitted in this study was podcasts. Cell, Science, and Nature all produce podcasts about some of the most relevant research that they publish. It is unclear how a podcast would perform relative to videos, graphics, and plain language summaries. We also followed the rules from Cell about how to create graphical abstracts (Cell Press, 2019). It would be interesting to see how an infographic of the research which contains more words, phrases, and data would perform. Participants of our survey often commented on the graphical abstracts saying that they wished they had words or even a small description to go with the image, which suggests that infographics might be more helpful at conveying information. Currently, Cell does not allow any phrases or data in their graphical abstracts (Cell Press, 2019).

Science communication research is an exciting new area that is necessary for effective communication between researchers and outside of the academic community. The work I presented in Chapter 4 is one small piece of the puzzle, but it provides the groundwork for future science summary studies.

Chapter 6
Materials and Methods

Sections 6.1-6.7 are the materials and methods for the biological work presented in Chapters 2 and 3 on protease, retroCHMP3, and Vpr. If a method is specific to one of the projects and not to the others, the specific project will be mentioned. For example, section 6.6 is a description of the plasmids used, and it is separated into Vpr, retroCHMP3, and protease plasmids subsections.

Section 6.8 is the full methods for Chapter 4 regarding the consequence of different methods for summarizing research.

6.1 Cell Maintenance

HeLa and Hek293T cells were grown in Dulbecco's Modified Eagle's medium (DMEM, Gibco #11995065) supplemented with l-glutamine, sodium pyruvate, and 10% fetal bovine serum (FBS, Sigma #F4135). HeLa and Hek293T cells for live cell imaging were seeded onto MatTek dishes with no. 1.5 coverslips coated with fibronectin (Invitrogen #33010-018). HeLa cells were transfected 6 hours before imaging with Fugene 6 (Promega #E2691) and 1000ng of DNA. Hek293T cells were transfected with Lipofectamine 2000 (Thermo Fisher #11668019) and 1000ng of DNA 5 hours before imaging. Prior to imaging, DMEM was replaced with cell imaging media (HBSS (Sigma #55037C), 10mM HEPES, pH7.4) supplemented with 1% FBS.

For VLP work, Hek293T cells were transfected with Lipofectamine 2000 (Thermo Fisher #11668019) and 1000ng of DNA 24 hours before VLP collection for imaging and 48 hours before VLP collection for westerns.

6.2 VLP Collection

Supernatant from Hek293T cells in a 6-well dish was collected with a 10ml syringe and filtered through a 0.22μm filter (Millex GP 33mm) into a 15ml Falcon tube and placed on ice. 1ml of the supernatant was carefully pipetted over 500ul of 20% sucrose in PBS (Corning #21-040) to create two layers. Tubes were spun at >30,000g for 1 hour. All supernatant was removed and VLPs were resuspended in either 100ul PBS for imaging or 65ul of RIPA (Sigma) with a protease inhibitor (GE Healthcare Life Sciences #80-6501-23) for western blotting. VLPs for imaging were plated onto MatTek dishes with no. 1.5 coverslips coated with Poly D Lysine (Trevigen #3439-100-01).

6.3 Biochemistry

Hek293T cell lysates were collected by adding 200uL RIPA buffer containing protease inhibitor mix (GE Healthcare Life Sciences #80-6501-23) directly to cells growing in a 6-well plate after removing media. Cells were kept on ice for 20 minutes before supernatant was collected, vortexed, and frozen overnight. Collected VLPs and cell lysate were run on a 4-12% Tris-Glycine gel (Novex), transferred via an iBlot 2 dry blotting system (Thermofisher), and blocked in 5% dry milk powder in TBS-T for 1 hour. A variety of primary antibodies were used as seen in Table 6.1. If the primary antibody was mouse derived, goat anti-mouse HRP-coupled secondaries (Sigma-Aldrich A9917) were used. If the primary antibody was rabbit derived, goat anti-rabbit HRP-coupled secondaries (Sigma-Aldrich A0545) were used. Western blots were visualized on a LiCOR system using Amersham ECL Prime (GE Healthcare Life Sciences).

Table 6.1 Primary Antibodies used in this work

Antibody	Derived from	Company	Concentration
Anti-HIV-1 p24 monoclonal (183-H12-5C)	mouse	NIH AIDS Reagent Program (Toohey et al., 1995; Wehrly and Chesebro, 1997)	1:10,000
monoclonal anti-GFP (JL-8)	mouse	Living Colors, Clontech	1:8,000
monoclonal anti-β-actin	mouse	Sigma-Aldrich	1:5,000
anti-HA, affinity isolated	rabbit	Sigma-Aldrich	1:1,000
dsRed polyclonal	rabbit	Living Colors, Clontech	1:1,000

6.4 Imaging

Live cell and VLP imaging were done with a custom-built microscope that is based on an Olympus IX-81 frame and equipped with a custom-built through-the-objective polarized TIRF illuminator (Johnson et al., 2014). A 100X PLANAPO 1.50NA Olympus Objective was used. A 488nm laser (100mW LuxX diode laser, Omicron), a 594nm laser (100mW iode-pumped solid-state laser, Cobolt AB), and a 405nm laser (100mW LuxX diode laser, Omicron) were used at 25mW, 30mW, and 2mW respectively. The temperature was maintained at 37C throughout imaging using custom-built housing for the microscope. For non-polarized imaging, TIRF light was azimuthally scanned at 100Hz with mirror galvanometers (Nutfield Technology). For anisotropy imaging, an electrooptic modifier (EOM, Conoptics) was used and the 488nm laser was polarized in a fixed parallel polarization through a quarter-wave plate (Thorlabs). The mirror galvanometers were used to add a 10-degree quiver to the excitation light to limit field aberrations.

Emission light was collected after passing through a multiband polychroic (zt405/488/594/647rpc 2mm substrate, Chroma). For anisotropy imaging, emission was

additionally passed through a ½" polarization cube (Thorlabs) and a cleanup polarizer (Chroma) within a cairn splitter. A CMOS camera (Flash-4.0, Hamamatsu) was used to collect images. Image acquisition was done with Metamorph software.

For VLP acceptor bleaching, VLPs were imaged with a 488nm laser, then bleached for 1 second with a 543nm laser and a 589nm laser both set to 30mW, followed by another image with a 488nm laser. For Vpr and protease imaging, live cell images were taken every 10 seconds. For retroCHMP3 imaging, images of GagPol were taken every 20 seconds and ESCRT images were taken every 5 seconds. All exposure times are 200ms.

6.5 Image Processing, Plotting, and Statistics

6.5.1 Vpr

The time course of the assembly of HIV-1 in HeLa cells was analyzed with Metamorph software. Each assembly video had a standard 100 au subtracted from all frames that is automatically added as a camera offset. From there, individual HIV-1 assemblies were selected and trimmed to the first time the assembling punctum was visible and the last time the punctum was visible. This automatically sets the first frame of the assembly as time zero. To account for the differing intensities between mEGFP and mCherry and for the differing intensities between different cells, the intensities for each assembly trace were rescaled by the following equation: $(I-I_{min})/(I_{max}-I_{min})$ where I is intensity. The rescaled max intensity for each frame of the assemblies were plotted together using python.

VLPs from cells transfected only with GagPol-mCherry or GagPol-mCherry-LXXLF were collected and imaged with excitation at 488nm and 594nm. Puncta present when imaged with 594nm excitation were selected via a 16x16 pixel circular region and the max intensities were recorded. The same regions were used to measure the max intensities during excitation at 488nm. The percentage of mCherry excitation at 488nm was calculated to be 20.551% of the excitation at 594nm.

For VLPs from cells transfected with GagPol-mCherry and mEGFP-Vpr or GagPol-mCherry-LXXLF and mEGFP-Vpr, puncta that were present when excited at 594nm were selected with circular regions and the max intensity was recorded. The same regions were then applied to an image taken with excitation at 488nm and the max intensities were recorded. The max intensities from excitation at 488nm had 20.551% of the max intensities with excitation at 594nm subtracted from them. If the resulting value of max intensity with 488nm excitation after subtraction was greater than zero, then that represented a red puncta that was also positive for green fluorescence. P values for VLP quantification were calculated via a Chi-square test.

6.5.2 retroCHMP3

The time course of the assembly in HeLa and Hek293T cells was analyzed with Metamorph software. Each HIV-1 assembly video had a standard 100 au subtracted

from all frames due to camera offset. The video of GagPol assembly was analyzed first and all assemblies were marked with circular regions that encompassed the entire assembling particle. Assemblies were confirmed by the shape of the intensity curve over time which shows the classic accumulation and plateau as shown previously (Jouvenet et al., 2008). After all assemblies were selected, the regions from the assemblies were overlaid onto the ESCRT video of the same assembly. Any spikes in intensity from the ESCRT regions were checked to confirm that they correspond to assembling Gag. This was done by testing if the ESCRT fluorescence had a Gaussian distribution that colocalized with the fluorescence of puncta of GagPol. For each puncta of the ESCRT, I recorded the number of frames that it was resident and the timing of that recruitment relative to the plateau of Gag assembly. To plot the overall number of repeat recruitments and length of recruitment, histograms were made which plotted the percent of total counts for either CHMP4B or VPS4A with or without retroCHMP3. Statistical differences between histograms were calculated using a one-tailed T-test with significance set at $p<.01$.

6.5.3 Protease

FRET Imaging

Acceptor bleaching on collected VLPs was performed by taking an image with 488nm laser to excite the mEGFP followed by an image with 543nm laser to image the mCherry. The mCherry was then bleached with 589nm and 543nm lasers simultaneously for 1 second. After bleach, an image was taken using 488nm excitation then another image with 543nm excitation. FRET efficiency was calculated by the Donor Intensity post-bleach minus Donor Intensity pre-bleach divided by the Donor Intensity post-bleach. All analysis was done using Metamorph software.

Anisotropy Assemblies

Live assemblies of HIV-1 in HeLa cells were analyzed with Metamorph software. Anisotropy imaging creates one channel that is the emission polarized parallel to the excitation light and one channel that is the emission polarized perpendicular to the excitation light. Videos of GagPol assembly were analyzed first by aligning the parallel and perpendicular channels of the image. After alignment, all assemblies in the parallel channel were marked with square regions that encompassed the entire assembling particle. Assemblies were confirmed by the shape of the intensity curve over time which shows the classic accumulation and plateau as shown previously (Jouvenet et al., 2008). The same square assembly regions used to define the assemblies in the parallel channel were used to cut out the fluorescent signal from the perpendicular channel. Each fluorescent signal was trimmed to the first time and the last time the assembling puncta could be seen within the square region. Assemblies shorter than 10 minutes were not analyzed.

Aligned and trimmed assemblies were then analyzed using a MATLAB analysis algorithm written by Joan Pulupa. The algorithm identifies the puncta in each frame of the trimmed parallel channel assembly using an automated algorithm which uses the Laplacian of Gaussian (LoG) algorithm (written by Vincent Garcia, based on (Lindeberg, 1998)). The puncta identified in each frame are excised and the same excision mask is applied to the trimmed perpendicular channel assembly. The maximum intensity pixel from each punctum in each frame from the parallel and perpendicular channels are then used to calculate the anisotropy via an anisotropy calculation algorithm written by Daniel Johnson. The anisotropy values for each trace were then plotted together using python to create an average anisotropy over time for each condition.

The total intensity for each trace was calculated by using ($Intensity_{parallel}$-2*$Intensity_{perpendicular}$). The calculated total intensity was then rescaled to be on a 0-1 axis via (Intensity - $Intensity_{min}$)/($Intensity_{max}$ - $Intensity_{min}$) prior to plotting. The intensity values for each trace were then plotted together using python to create an average intensity over time for each condition.

Anisotropy VLPs

VLPs were analyzed with ImageJ software. VLP images were analyzed first by aligning the image from the emission that was parallel to the excitation light and the image from the emission perpendicular to the excitation light using the TurboReg ImageJ plugin. After alignment, parallel and perpendicular images were analyzed using a MATLAB algorithm written by Joan Pulupa. VLPs are identified in the image via an automated algorithm which uses the Laplacian of Gaussian (LoG) algorithm (written by Vincent Garcia, based on (Lindeberg, 1998)). The identified VLPs are then excised from the image and fit to a Gaussian (Gaussian fitting algorithm, Daniel Johnson). If either the parallel or perpendicular excised VLP did not fit to a Gaussian, the data point was rejected. For VLPs which passed this quality control, the maximum intensity pixel was identified and used to calculate the anisotropy via an anisotropy calculation algorithm written by Daniel Johnson. The anisotropy values for each VLP were then plotted using python. The total intensity for each VLP was calculated by using ($Intensity_{parallel}$ - 2*$Intensity_{perpendicular}$). The calculated total intensity of all VLPs were rescaled to be on a 0-1 axis prior to plotting via (I - I_{min})/(I_{max} - I_{min}) where I is intensity. The rescaled total intensity values for each VLP were then plotted using python.

Statistical differences between three or more means were calculated via one-way ANOVA. Statistical differences between two means were calculated via independent two-tailed T-test. Significance for both ANOVA and T-tests was set at $p<.01$.

Anisotropy Control Cells

HeLa cells transiently transfected with either mEGFP, palm-mEGFP, or MA-mEGFP were analyzed with Metamorph software. Cells were analyzed first by aligning

the parallel and perpendicular channels of the image. After alignment, 50 square selections of 1x1 pixel were chosen at random across the surface of the cell. The intensity of the pixel in both the parallel and perpendicular channels was recorded and the anisotropy of the region was calculated using an anisotropy calculation algorithm written by Daniel Johnson. The anisotropies for the control cells were then plotted using python.

The total intensity for each region was calculated by using ($Intensity_{parallel}$ - 2*$Intensity_{perpendicular}$). The calculated total intensity of all regions were rescaled to be on a 0-1 axis prior to plotting via ($I - I_{min}$)/($I_{max} - I_{min}$) where I is intensity. The rescaled total intensity values for each region were then plotted using python.

Statistical differences between three or more means were calculated via one-way ANOVA. Statistical differences between two means were calculated via independent two-tailed T-test. Significance for both ANOVA and T-tests was set at $p<.01$.

6.6 Plasmids

6.6.1 Vpr Plasmids

GagPol-mCherry, GagPol-mEGFP, GagPol-LXXLF, and GagPol-mCherry-LXXLF were all created from the PCRV1-NL4.3-GagPol packaging vector which was a gift from the Paul Bieniasz at Rockefeller University. Both mCherry and mEGFP were cloned with no linker after the Matrix domain in Gag via Gibson assembly with the NEBuilder® HiFi DNA Assembly Cloning Kit (New England BioLabs).

The LXXLF mutation inserts a premature stop codon at amino acid 43 within the p6 domain which removes the last 10 amino acids of p6. This stop codon affects the Gag coding sequence but makes no amino acid changes to the Pol reading frame. This mutation was created with the Quikchange site-directed mutagenesis kit (Agilent).

The mEGFP-Vpr construct was altered from the Addgene 110200 plasmid containing TEV-Vpr which was a gift from Sergi Padilla Parra (Jones and Padilla-Parra, 2015). TEV was removed from the original plasmid and mEGFP was inserted in its place using a Gibson reaction via the NEBuilder® HiFi DNA Assembly Cloning Kit (New England BioLabs).

Table 6.2 Primers for Vpr constructs

Plasmid	Parental Plasmid	Primer 1 (mutagenesis/ insert for HiFi)	Primer 2 (mutagenesis/ insert for HiFi)	HiFi Backbone Primers
PCRV1-NL4.3-GagPol-mCherry	PCRV1-NL4.3-GagPol	5'-ggaaacaacagccagGTGAGCAAGGGCGAG-3'	5'-gggtaattttggctgacCTTGTACAGCTCGTC-3'	5'-ctggctgttgtttcctgtgtcagctg-3' and 5'-gtcagccaaaattaccctatagtgcagaacctc-3'
PCRV1-NL4.3-GagPol-mEGFP	PCRV1-NL4.3-GagPol	5'-gggtaattttggctgacCTTGTACAGCTCGTC-3'	5'-gccaaaattaccctatagtgAAGGGCGAGGAGCTGTTCACC-3'	5'-atagggtaattttggctcacctggctgttgtttcctgtgtc-3' and 5'-gtcagccaaaattaccctatagtgcagaacctc-3'
PCRV1-NL4.3-GagPol-LXXLF	PCRV1-NL4.3-GagPol	5'-gcttccctcagatAactctttggcagcgac-3'	5'-gtcgctgccaaagagtTatctgagggaagc-3'	N/A
PCRV1-NL4.3-GagPol-mCherry-LXXLF	PCRV1-NL4.3-GagPol-mCherry	5'-gcttccctcagatAactctttggcagcgac-3'	5'-gtcgctgccaaagagtTatctgagggaagc-3'	N/A
mEGFP-Vpr	TEV-Vpr	5'-ccgtcagatccgctagcatgGTGAGCAAGGGCGAGGAGCTG-3'	5'-gcttgagctcgagatctgagtaCTTGTACAGCTCGTCCATGCCG-3'	5'-catgctagcggatctgacgg-3' and 5'-tactcagatctcgagctcaagc-3'

6.6.2 retroCHMP3 Plasmids

The ESCRT plasmids pLNCX2-mCherry-CHMP4B and pLNCX2-mCherry-VPS4A were used as previously published (Bleck et al., 2014; Johnson et al., 2018). The mCherry-TSG101 plasmid was a gift from James Hurley (Addgene plasmid # 21505 ; http://n2t.net/addgene:21505 ; RRID:Addgene_21505) (Lee et al., 2008). The PCRV1-NL4.3-GagPol packaging vector was a gift from Paul Bieniasz at Rockefeller University. The PCRV1-NL4.3-GagPol-PR-D25A plasmid was created using site-directed mutagenesis to create the protease inactivating D25A mutation. GagPol-mEGFP and GagPol-mEGFP-D25A constructs were created from the PCRV1-NL4.3-GagPol plasmid or PCRV1-NL4.3-GagPol-PR-D25A plasmid respectively via Gibson assembly with the NEBuilder® HiFi DNA Assembly Cloning Kit (New England BioLabs). For both plasmids, mEGFP is in the Matrix domain with a Matrix/Capsid cleavage site on either side of the mEGFP.

The EF1-alpha_sm-retroCHMP3-T2A-H2B-tagBFP construct was created from the EF1-alpha_sm-retroCHMP3 construct which was a gift from Wes Sundquist at the University of Utah. The T2A-H2B-BFP was added to the retroCHMP3 in two steps. First, the T2A was added via site-directed mutagenesis (Quikchange Lightning, Agilent), then Gibson assembly with the NEBuilder® HiFi DNA Assembly Cloning Kit (New England BioLabs) was used to add the H2B-tagBFP.

Data in Figures 3.1 and 3.2 used the NL4.3 derived expression vector NLENG1-IRES-GFP for production of HIV-1 virus, which was a gift to the Sundquist Lab from David Levy (Levy et al., 2004).

Table 6.3 Primers for retroCHMP3 constructs

Plasmid	Parental Plasmid	Primer 1 (mutagenesis/ insert for HiFi)	Primer 2 (mutagenesis/ insert for HiFi)	HiFi Backbone Primers
PCRV1-NL4.3-GagPol-PR-D25A	PCRV1-NL4.3-GagPol	5'-actgtatcatctgctcctgttgctaatagagcttcctttaattgcc-3'	5'-ggcaattaaaggaagctctattagcaacaggagcagatgatacagt-3'	N/A
PCRV1-NL4.3-GagPol-mEGFP	PCRV1-NL4.3-GagPol	5'-gggtaattttggctgacCTTGTACAGCTCGTC-3'	5'-gccaaaattacccctatagtgAAGGGCGAGGAGCTGTTCACC-3'	5'-atagggtaattttggctcacctggctgttgttttcctgtgtc-3' and 5'-gtcagccaaaattaccctatagtgcagaacctc-3'
PCRV1-NL4.3-GagPol-mEGFP-D25A	PCRV1-NL4.3-GagPol-PR-D25A	5'-gggtaattttggctgacCTTGTACAGCTCGTC-3'	5'-gccaaaattacccctatagtgAAGGGCGAGGAGCTGTTCACC-3'	5'-atagggtaattttggctcacctggctgttgttttcctgtgtc-3' and 5'-gtcagccaaaattaccctatagtgcagaacctc-3'
EF1-alpha_sm-retroCHMP3-T2A	EF1-alpha_sm-retroCHMP3	5'-CGCATGTTAGCAGACTTCCTCTGCCCTCagcgtaatctggaacATCGTATGGG-3'	5'-ACATGCGGTGACGTCGAGGAGAATCCTGGCCCAtgaaagcttGCGGCCGCACTCCTCAG-3'	N/A
EF1-alpha_sm-retroCHMP3-T2A-H2B	EF1-alpha_sm-retroCHMP3-T2A	5'-CGAGGAGAATCCTGGCCCAatgcctgaaccctctaag-3'	5'-GTTCTCCTTAATCAGCTCGCTcaccatggtggcgaccggtg-3'	5'-TGGGCCAGGATTCTCCTCGACGTCAC-3' and 5'-tgaaagcttGCGGCCGCACTCCTC-3'

EF1-alpha_sm-retroCHMP3-T2A-H2B-tagBFP	EF1-alpha_sm-retroCHMP3-T2A-H2B	5'-caccggtcgccaccatggtgAGCGAGCTGATTAAGGAGAAC-3'	5'-CTGCACCTGAGGAGTGCGGCCGCaagctttcattaCTTGTACAGCTCGTCCATG-3'	5'-TGGGCCAGGATTCTCCTCGACGTCAC-3' and 5'-tgaaagcttGCGGCCGCACTCCTC-3'

6.6.3 Protease Plasmids

FRET

Syngag constructs for FRET as presented in Chapter 2 section 2.1.1 were created using In-Fusion® HD Cloning (Clontech). All mEGFP/mCherry containing constructs were able to use the same In-Fusion® HD primers to add either mEGFP or mCherry to the MA site with a cleavage between the fluorescent protein and CA (Table 6.4). To create Syngag-MA(mEGFP) and Syngag-MA(mCherry), the untagged Syngag was used as the parental plasmid. For Syngag-MA(mEGFP)-mCherry, the previously published Syngag-mCherry was used as the parental plasmid (Jouvenet et al., 2006). For Syngag-MA(mCherry)-mEGFP, the previously published Syngag-mEGFP was used as the parental plasmid (Jouvenet et al., 2006).

Clover, Clover3, Ruby2, and Ruby3 were all a gift from Michael Lin (Bajar and Wang et al., 2016A; Lam et al., 2012). The previously published Syngag-mEGFP (Jouvenet et al., 2006) was used as the parental plasmid and each Clover or Ruby variant was inserted in place of the mEGFP via In-Fusion® HD Cloning (Clontech).

Table 6.4 Primers for FRET protease constructs

Plasmid	Parental Plasmid	In-Fusion Primer 1	In-Fusion Primer 2
Syngag-Clover	Syngag-mEGFP	5'-CGTCACAATCGGATCCGGCCACCATGGTGAGCAA-3'	5'-TCTAGAGTCGCGGCCGCTTTACTTGTACAGCTCGTCC-3'
Syngag-Clover3	Syngag-mEGFP	5'-CGTCACAATCGGATCCGGCCACCATGGTGAGCAA-3'	5'-TCTAGAGTCGCGGCCGCTTTACTTGTACAGCTCGTCC-3'
Syngag-Ruby2	Syngag-mEGFP	5'-CGTCACAATCGGATCCGGCCACCATGGTGTCTAA-3'	5'-TCTAGAGTCGCGGCCGCTTTACTTGTACAGCTCGTCC-3'
Syngag-Ruby3	Syngag-mEGFP	5'-CGTCACAATCGGATCCGGCCACCATGGTGTCTAA-3'	5'-TCTAGAGTCGCGGCCGCTTTACTTGTACAGCTCGTCC-3'
Syngag-MA(mEGFP)	Syngag	5'-CACAGCAACCAGGATATCATGGTGAGCAAGGGCGAG-3'	5'-GTTCTGGCTGACGATATCCTTGTACAGCTCGTCCATG-3'
Syngag-MA(mCherry)	Syngag	5'-CACAGCAACCAGGATATCATGGTGAGCAAGGGCGAG-3'	5'-GTTCTGGCTGACGATATCCTTGTACAGCTCGTCCATG-3'
Syngag-MA(mEGFP)-mCherry	Syngag-mCherry	5'-CACAGCAACCAGGATATCATGGTGAGCAAGGGCGAG-3'	5'-GTTCTGGCTGACGATATCCTTGTACAGCTCGTCCATG-3'
Syngag-MA(mCherry)-mEGFP	Syngag-mEGFP	5'-CACAGCAACCAGGATATCATGGTGAGCAAGGGCGAG-3'	5'-GTTCTGGCTGACGATATCCTTGTACAGCTCGTCCATG-3'

Cleavage-sensitive reporters

Cleavage-sensitive reporters used in Chapter 2 section 2.1.2 were created using site-directed mutagenesis (Quikchange Lightning, Agilent). pCDH-puro-CMV-VC3AI was a gift from Binghui Li (Addgene plasmid # 78907 ; http://n2t.net/addgene:78907 ; RRID:Addgene_78907). The DEVDG cleavage site was replaced with either the RT/IN cleavage site or the MA/CA cleavage site using the Quikchange Lightning kit and the primers shown in Table 6.5.

ZipGFP1-10_TEV and ZipGFP11_TEV were gifts from Xiaokun Shu (Addgene plasmid # 81242 ; http://n2t.net/addgene:81242 ; RRID:Addgene_81242 and Addgene plasmid # 81243 ; http://n2t.net/addgene:81243 ; RRID:Addgene_81243 respectively). The TEV cleavage site was replaced with either the RT/IN cleavage site or the MA/CA cleavage site using the Quikchange Lightning kit and the primers shown in Table 6.5.

The single polypeptide FPX biosensor for caspase-3 was a gift from Robert Campbell (Addgene plasmid # 60883 ; http://n2t.net/addgene:60883 ; RRID:Addgene_60883). For clarity purposes, this plasmid was named ddRFP-A_ddFP-B_DEVD_ddGFP-A in this thesis. The DEVD cleavage site was replaced with either the RT/IN cleavage site or the MA/CA cleavage site using the Quikchange Lightning kit and the primers shown in Table 6.5.

Table 6.5 Primers for cleavage-sensitive reporter constructs

Plasmid	Parental Plasmid	Mutagenesis Primer 1	Mutagenesis Primer 2
VC3AI-RT/IN	pCDH-puro-CMV-VC3AI	5'-AGGAAAGTACTATTTTTAGATGGAATATTCACCGGGGTGGTGCCCATCCTGGTCGAGCTG-3'	5'-TATTCCATCTAAAAATAGTACTTTCCTGATCCCGGCGGCGGTCACGAACTCCAGCAGGAC-3'
VC3AI-MA/CA	pCDH-puro-CMV-VC3AI	5'-gtcagccaaaattaccctatagtgcagaacGGCTTCACCGGGGTGGTGCCCATCCTGGTC-3'	5'-gttctgcactatagggtaattttggctgacCCCGGCGGCGGTCACGAACTCCAGCAGGAC-3'
zipGFP1-10-RT/IN	zipGFP1-10-TEV_T2A-mCherry	5'-ATCAGGAAAGTACTATTTTTAGATGGAATAGAATTCGGCGGCAGCAAGGTGTCTGCACTT-3'	5'-TATTCCATCTAAAAATAGTACTTTCCTGATTTTTTCATTTGGATCTTTGCTCAGGACTGT-3'
zipGFP1-10-MA/CA	zipGFP1-10-TEV_T2A-mCherry	5'-GTCAGCCAAAATTACCCTATAGTGCAGAACGAATTCGGCGGCAGCAAGGTGTCTGCACTT-3'	5'-GTTCTGCACTATAGGGTAATTTTGGCTGACTTTTTCATTTGGATCTTTGCTCAGGACTGT-3'
zipGFP11-RT/IN	zipGFP11-TEV	5'-AGGAAAGTACTATTTTTAGATGGAATACTCGAGGGAGGCAGCGAAGTGAGCGCGCTG-3'	5'-TATTCCATCTAAAAATAGTACTTTCCTGATGCCGGCGGCGTTCACGTACTCGTGCAG-3'
zipGFP11-MA/CA	zipGFP11-TEV	5'-GTCAGCCAAAATTACCCTATAGTGCAGAACCTCGAGGGAGGCAGCGAAGTGAGCGCGCTG-3'	5'-GTTCTGCACTATAGGGTAATTTTGGCTGACGCCGGCGGCGTTCACGTACTCGTGCAGCAC-3'

ddRFP-A_ddFP-B_RT/IN_ddGFP-A	ddRFP-A_ddFP-B_DEVD_ddGFP-A	5'atcaggaaagtactatttttagatggaataGCCGTCATCAAAGAGTTCATGCGCTTCAAG-3'	5'TATTCCATCTAAAAATAGTACTTTCCTGATGCCGGAGGCGGATCCGGAGCTGCCGCTGCC-3'
ddRFP-A_ddFP-B_MA/CA_ddGFP-A	ddRFP-A_ddFP-B_DEVD_ddGFP-A	5-gtcagccaaaattaccctatagtgcagaacGGAGCCGTCATCAAAGAGTTCATGCGCTTC-3'	5'-gttctgcactatagggtaattttggctgacGCCGGAGGCGGATCCGGAGCTGCCGCTGCC-3'

Anisotropy

Constructs used for the anisotropy measurements in Chapter 2 section 2.2 were created using a combination of site-directed mutagenesis (Quikchange Lightning, Agilent) and Gibson assembly with the NEBuilder® HiFi DNA Assembly Cloning Kit (New England BioLabs). The PCRV1-NL4.3-GagPol plasmid was a gift from Paul Bieniasz at Rockefeller University. The PCRV1-NL4.3-GagPol-PR-D25A plasmid was created using site-directed mutagenesis to create the protease inactivating D25A mutation. PCRV1-NL4.3-GagPol was also used as the parental plasmid for PCRV1-NL4.3-GagPol-MA-mEGFP and PCRV1-NL4.3-GagPol-PR-D25A was used as the parental plasmid for PCRV1-NL4.3-GagPol-MA-mEGFP-PR-D25A which were both created with the NEBuilder® HiFi Kit. Another copy of the MA/CA cleavage site was added to both PCRV1-NL4.3-GagPol-MA-mEGFP and PCRV1-NL4.3-GagPol-MA-mEGFP-PR-D25A using site-directed mutagenesis to create PCRV1-NL4.3-GagPol-MA-mEGFP-DC and PCRV1-NL4.3-GagPol-MA-mEGFP-DC-PR-D25A. Finally, the control plasmid PCRV1-NL4.3-MA(mEGFP) was created by removing the rest of GagPol from PCRV1-NL4.3-GagPol-MA-mEGFP with site-directed mutagenesis. All primers for this work are in Table 6.6.

Other plasmids used in the anisotropy work are N1-mEGFP which was a gift from Micheal Davidson (Addgene plasmid # 54767 ; http://n2t.net/addgene:54767 ; RRID:Addgene_54767) and Palmitoylated-mEGFP (Atkinson et al., 2013).

Table 6.6 Primers for protease anisotropy constructs

Plasmid	Parental Plasmid	Primer 1 (mutagenesis/ insert for HiFi)	Primer 2 (mutagenesis/ insert for HiFi)	HiFi Backbone Primers
PCRV1-NL4.3-GagPol-PR-D25A	PCRV1-NL4.3-GagPol	5'-actgtatcatctgctcctgttgctaatagagcttcctttaattgcc-3'	5'-ggcaattaaaggaagctctattagcaacaggagcagatgatacagt-3'	N/A
PCRV1-NL4.3-GagPol-MA-mEGFP	PCRV1-NL4.3-GagPol	5'-ggaaacaacagccagGTGAGCAAGGGCGAG-3'	5'gggtaattttggctgacCTTGTACAGCTCGTC-3'	5'ctggctgttgtttcctgtgtcagctg-3' and 5'-gtcagccaaaattaccctatagtgcagaacctc-3'
PCRV1-NL4.3-GagPol-MA-mEGFP-PR-D25A	PCRV1-NL4.3-GagPol-PR-D25A	5'-ggaaacaacagccagGTGAGCAAGGGCGAG-3'	5'-gggtaattttggctgacCTTGTACAGCTCGTC-3'	5'ctggctgttgtttcctgtgtcagctg-3' and 5'-gtcagccaaaattaccctatagtgcagaacctc-3'
PCRV1-NL4.3-GagPol-mEGFP-DC	PCRV1-NL4.3-GagPol-MA-mEGFP	5'-gccaaaattacccctatagtgAAGGGCGAGGAGCTGTTCACC-3'	5'-atagggtaattttggctcacctggctgttgtttcctgtgtc-3'	N/A
PCRV1-NL4.3-GagPol-mEGFP-DC-PR-D25A	PCRV1-NL4.3-GagPol-MA-mEGFP-PR-D25A	5'-gccaaaattacccctatagtgAAGGGCGAGGAGCTGTTCACC-3'	5'-atagggtaattttggctcacctggctgttgtttcctgtgtc-3'	N/A
PCRV1-NL4.3-MA(mEGFP)	PCRV1-NL4.3-GagPol-MA-mEGFP	5'-taagcggccgctcgacatagcag-3'	5'-ctatgtcgagcggccgcTTACTTGTACAGCTCG-3'	N/A

6.7 Protease Inhibitors

The protease inhibitor cocktail used in the protease anisotropy experiments In Chapter 2 section 2.2 is a combination of 150μM Darunavir and 100μM Atazanavir. These reagents were obtained through the NIH AIDS Reagent Program, Division of AIDS, NIAID, NIH: Darunavir (Cat# 11447) from Tibotec, Inc. and Atazanavir Sulfate from NIAID, DAIDS (cat# 10003). For live cell imaging, DMEM on HeLa cells was replaced with phenol red free DMEM (Gibco #11995065) with 10% FBS along with 150μM Darunavir and 100μM Atazanavir at the time of transfection. This media was not replaced prior to imaging. For VLPs with protease inhibitors, 150μM Darunavir and 100μM Atazanavir in DMEM were applied to Hek293T cells at the time of transfection. No additional protease inhibitors were applied after collection.

6.8 Survey Methods

This section is the full methods from Chapter 4 on how to summarize your research findings. They are adapted from my previous publication (Bredbenner and Simon, 2019).

6.8.1 Science Summary Design

This work was granted exempt status from the Rockefeller University IRB (ref #342107). We chose two recently published papers as the subject of study. Cohn et al. was published in Nature Medicine in April 2018 and outlines a method for recovering latent cells from HIV-1+ patient blood in order to study the latent cells for a possible future cure. It also sequences these latent cells and shows that they are often clonal (Cohn et al., 2018). Takata et al. was published in Nature in September 2017 and shows that HIV-1 has selectively removed CG dinucleotides from its genome to more closely mimic the nucleotide content of its human host. Specifically, HIV-1 has removed CG dinucleotides to avoid the host protein ZAP which recognizes and destroys RNA in the cell that has these dinucleotides (Takata et al., 2017). Both papers are within the HIV-1 field, and both were published at similar times in similar journals. Both papers were also first-authored by graduate students both at Rockefeller University and both in the same year of graduate school.

The abstracts of both papers were taken, as published, to place into a survey. From there, a plain language summary was written for each paper. The main takeaways that were highlighted in the published abstracts were also the main focus of the plain language summaries. Every effort was taken to eliminate any jargon and to provide real-world context for each of the findings. Both plain language summaries were of similar length (422 words for Cohn et al.; 433 words for Takata et al.). The plain language summaries followed the guidelines put into place by eLife, including their list of questions that they ask the scientists to make the summaries easier for the editors to write (Inside eLife, 2017). The abstracts and plain language summaries were put into a readability calculator to obtain the Flesch Reading Ease Score (FRES) and the Flesch-

Kincaid Grade Level (FKGL) similar to previously published work on plain language summaries (Carvalho et al., 2019). The scores can be seen in Table 6.5.

Table 6.7 Readability of published abstracts and plain language summaries for Cohn et al. and Takata et al.

	Cohn et al.		**Takata et al.**	
	Abstract	**Plain Language**	**Abstract**	**Plain Language**
FRES[a]	24.2	63	15.2	58
FKGL[b]	16.2	9.5	16.1	10

All scores were obtained from www.readability-score.com.
[a] Flesch Reading Ease Score
[b] Flesch-Kincaid Grade Level

The plain language summaries were used as the spoken script for the video abstracts. The videos of each paper were illustrated using similar visual motifs and the videos were of similar lengths (2:33 for Cohn et al.; 2:49 for Takata et al.). Both videos followed the "whiteboard explainer" style where images are drawn on a screen and the drawing is either freeze-framed or sped up to match the narration. Both videos were uploaded to YouTube and were made unlisted so only survey participants could see them. The YouTube generated closed captions were edited to reflect the actual script, and closed captions were set to automatically appear anytime the videos were played. The closed captions could be turned off by the participants if they wanted.

The videos followed all of the qualifications set by Cell for their video abstracts (Cell Press, 2019). All technical specifications were met or exceeded, and the videos were within the requested length. The first author has made several of these Cell video abstracts and is familiar with the qualifications necessary. Audio quality was also carefully controlled as it plays a role in how favorable participants find the research (Newman and Schwarz, 2018).

The graphical abstracts were created using Keynote software and they followed the same visual motifs that were in the videos. The graphical abstracts were placed into a color-blindness simulator to be sure that all possible participants could see the image equally well (Coblis, 2000). The graphical abstracts were also created based on the

guidelines set up by Cell for their graphical abstracts (Cell Press, 2019). All technical specifications were met or exceeded where possible.

All summaries were created with the intent that the videos, graphics, and plain language summaries should be content-identical.

6.8.2 Survey Design

The survey was created in the Google Forms platform. Eight surveys were created that were mostly identical except for the type of summary shown. Two surveys showed video abstracts, two showed graphical abstracts, two showed plain language summaries, and two showed published abstracts. Each pair of surveys showed both the Cohn et al. summary and the Takata et al. summary, but one version showed the Cohn et al. summary first and one showed the Takata et al. summary first (Fig 6.1). Switching which paper was shown first was done to be able to prove that the responses received did not differ based on which paper summary was seen first. Participants were randomly assorted to one of the eight surveys via a random URL generator embedded into the button on the survey website. Each participant only completed one survey meaning that they only saw one type of science summary, but they saw that type of summary for both papers (Fig 6.1).

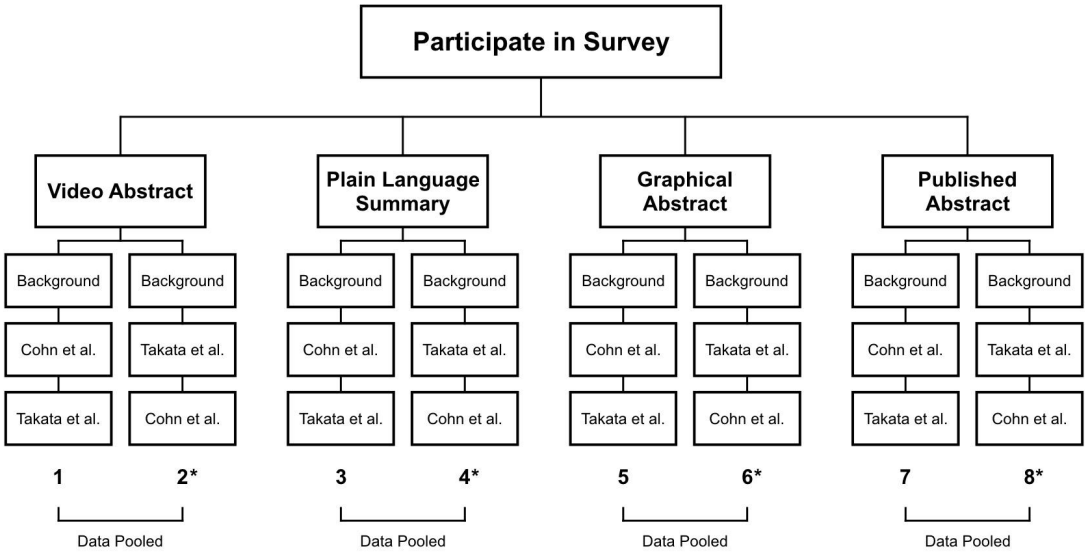

Figure 6.1 Flowchart of survey assignment and pooling
A flowchart representing the eight survey versions created for this research. Once participants click on the button “Participate in Survey”, they are randomly assorted to one of the eight possible surveys including two versions each of video abstracts, plain language summaries, graphical abstracts, and published abstracts where one version shows the Cohn et al. summary first and one shows the Takata et al. summary first. All surveys ask background questions prior to showing a summary. The asterisks denote surveys that contained an error which only showed participants with science careers both the Takata et al. and Cohn et al. summaries. All other participants were only shown the Cohn et al. summary. The error was corrected shortly after publicizing the survey. Data from both versions of each type of summary were pooled, as denoted by brackets and the phrase “Data Pooled.”

Four of the surveys contained a collection error that was corrected part way through data collection (Fig 6.1). If participants were funneled to one of the surveys with the error, only participants who marked that they had science careers were shown both the Cohn et al. and Takata et al. summaries. All other participants only saw the Cohn et al. summary. This error led to fewer non-science and science-related participants for the Takata et al. paper, but the error was corrected in time to still get usable data.

Before presenting the created summaries, all surveys asked participants to report their career type (science, science-related, non-science, or undergraduate), input their gender if they so desired (a fill-in-the-blank that was not required), and report their preference for receiving science updates (written summaries, video, audio, reading the original research paper, or graphics).

Participants that reported they had science careers were asked an additional series of questions about how they prefer to receive research updates in their field versus outside of their field. This list of options included newspaper articles, social media, recommendations from friends and colleagues, scientific journals, and PubMed/other alerts.

After the background information was collected, participants were shown one of the summaries and asked follow up questions about it. There was a 6-question quiz associated with each of the papers to determine comprehension (Table 6.6). The quiz was one multiple choice question and five true/false questions. These questions were designed to be answerable regardless of which summary type the participant had seen. Other follow up questions were asked to determine how much the participants enjoyed and understood the research and also how much they wanted to see more summaries of the type that they were presented (Table 6.6). The full survey is available as supplementary file 6.

Table 6.8 Follow up questions for Cohn et al. and Takata et al.

Type of Question	Cohn et al.	Takata et al.
Comprehension – Multiple Choice	This research focuses on: **(a) HIV** (b) FIV (c) Influenza (d) I don't know	This research focuses on: **(a) HIV** (b) FIV (c) Influenza (d) I don't know
Comprehension – T/F	This research created a capture technique to collect all T-cells from patients. **False**	Vertebrates have evolved less AG nucleotide pairs. **False**
Comprehension – T/F	The capture technique is a type of cure for the virus discussed in the summary. **False**	The virus mentioned has evolved to lack CG pairs to avoid cell anti-viral defenses. **True**
Comprehension – T/F	Latent cells captured from patient blood are mostly from a single latent cell that divided. **True**	ZAP interacts with the DNA of the virus mentioned in the summary. **False**

Comprehension – T/F	Captured latent cells have higher expression of genes that increase virus activation. **False**	All possible DNA nucleotide pairs show up at the same rate as each other in vertebrates (eg. AT is present at the same frequency as GT or CG or GC). **False**
Comprehension – T/F	Latent cells are a consequence of the lifecycle of the virus mentioned. **True**	ZAP is a protein that is made by the infected host cell. **True**
Enjoyment	I enjoyed reading[a] this abstract[b]: (0) Not at all (1) A bit (2) Average (3) Mostly (4) Very Much	I enjoyed reading[a] this abstract[b]: (0) Not at all (1) A bit (2) Average (3) Mostly (4) Very Much
Understanding	I understand this research more after reading[a] this abstract[b]: (0) Not at all	I understand this research more after reading[a] this abstract[b]: (0) Not at all

	(1) A bit (2) Average (3) Mostly (4) Very Much	(1) A bit (2) Average (3) Mostly (4) Very Much
Desire for Updates	I want to get more science updates via written abstract[b] after reading[a] this: (0) Not at all (1) A bit (2) Average (3) Mostly (4) Very Much	I want to get more science updates via written abstract[b] after reading[a] this: (0) Not at all (1) A bit (2) Average (3) Mostly (4) Very Much

Follow up questions for comprehension have the correct answer noted in bold. For enjoyment, understanding, and desire for updates, participants were only presented with the phrases “Not at all”, “A bit”, “Average”, “Mostly”, and “Very Much”. The numbers in parentheses were added for analysis and presentation of data.

[a] The word ‘reading’ was removed or changed to ‘viewing’ for surveys with video or graphical abstracts.

[b] The word ‘abstract’ was changed to ‘video summary’ or ‘summary’ for surveys with video abstracts, ‘summary’ for surveys with plain language summaries, and ‘graphical summary’ or ‘summary’ for surveys with graphical abstracts.

6.8.3 Survey Recruitment

Recruitment was done using the snowball method used in studies similar to this research (Gardiner et al., 2018). Participants were recruited online via the first author’s social media pages using appropriate hashtags. Emails were also sent to a number of

science groups including the National Alliance for Broader Impacts (NABI), The Falling Walls organization, the BioBus, all attendees of the 2019 SciOut conference, all attendees of the Science Alliance Leadership Training (SALT) up to 2018, and all members of the Rockefeller University Community.

6.8.4 Survey Analysis

Results were downloaded from Google Forms and put into Google Sheets for analysis. Results from surveys which showed the Takata et al. summary first and results from surveys which showed the Cohn et al. summary first were compared via the Mann-Whitney U-Test to see if the populations were different based on which summary was presented first. In all cases of all summary types, it did not matter which summary was shown first, so Takata et al. data from both versions were pooled and Cohn et al. data from both versions were pooled (Fig 6.1).

The results were then checked between Cohn et al. and Takata et al. to see if the two papers yielded different results. The two papers showed statistically significant differences between the Cohn et al. and Takata et al. published abstracts in comprehension scores and the desire for more updates. Since the published abstracts were significantly different in these categories, the two papers were kept separate for analysis.

Participants who marked that they were undergraduates were pooled with participants who marked that they had non-science careers since undergraduates were in the minority of participants and they often have the same schooling as adults without science careers. There were no significant differences in the results between these two populations, so pooling seemed appropriate.

The results from the separate careers (science, science-related, and non-science) in the two papers were compared to see if there were significant differences. There were statistically significant differences between careers in every scoring category in each of the two papers, so the careers were kept separate for analysis.

All statistical significance between populations was calculated by the Mann-Whitney U Test. All correlation values were calculated by the Pearson’s r correlation coefficient.

References

Women, Minorities, and Persons with Disabilities in Science and Engineering: 2019. (2019). National Science Foundation, National Center for Science and Engineering Statistics. https://ncses.nsf.gov/pubs/nsf19304/digest/occupation#science-and-engineering-occupations

Video Abstract Guidelines. (2019). Cell Press. https://www.cell.com/video-abstract-guidelines

Cell Press Graphical Abstract Guidelines. (2019). *Cell Press*. https://www.cell.com/pb/assets/raw/shared/figureguidelines/GA_guide.pdf

Plain-language Summaries: How to write an eLife digest. (2017, March). *Inside ELife*. https://elifesciences.org/inside-elife/85518309/plain-language-summaries-how-to-write-an-elife-digest

State of Science Index Survey. (2019). 3M. https://www.3m.com/3M/en_US/state-of-science-index-survey/interactive-3m-state-of-science-survey/

Abram, M. E., & Parniak, M. A. (2005). Virion Instability of Human Immunodeficiency Virus Type 1 Reverse Transcriptase (RT) Mutated in the Protease Cleavage Site between RT p51 and the RT RNase H Domain. *Journal of Virology*, *79*(18), 11952–11961. https://doi.org/10.1128/jvi.79.18.11952-11961.2005

Aiken, C., & Trono, D. (1995). Nef stimulates human immunodeficiency virus type 1 proviral DNA synthesis. *Journal of Virology*, *69*(8), 5048–5056. https://doi.org/10.1128/jvi.69.8.5048-5056.1995

Aiken, C., Konner, J., Landau, N. R., Lenburg, M. E., & Trono, D. (1994). Nef induces CD4 endocytosis: Requirement for a critical dileucine motif in the membrane-proximal CD4 cytoplasmic domain. *Cell*, *76*(5), 853–864. https://doi.org/10.1016/0092-8674(94)90360-3

Atkinson, C. E., Mattheyses, A. L., Kampmann, M., & Simon, S. M. (2013). Conserved spatial organization of FG domains in the nuclear pore complex. *Biophysical Journal*, *104*(1), 37–50. https://doi.org/10.1016/j.bpj.2012.11.3823

Bajar, B. T., Wang, E. S., Lam, A. J., Kim, B. B., Jacobs, C. L., Howe, E. S., Davidson, M. W., Lin, M. Z., & Chu, J. (2016). Improving brightness and photostability of green and red fluorescent proteins for live cell imaging and FRET reporting. *Scientific Reports*, *6*(January), 1–12. https://doi.org/10.1038/srep20889

Bajar, B. T., Wang, E. S., Zhang, S., Lin, M. Z., & Chu, J. (2016). A guide to fluorescent protein FRET pairs. *Sensors (Switzerland)*, *16*(9), 1–24. https://doi.org/10.3390/s16091488

Barnfield, S., Pitts, A. C., Kalaria, R., Allan, L., & Tullo, E. (2017). “Is all the stuff about neurons necessary?” The development of lay summaries to disseminate findings from the Newcastle Cognitive Function after Stroke (COGFAST) study. *Research Involvement and Engagement*, *3*(1), 1–14. https://doi.org/10.1186/s40900-017-0066-y

Baumgärtel, V., Ivanchenko, S., Dupont, A., Sergeev, M., Wiseman, P. W., Kräusslich, H. G., Bräuchle, C., Müller, B., & Lamb, D. C. (2011). Live-cell visualization of

dynamics of HIV budding site interactions with an ESCRT component. *Nature Cell Biology*, *13*(4), 469–476. https://doi.org/10.1038/ncb2215

Bendjennat, M., & Saffarian, S. (2016). The Race against Protease Activation Defines the Role of ESCRTs in HIV Budding. *PLoS Pathogens*, *12*(6), 1–25. https://doi.org/10.1371/journal.ppat.1005657

Bentham, M., Mazaleyrat, S., & Harris, M. (2006). Role of myristoylation and N-terminal basic residues in membrane association of the human immunodeficiency virus type 1 Nef protein. *Journal of General Virology*, *87*(3), 563–571. https://doi.org/10.1099/vir.0.81200-0

Bieniasz, P. D. (2009). The Cell Biology of HIV-1 Virion Genesis. *Cell Host and Microbe*, *5*(6), 550–558. https://doi.org/10.1016/j.chom.2009.05.015

Bleck, M., Itano, M. S., Johnson, D. S., Thomas, V. K., North, A. J., Bieniasz, P. D., & Simon, S. M. (2014). Temporal and spatial organization of ESCRT protein recruitment during HIV-1 budding. *Proceedings of the National Academy of Sciences of the United States of America*, *111*(33), 12211–12216. https://doi.org/10.1073/pnas.1321655111

Bouyac-Bertoia, M., Dvorin, J. D., Fouchier, R. A. M., Jenkins, Y., Meyer, B. E., Wu, L. I., Emerman, M., & Malim, M. H. (2001). HIV-1 Infection Requires a Functional Integrase NLS. *Molecular Cell*, *7*(5), 1025–1035. https://doi.org/10.1016/S1097-2765(01)00240-4

Bredbenner, K., & Simon, S. M. (2019). Video abstracts and plain language summaries are more effective than graphical abstracts and published abstracts. *PLoS ONE*, *14*(11), 1–19. https://doi.org/10.1371/journal.pone.0224697

Brown, P. O., Bowerman, B., Varmus, H. E., & Bishop, J. M. (1989). Retroviral integration: Structure of the initial covalent product and its precursor, and a role for the viral IN protein. *Proceedings of the National Academy of Sciences of the United States of America*, *86*(8), 2525–2529. https://doi.org/10.1073/pnas.86.8.2525

Burghardt, T. P. (1984). Model-Independent fluorescence polarization for measuring order in a biological assembly. *Biopolymers*, *23*(11), 2383–2406. https://doi.org/10.1002/bip.360231118

Caliendo, A. M., & Kraft, C. S. (2016). Human immunodeficiency virus type 1. *Molecular Pathology in Clinical Practice:Second Edition*, *63*(9), 629–640. https://doi.org/10.1007/978-3-319-19674-9_45

Campbell, E. M., Perez, O., Melar, M., & Hope, T. J. (2007). Labeling HIV-1 virions with two fluorescent proteins allows identification of virions that have productively entered the target cell. *Virology*, *360*(2), 286–293. https://doi.org/10.1016/j.virol.2006.10.025

Carlson, L. A., Briggs, J. A. G., Glass, B., Riches, J. D., Simon, M. N., Johnson, M. C., Muller, B., Grunewald, K., & Krausslich, H. G. (2008). Three-Dimensional Analysis of Budding Sites and Released Virus Suggests a Revised Model for HIV-1 Morphogenesis. *Cell Host and Microbe*, *4*(6), 592–599. https://doi.org/10.1016/j.chom.2008.10.013

Carvalho, F. A., Elkins, M. R., Franco, M. R., & Pinto, R. Z. (2019). Are plain-language summaries included in published reports of evidence about physiotherapy interventions? Analysis of 4421 randomised trials, systematic reviews and guidelines on the Physiotherapy Evidence Database (PEDro). *Physiotherapy*, *105*(3), 354–361.

Cashikar, A. G., Shim, S., Roth, R., Maldazys, M. R., Heuser, J. E., & Hanson, P. I. (2014). Structure of cellular ESCRT-III spirals and their relationship to HIV budding. *ELife*, *3*, 1–17. https://doi.org/10.7554/eLife.02184

Cassan, M., Delaunay, N., Vaquero, C., & Rousset, J. P. (1994). Translational frameshifting at the gag-pol junction of human immunodeficiency virus type 1 is not increased in infected T-lymphoid cells. *Journal of Virology*, *68*(3), 1501–1508. https://doi.org/10.1128/jvi.68.3.1501-1508.1994

Cavrois, M., Neidleman, J., Kreisberg, J. F., & Greene, W. C. (2007). In vitro derived dendritic cells trans-infect CD4 T cells primarily with surface-bound HIV-1 virions. *PLoS Pathogens*, *3*(1), 0038–0045. https://doi.org/10.1371/journal.ppat.0030004

Chang, D. D., & Sharp, P. A. (1989). Regulation by HIV Rev depends upon recognition of splice sites. *Cell*, *59*(5), 789–795. https://doi.org/10.1016/0092-8674(89)90602-8

Chang, F., Re, F., Sebastian, S., Sazer, S., & Luban, J. (2004). HIV-1 Vpr Induces Defects in Mitosis, Cytokinesis, Nuclear Structure, and Centrosomes. *Molecular Biology of the Cell*, *15*, 1793–1801. https://www.molbiolcell.org/doi/pdf/10.1091/mbc.e03-09-0691

Chiang, C.-C., Wang, S.-M., Pan, Y.-Y., Huang, K.-J., & Wang, C.-T. (2010). A Single Amino Acid Substitution in HIV-1 Reverse Transcriptase Significantly Reduces Virion Release. *Journal of Virology*, *84*(2), 976–982. https://doi.org/10.1128/jvi.01532-09

Chowers, M. Y., Pandori, M. W., Spina, C. A., Richman, D. D., & Guatelli, J. C. (1995). The growth advantage conferred by HIV-1 nef is determined at the level of viral DNA formation and is independent of CD4 downregulation. *Virology*, *212*, 451–457.

Chutiwitoonchai, N., Siarot, L., Takeda, E., Shioda, T., Ueda, M., & Aida, Y. (2016). HIV-1 Vpr abrogates the effect of TSG101 overexpression to support virus release. *PLoS ONE*, *11*(9), 1–17. https://doi.org/10.1371/journal.pone.0163100

Clayton, A. H. A., Hanley, Q. S., Arndt-Jovin, D. J., Subramaniam, V., & Jovin, T. M. (2002). Dynamic fluorescence anisotropy imaging microscopy in the frequency domain (rFLIM). *Biophysical Journal*, *83*(3), 1631–1649. https://doi.org/10.1016/S0006-3495(02)73932-5

Clever, J., Sassetti, C., & Parslow, T. G. (1995). RNA secondary structure and binding sites for gag gene products in the 5' packaging signal of human immunodeficiency virus type 1. *Journal of Virology*, *69*(4), 2101–2109. https://doi.org/10.1128/jvi.69.4.2101-2109.1995

Coblis, W. M. (2000). *Color Blindness Simulator*. https://www.color-blindness.com/coblis-color-blindness-simulator/

Cohen, E. A., Subbramanian, R. A., & Gottlinger, H. G. (1996). Role of Auxiliary Proteins in Retroviral Morphogenesis. In *Morphogenesis and Maturation of Retroviruses* (pp. 219–235).

Cohn, L. B., Da Silva, I. T., Valieris, R., Huang, A. S., Lorenzi, J. C. C., Cohen, Y. Z., Pai, J. A., Butler, A. L., Caskey, M., Jankovic, M., & Nussenzweig, M. C. (2018). Clonal CD4+ T cells in the HIV-1 latent reservoir display a distinct gene profile upon reactivation. *Nature Medicine*, *24*(5), 604–609. https://doi.org/10.1038/s41591-018-0017-7

Corrie, J. E. T., Brandmeier, B. D., Ferguson, R. E., Trentham, D. R., Kendrick-Jones, J., Hopkins, S. C., Van Der Heide, U. A., Goldman, Y. E., Sabido-David, C., Dale, R. E., Criddle, S., & Irving, M. (1999). Dynamic measurement of myosin light-chain-domain tilt and twist in muscle contraction. *Nature*, *400*(6743), 425–430. https://doi.org/10.1038/22704

Dale, R. E., Hopkins, S. C., An Der Heide, U. A., Marszałek, T., Irving, M., & Goldman, Y. E. (1999). Model-independent analysis of the orientation of fluorescent probes with restricted mobility in muscle fibers. *Biophysical Journal*, *76*(3), 1606–1618. https://doi.org/10.1016/S0006-3495(99)77320-0

de Marco, A., Heuser, A.-M., Glass, B., Krausslich, H.-G., Muller, B., & Briggs, J. A. G. (2012). Role of the SP2 Domain and Its Proteolytic Cleavage in HIV-1 Structural Maturation and Infectivity. *Journal of Virology*, *86*(24), 13708–13716. https://doi.org/10.1128/jvi.01704-12

Deml, L., Bojak, A., Steck, S., Graf, M., Wild, J., Schirmbeck, R., Wolf, H., & Wagner, R. (2001). Multiple Effects of Codon Usage Optimization on Expression and Immunogenicity of DNA Candidate Vaccines Encoding the Human Immunodeficiency Virus Type 1 Gag Protein. *Journal of Virology*, *75*(22), 10991–11001. https://doi.org/10.1128/jvi.75.22.10991-11001.2001

Desai, T. M., Marin, M., Sood, C., Shi, J., Nawaz, F., Aiken, C., & Melikyan, G. B. (2015). Fluorescent protein-tagged Vpr dissociates from HIV-1 core after viral fusion and rapidly enters the cell nucleus. *Retrovirology*, *12*(1), 1–20. https://doi.org/10.1186/s12977-015-0215-z

Ding, Y., Li, J., Enterina, J. R., Shen, Y., Zhang, I., Tewson, P. H., Mo, G. C. H., Zhang, J., Quinn, A. M., Hughes, T. E., Maysinger, D., Alford, S. C., Zhang, Y., & Campbell, R. E. (2015). Ratiometric biosensors based on dimerization-dependent fluorescent protein exchange. *Nature Methods*, *12*(3), 195–198. https://doi.org/10.1038/nmeth.3261

Dorfman, T., Mammano, F., Haseltine, W. A., & Göttlinger, H. G. (1994). Role of the matrix protein in the virion association of the human immunodeficiency virus type 1 envelope glycoprotein. *Journal of Virology*, *68*(3), 1689–1696. https://doi.org/10.1128/jvi.68.3.1689-1696.1994

Fabrikant, G., Lata, S., Riches, J. D., Briggs, J. A. G., Weissenhorn, W., & Kozlov, M. M. (2009). Computational model of membrane fission catalyzed by ESCRT-III. *PLoS Computational Biology*, *5*(11). https://doi.org/10.1371/journal.pcbi.1000575

Feinberg, M. B., Baltimore, D., & Frankel, A. D. (1991). The role of Tat in the human immunodeficiency virus life cycle indicates a primary effect on transcriptional elongation. *Proceedings of the National Academy of Sciences of the United States of America*, *88*(9), 4045–4049. https://doi.org/10.1073/pnas.88.9.4045

Feng, Y., Broder, C. C., Kennedy, P. A., & Berger, E. A. (1996). HIV-1 entry cofactor: Functional cDNA cloning of a seven-transmembrane, G protein-coupled receptor. *Science*, *272*(5263), 872–877.

Fischer, U., Huber, J., Boelens, W. C., Mattajt, L. W., & Lührmann, R. (1995). The HIV-1 Rev Activation Domain is a nuclear export signal that accesses an export pathway used by specific cellular RNAs. *Cell*, *82*(3), 475–483. https://doi.org/10.1016/0092-8674(95)90436-0

Fisher, R. D., Chung, H. Y., Zhai, Q., Robinson, H., Sundquist, W. I., & Hill, C. P. (2007). Structural and Biochemical Studies of ALIX/AIP1 and Its Role in Retrovirus Budding. *Cell*, *128*(5), 841–852. https://doi.org/10.1016/j.cell.2007.01.035

Fletcher, T. M., Soares, M. A., McPhearson, S., Hui, H., Wiskerchen, M. A., Muesing, M. A., Shaw, G. M., Leavitt, A. D., Boeke, J. D., & Hahn, B. H. (1997). Complementation of integrase function in HIV-1 virions. *EMBO Journal*, *16*(16), 5123–5138. https://doi.org/10.1093/emboj/16.16.5123

Fontenot, D., He, H., Hanabuchi, S., Nehete, P. N., Zhang, M., Chang, M., Nehete, B., Wang, Y. H., Wang, Y. H., Ma, Z. M., Lee, H. C., Ziegler, S. F., Courtney, A. N., Miller, C. J., Sun, S. C., Liu, Y. J., & Jagannadha Sastry, K. (2009). TSLP production by epithelial cells exposed to immunodeficiency virus triggers DC-mediated mucosal infection of CD4+ T cells. *Proceedings of the National Academy of Sciences of the United States of America*, *106*(39), 16776–16781. https://doi.org/10.1073/pnas.0907347106

Gallay, P., Stitt, V., Trono, D., Mundy, C., & Oettinger, M. (1996). Role of the karyopherin pathway in human immunodeficiency virus type 1 nuclear import. *Journal of Virology*, *70*(2), 1027–1032.

Gamble, T. R., Yoo, S., Vajdos, F. F., Von Schwedler, U. K., Worthylake, D. K., Wang, H., McCutcheon, J. P., Sundquist, W. I., & Hill, C. P. (1997). Structure of the carboxyl-terminal dimerization domain of the HIV-1 capsid protein. *Science*, *278*(5339), 849–853. https://doi.org/10.1126/science.278.5339.849

Gardiner, A., Sullivan, M., & Grand, A. (2018). Who Are You Writing for? Differences in Response to Blog Design Between Scientists and Nonscientists. *Science Communication*, *40*(1), 109–123. https://doi.org/10.1177/1075547017747608

Garrus, J. E., Von Schwedler, U. K., Pornillos, O. W., Morham, S. G., Zavitz, K. H., Wang, H. E., Wettstein, D. A., Stray, K. M., Côté, M., Rich, R. L., Myszka, D. G., & Sundquist, W. I. (2001). Tsg101 and the vacuolar protein sorting pathway are essential for HIV-1 budding. *Cell*, *107*(1), 55–65. https://doi.org/10.1016/S0092-8674(01)00506-2

Ghosh, A. K., Osswald, H. L., & Prato, G. (2016). Recent Progress in the Development of HIV-1 Protease Inhibitors for the Treatment of HIV/AIDS. *Journal of Medicinal Chemistry*, *59*(11), 5172–5208. https://doi.org/10.1021/acs.jmedchem.5b01697

Gibbs, J. S., Lackner, A. A., Lang, S. M., Simon, M. A., Sehgal, P. K., Daniel, M. D., & Desrosiers, R. C. (1995). Progression to AIDS in the absence of a gene for vpr or vpx. *Journal of Virology*, *69*(4), 2378–2383. http://www.ncbi.nlm.nih.gov/pubmed/7884883%0Ahttp://www.pubmedcentral.nih.gov/articlerender.fcgi?artid=PMC188910

Gottlinger, H. G., Sodroski, J. G., & Haseltine, W. A. (1989). Role of capsid precursor processing and myristoylation in morphogenesis and infectivity of human immunodeficiency virus type 1. *Proceedings of the National Academy of Sciences of the United States of America*, *86*(15), 5781–5785. https://doi.org/10.1073/pnas.86.15.5781

Göttlinger, H. G., Bukovsky, A. A., Dorfman, T., & Weimann, A. (1997). Nef association with human immunodeficiency virus type 1 virions and cleavage by the viral protease. *Journal of Virology*, *71*(2), 1013–1018.

Hahn, F., Schmalen, A., Setz, C., Friedrich, M., Schlößer, S., Kölle, J., Spranger, R., Rauch, P., Fraedrich, K., Reif, T., Karius-Fischer, J., Balasubramanyam, A., Henklein, P., Fossen, T., & Schubert, U. (2017). Proteolysis of mature HIV-1 p6 Gag protein by the insulin-degrading enzyme (IDE) regulates virus replication in an Env-dependent manner. *PLoS ONE*, *12*(4), 1–29. https://doi.org/10.1371/journal.pone.0174254

Harris, R. S., Bishop, K. N., Sheehy, A. M., Craig, H. M., Petersen-Mahrt, S. K., Watt, I. N., Neuberger, M. S., & Malim, M. H. (2003). DNA deamination mediates innate immunity to retroviral infection. *Cell*, *113*(6), 803–809. https://doi.org/10.1016/S0092-8674(03)00423-9

Harrison, G. P., & Lever, A. M. (1992). The human immunodeficiency virus type 1 packaging signal and major splice donor region have a conserved stable secondary structure. *Journal of Virology*, *66*(7), 4144–4153. https://doi.org/10.1128/jvi.66.7.4144-4153.1992

Harte Jr., W. E., Swaminathan, S., Mansuri, M. M., Martin, J. C., Rosenberg, I. E., & Beveridge, D. L. (1990). Domain communication in the dynamical structure of human immunodeficiency virus 1 protease. *Proceedings of the National Academy of Sciences of the United States of America*, *87*(22), 8864–8868. https://doi.org/10.1073/pnas.87.22.8864

Heinzinger, N. K., Bukrinsky, M. I., Haggerty, S. A., Ragland, A. M., Kewalramani, V., Lee, M. A., Gendelman, H. E., Ratner, L., Stevenson, M., & Emerman, M. (1994). The Vpr protein of human immunodeficiency virus type 1 influences nuclear localization of viral nucleic acids in nondividing host cells. *Proceedings of the National Academy of Sciences of the United States of America*, *91*(15), 7311–7315. https://doi.org/10.1073/pnas.91.15.7311

Hellen, C. U. T., Kräusslich, H. G., & Wimmer, E. (1989). Proteolytic Processing of Polyproteins in the Replication of RNA Viruses. *Biochemistry*, *28*(26), 9881–9890. https://doi.org/10.1021/bi00452a001

Hirsch, V. M., Sharkey, M. E., Brown, C. R., Brichacek, B., Goedstein, S., Wakefield, J., Byrum, R., Elkins, W. R., Hahn, B. H., Lifson, J. D., & Stevenson, M. (1998). Vpx is required for dissemination and pathogenesis of SIV(SM) PBj: Evidence of

macrophage-dependent viral amplification. *Nature Medicine*, *4*(12), 1401–1408. https://doi.org/10.1038/3992

Hornak, V., Okur, A., Rizzo, R. C., & Simmerling, C. (2006). HIV-1 protease flaps spontaneously open and reclose in molecular dynamics simulations. *Proceedings of the National Academy of Sciences of the United States of America*, *103*(4), 915–920. https://doi.org/10.1073/pnas.0508452103

Hrimech, M., Yao, X. J., Bachand, F., Rougeau, N., & Cohen, E. A. (1999). Human immunodeficiency virus type 1 (HIV-1) Vpr functions as an immediate-early protein during HIV-1 infection. *Journal of Virology*, *73*(5), 4101–4109. http://www.ncbi.nlm.nih.gov/pubmed/10196306%0Ahttp://www.pubmedcentral.nih.gov/articlerender.fcgi?artid=PMC104189

Huang, M., Orenstein, J. M., Martin, M. A., & Freed, E. O. (1995). p6Gag is required for particle production from full-length human immunodeficiency virus type 1 molecular clones expressing protease. *Journal of Virology*, *69*(11), 6810–6818. http://www.pubmedcentral.nih.gov/articlerender.fcgi?artid=189593&tool=pmcentrez&rendertype=abstract

Inoué, S., Shimomura, O., Goda, M., Shribak, M., & Tran, P. T. (2002). Fluorescence polarization of green fluorescence protein. *Proceedings of the National Academy of Sciences of the United States of America*, *99*(7), 4272–4277. https://doi.org/10.1142/9789812790866_0070

Jacks, T., Powert, M. D., Masiarzt, F. R., Luciwt, P. A., Barrt, P. J., & Varmus, H. E. (1988). Characterization of ribosomal frameshifting in HIV-1 gag-pol expression. *Nature*, *331*(21), 280–283.

Jenkins, Y., Pornillos, O., Rich, R. L., Myszka, D. G., Sundquist, W. I., & Malim, M. H. (2001). Biochemical Analyses of the Interactions between Human Immunodeficiency Virus Type 1 Vpr and p6Gag. *Journal of Virology*, *75*(21), 10537–10542. https://doi.org/10.1128/jvi.75.21.10537-10542.2001

JH, H. (2015). ESCRTs are everywhere. *Embo J*, *34*(19), 2398–2407. http://dx.doi.org/10.15252/embj.201592484

Johnson, D. S., Bleck, M., & Simon, S. M. (2018). Timing of ESCRT-III protein recruitment and membrane scission during HIV-1 assembly. *ELife*, *7*, 1–20. https://doi.org/10.7554/eLife.36221

Johnson, D. S., Toledo-Crow, R., Mattheyses, A. L., & Simon, S. M. (2014). Polarization-controlled TIRFM with focal drift and spatial field intensity correction. *Biophysical Journal*, *106*(5), 1008–1019. https://doi.org/10.1016/j.bpj.2013.12.043

Jones, D. M., & Padilla-Parra, S. (2015). Imaging real-time HIV-1 virion fusion with FRET-based biosensors. *Scientific Reports*, *5*, 1–10. https://doi.org/10.1038/srep13449

Jouvenet, N., Bieniasz, P. D., & Simon, S. M. (2008). Imaging the biogenesis of individual HIV-1 virions in live cells. *Nature*, *454*(7201), 236–240. https://doi.org/10.1038/nature06998

Jouvenet, N., Neil, S. J. D., Bess, C., Johnson, M. C., Virgen, C. A., Simon, S. M., & Bieniasz, P. D. (2006). Plasma membrane is the site of productive HIV-1 particle

assembly. *PLoS Biology*, *4*(12), 2296–2310. https://doi.org/10.1371/journal.pbio.0040435

Jouvenet, N., Simon, S. M., & Bieniasz, P. D. (2009). Imaging the interaction of HIV-1 genomes and Gag during assembly of individual viral particles. *Proceedings of the National Academy of Sciences of the United States of America*, *106*(45), 19114–19119. https://doi.org/10.1073/pnas.0907364106

Jouvenet, N., Zhadina, M., Bieniasz, P. D., & Simon, S. M. (2011). Dynamics of ESCRT protein recruitment during retroviral assembly. *Nature Cell Biology*, *13*(4), 394–402. https://doi.org/10.1038/ncb2207

Kahn, J. O., & Walker, B. D. (1998). Acute Human Immunodeficiency Virus Type 1 Infection. *The New England Journal of Medicine*, *339*(1), 33–39.

Kampmann, M., Atkinson, C. E., Mattheyses, A. L., & Simon, S. M. (2011). Mapping the orientation of nuclear pore proteins in living cells with polarized fluorescence microscopy. *Nature Structural and Molecular Biology*, *18*(6), 643–649. https://doi.org/10.1038/nsmb.2056

Kao, S., Khan, M. A., Miyagi, E., Plishka, R., Buckler-White, A., & Strebel, K. (2003). The Human Immunodeficiency Virus Type 1 Vif Protein Reduces Intracellular Expression and Inhibits Packaging of APOBEC3G (CEM15), a Cellular Inhibitor of Virus Infectivity. *Journal of Virology*, *77*(21), 11398–11407. https://doi.org/10.1128/jvi.77.21.11398-11407.2003

Karacostas, V., Wolffe, E. J., Nagashima, K., Gonda, M. A., & Moss, B. (1993). Overexpression of the HIV-1 gag-pol polyprotein results in intracellular activation of HIV-1 protease and inhibition of assembly and budding of virus-like particles. In *Virology* (Vol. 193, pp. 661–671). https://doi.org/S0042-6822(83)71174-8 [pii]\r10.1006/viro.1993.1174

Khan, M. A., Aberham, C., Kao, S., Akari, H., Gorelick, R., Bour, S., & Strebel, K. (2001). Human Immunodeficiency Virus Type 1 Vif Protein Is Packaged into the Nucleoprotein Complex through an Interaction with Viral Genomic RNA. *Journal of Virology*, *75*(16), 7252–7265. https://doi.org/10.1128/jvi.75.16.7252-7265.2001

Kirkpatrick, E., Gaisford, W., Williams, E., Brindley, E., Tembo, D., & Wright, D. (2017). Understanding Plain English summaries. A comparison of two approaches to improve the quality of Plain English summaries in research reports. *Research Involvement and Engagement*, *3*(1), 17. https://doi.org/10.1186/s40900-017-0064-0

Kohl, N. E., Emini, E. A., Schleif, W. A., Davis, L. J., Heimbach, J. C., Dixon, R. A. F., Scolnick, E. M., & Sigal, I. S. (1988). Active human immunodeficiency virus protease is required for viral infectivity. *Proceedings of the National Academy of Sciences of the United States of America*, *85*(13), 4686–4690. https://doi.org/10.1073/pnas.85.13.4686

Kondo, E., & Göttlinger, H. G. (1996). A conserved LXXLF sequence is the major determinant in p6gag required for the incorporation of human immunodeficiency virus type 1 Vpr. *Journal of Virology*, *70*(1), 159–164. http://www.ncbi.nlm.nih.gov/pubmed/8523520%0Ahttp://www.pubmedcentral.nih.gov/articlerender.fcgi?artid=PMC189800

Krausslich, H., & Wimmer, E. (1988). Viral proteinases. *Annual Review of Biochemistry*, *57*, 701–754.

Lam, A. J., St-Pierre, F., Gong, Y., Marshall, J. D., Cranfill, P. J., Baird, M. A., McKeown, M. R., Wiedenmann, J., Davidson, M. W., Schnitzer, M. J., Tsien, R. Y., & Lin, M. Z. (2012). Improving FRET dynamic range with bright green and red fluorescent proteins. *Nature Methods*, *9*(10), 1005–1012. https://doi.org/10.1038/nmeth.2171

Larson, D. R., Johnson, M. C., Webb, W. W., & Vogt, V. M. (2005). Visualization of retrovirus budding with correlated light and electron microscopy. *Proceedings of the National Academy of Sciences of the United States of America*, *102*(43), 15453–15458. https://doi.org/10.1073/pnas.0504812102

Lata, S., Schoehn, G., Jain, A., Pires, R., Piehler, J., Gottlinger, H. G., & Weissenhorn, W. (2008). Helical structures of ESCRT-III are disassembled by VPS4. *Science*, *321*(5894), 1354–1357. https://doi.org/10.1126/science.1161070

Lecossier, D., Bouchonnet, F., Clavel, F., & Hance, A. J. (2003). Hypermutation of HIV-1 DNA in the absence of the Vif protein. *Science*, *300*(5622), 1112. https://doi.org/10.1126/science.1083338

Lee, H. H., Elia, N., Ghirlando, R., Lippincott-Schwartz, J., & Hurley, J. H. (2008). Midbody targeting of the ESCRT machinery by a noncanonical coiled coil in CEP55. *Science*, *322*(5901), 576–580. https://doi.org/10.1126/science.1162042

Lee, S. K., Potempa, M., Kolli, M., Özen, A., Schiffer, C. A., & Swanstrom, R. (2012). Context surrounding processing sites is crucial in determining cleavage rate of a subset of processing sites in HIV-1 gag and gag-pro-pol polyprotein precursors by viral protease. *Journal of Biological Chemistry*, *287*(16), 13279–13290. https://doi.org/10.1074/jbc.M112.339374

Lever, A., Gottlinger, H., Haseltine, W., & Sodroski, J. (1989). Identification of a Sequence Required for Efficient Packaging of Human Immunodeficiency Virus Type 1 RNA into Virions. *Journal of Virology*, *63*(9), 4085–4087. https://doi.org/10.1007/978-3-319-19674-9_45

Levy, D. N., Aldrovandi, G. M., Kutsch, O., & Shaw, G. M. (2004). Dynamics of HIV-1 recombination in its natural target cells. *Proceedings of the National Academy of Sciences of the United States of America*, *101*(12), 4204–4209. https://doi.org/10.1073/pnas.0306764101

Lindeberg, T. (1998). Feature Detection with Automatic Scale Selection. *International Journal of Computer Vision*, *30*(2), 79–116. https://doi.org/10.1023/A:1008045108935

Liu, B., Yu, X., Luo, K., Yu, Y., & Yu, X.-F. (2004). Influence of Primate Lentiviral Vif and Proteasome Inhibitors on Human Immunodeficiency Virus Type 1 Virion Packaging of APOBEC3G. *Journal of Virology*, *78*(4), 2072–2081. https://doi.org/10.1128/jvi.78.4.2072-2081.2004

Liu, H., Wu, X., Xiao, H., Conway, J. A., & Kappes, J. C. (1997). Incorporation of functional human immunodeficiency virus type 1 integrase into virions independent of the Gag-Pol precursor protein. *Journal of Virology*, *71*(10), 7704–7710.

http://www.pubmedcentral.nih.gov/articlerender.fcgi?artid=192121&tool=pmcentrez&rendertype=abstract

Louis, J. M., Marius Clore, G., & Gronenborn, A. M. (1999). Autoprocessing of HIV-1 protease is tightly coupled to protein folding. *Nature Structural Biology*, *6*(9), 868–875. https://doi.org/10.1038/12327

Luban, J., & Goff, S. P. (1994). Mutational analysis of cis-acting packaging signals in human immunodeficiency virus type 1 RNA. *Journal of Virology*, *68*(6), 3784–3793. https://doi.org/10.1128/jvi.68.6.3784-3793.1994

Luo, T., Anderson, S. J., & Garcia, J. V. (1996). Inhibition of Nef- and phorbol ester-induced CD4 degradation by macrolide antibiotics. *Journal of Virology*, *70*(3), 1527–1534. https://doi.org/10.1128/jvi.70.3.1527-1534.1996

Maddon, P. J., Dalgleish, A. G., McDougal, J. S., Clapham, P. R., Weiss, R. A., & Axel, R. (1986). The T4 gene encodes the AIDS virus receptor and is expressed in the immune system and the brain. *Cell*, *47*(3), 333–348. https://doi.org/10.1016/0092-8674(86)90590-8

Malerød, L., & Stenmark, H. (2009). ESCRTing Membrane Deformation. *Cell*, *136*(1), 15–17. https://doi.org/10.1016/j.cell.2008.12.029

Mammano, F., Kondo, E., Sodroski, J., Bukovsky, A., & Göttlinger, H. G. (1995). Rescue of human immunodeficiency virus type 1 matrix protein mutants by envelope glycoproteins with short cytoplasmic domains. *Journal of Virology*, *69*(6), 3824–3830. https://doi.org/10.1128/jvi.69.6.3824-3830.1995

Mangeat, B., Turelli, P., Caron, G., Friedli, M., Perrin, L., & Trono, D. (2003). Broad antiretroviral defence by human APOBEC3G through lethal editing of nascent reverse transcripts. *Nature*, *424*(6944), 99–103. https://doi.org/10.1038/nature01709

Marin, M., Rose, K. M., Kozak, S. L., & Kabat, D. (2003). HIV-1 Vif protein binds the editing enzyme APOBEC3G and induces its degradation. *Nature Medicine*, *9*(11), 1398–1403. https://doi.org/10.1038/nm946

Martin Stoltzfus, C. (2009). Chapter 1 Regulation of HIV-1 Alternative RNA Splicing and Its Role in Virus Replication. In *Advances in Virus Research* (1st ed., Vol. 74, Issue 09). Elsevier Inc. https://doi.org/10.1016/S0065-3527(09)74001-1

Martin-Serrano, J., Zang, T., & Bieniasz, P. D. (2001). HIV-1 and Ebola virus encode small peptide motifs that recruit Tsg101 to sites of particle assembly to facilitate egress. *Nature Medicine*, *7*(12), 1313–1319. https://doi.org/10.1038/nm1201-1313

Martin-Serrano, J., Yaravoy, A., Perez-Caballero, D., & Bieniasz, P. D. (2003). Divergent retroviral late-budding domains recruit vacuolar protein sorting factors by using alternative adaptor proteins. *Proceedings of the National Academy of Sciences of the United States of America*, *100*(21), 12414–12419. https://doi.org/10.1073/pnas.2133846100

Mattei, S., Anders, M., Konvalinka, J., Krausslich, H.-G., Briggs, J. A. G., & Muller, B. (2014). Induced Maturation of Human Immunodeficiency Virus. *Journal of Virology*, *88*(23), 13722–13731. https://doi.org/10.1128/jvi.02271-14

Mattei, S., Tan, A., Glass, B., Müller, B., Kräusslich, H. G., & Briggs, J. A. G. (2018). High-resolution structures of HIV-1 Gag cleavage mutants determine structural switch for virus maturation. *Proceedings of the National Academy of Sciences of the United States of America*, *115*(40), E9401–E9410. https://doi.org/10.1073/pnas.1811237115

Mattheyses, A. L., Kampmann, M., Atkinson, C. E., & Simon, S. M. (2010). Fluorescence anisotropy reveals order and disorder of protein domains in the nuclear pore complex. *Biophysical Journal*, *99*(6), 1706–1717. https://doi.org/10.1016/j.bpj.2010.06.075

McNatt, M. W., Zang, T., & Bieniasz, P. D. (2013). Vpu Binds Directly to Tetherin and Displaces It from Nascent Virions. *PLoS Pathogens*, *9*(4), 40–44. https://doi.org/10.1371/journal.ppat.1003299

Mohammed, K. D., Topper, M. B., & Muesing, M. A. (2011). Sequential Deletion of the Integrase (Gag-Pol) Carboxyl Terminus Reveals Distinct Phenotypic Classes of Defective HIV-1. *Journal of Virology*, *85*(10), 4654–4666. https://doi.org/10.1128/jvi.02374-10

Morita, E., Sandrin, V., McCullough, J., Katsuyama, A., Baci Hamilton, I., & Sundquist, W. I. (2011). ESCRT-III protein requirements for HIV-1 budding. *Cell Host and Microbe*, *9*(3), 235–242. https://doi.org/10.1016/j.chom.2011.02.004

Muller, B., Tessmer, U., Schubert, U., & Krausslich, H.-G. (2000). Human Immunodeficiency Virus Type 1 Vpr Protein Is Incorporated into the Virion in Significantly Smaller Amounts than Gag and Is Phosphorylated in Infected Cells. *Journal of Virology*, *74*(20), 9727–9731. https://doi.org/10.1128/jvi.74.20.9727-9731.2000

Muthumani, K., Montaner, L. J., Ayyavoo, V., & Weiner, D. B. (2004). Vpr-GFP Virion Particle Identifies HIV-Infected Targets and Preserves HIV-1Vpr Function in Macrophages and T-Cells. *DNA and Cell Biology*, *19*(3). https://doi.org/https://www.liebertpub.com/doi/pdf/10.1089/104454900314564

Neil, S. J. D., Zang, T., & Bieniasz, P. D. (2008). Tetherin inhibits retrovirus release and is antagonized by HIV-1 Vpu. *Nature*, *451*(7177), 425–430. https://doi.org/10.1038/nature06553

Newman, E. J., & Schwarz, N. (2018). Good Sound, Good Research: How Audio Quality Influences Perceptions of the Research and Researcher. *Science Communication*, *40*(2), 246–257. https://doi.org/10.1177/1075547018759345

Ott, D. E., Coren, L. V., Chertova, E. N., Gagliardi, T. D., Nagashima, K., Sowder, R. C., Poon, D. T. K., & Gorelick, R. J. (2003). Elimination of Protease Activity Restores Efficient Virion Production to a Human Immunodeficiency Virus Type 1 Nucleocapsid Deletion Mutant. *Journal of Virology*, *77*(10), 5547–5556. https://doi.org/10.1128/jvi.77.10.5547-5556.2003

Ott, D. E., Coren, L. V., & Shatzer, T. (2009). The Nucleocapsid Region of Human Immunodeficiency Virus Type 1 Gag Assists in the Coordination of Assembly and Gag Processing: Role for RNA-Gag Binding in the Early Stages of Assembly. *Journal of Virology*, *83*(15), 7718–7727. https://doi.org/10.1128/jvi.00099-09

Pandori, M. W., Fitch, N. J., Craig, H. M., Richman, D. D., Spina, C. A., & Guatelli, J. C. (1996). Producer-cell modification of human immunodeficiency virus type 1: Nef is a virion protein. *Journal of Virology*, *70*(7), 4283–4290. http://www.ncbi.nlm.nih.gov/pubmed/8676450%0Ahttp://www.pubmedcentral.nih.gov/articlerender.fcgi?artid=PMC190360

Pereira, E. A., & DaSilva, L. L. P. (2016). HIV-1 Nef: Taking Control of Protein Trafficking. *Traffic*, *17*(9), 976–996. https://doi.org/10.1111/tra.12412

Perryman, A. L., Lin, J.-H., & McCammon, J. A. (2004). HIV-1 protease molecular dynamics of a wild-type and of the V82F/I84V mutant: Possible contributions to drug resistance and a potential new target site for drugs. *Protein Science*, *13*(4), 1108–1123. https://doi.org/10.1110/ps.03468904

Pettit, S. C., Moody, M. D., Wehbie, R. S., Kaplan, A. H., Nantermet, P. V, Klein, C. A., & Swanstrom, R. (1994). The p2 domain of human immunodeficiency virus type 1 Gag regulates sequential proteolytic processing and is required to produce fully infectious virions. *Journal of Virology*, *68*(12), 8017–8027. https://doi.org/10.1128/jvi.68.12.8017-8027.1994

Pettit, S. C., Clemente, J. C., Jeung, J. A., Dunn, B. M., & Kaplan, A. H. (2005). Ordered Processing of the Human Immunodeficiency Virus Type 1 GagPol Precursor Is Influenced by the Context of the Embedded Viral Protease. *Journal of Virology*, *79*(16), 10601–10607. https://doi.org/10.1128/jvi.79.16.10601-10607.2005

Pettit, S. C., Everitt, L. E., Choudhury, S., Dunn, B. M., & Kaplan, A. H. (2004). Initial Cleavage of the Human Immunodeficiency Virus Type 1 GagPol Precursor by Its Activated Protease Occurs by an Intramolecular Mechanism. *Journal of Virology*, *78*(16), 8477–8485. https://doi.org/10.1128/jvi.78.16.8477-8485.2004

Poon, B., Grovit-Ferbas, K., Stewart, S. A., & Chen, I. S. Y. (1998). Cell cycle arrest by Vpr in HIV-1 virions and insensitivity to antiretroviral agents. *Science*, *281*(5374), 266–269. https://doi.org/10.1126/science.281.5374.266

Rakedzon, T., Segev, E., Chapnik, N., Yosef, R., & Baram-Tsabari, A. (2017). Automatic jargon identifier for scientists engaging with the public and science communication educators. *PloS One*, *12*(8), e0181742. https://doi.org/10.1371/journal.pone.0181742

Rocheleau, J. V., Edidin, M., & Piston, D. W. (2003). Intrasequence GFP in class I MHC molecules, a rigid probe for fluorescence anisotropy measurements of the membrane environment. *Biophysical Journal*, *84*(6), 4078–4086. https://doi.org/10.1016/S0006-3495(03)75133-9

Rodgers, P. (2017, March). Plain-language Summaries of Research: Writing for different readers. *ELife*. https://doi.org/10.7554/eLife.25408

Rodríguez Estrada, F. C., & Davis, L. S. (2015). Improving Visual Communication of Science Through the Incorporation of Graphic Design Theories and Practices Into Science Communication. *Science Communication*, *37*(1), 140–148. https://doi.org/10.1177/1075547014562914

Schmalen, A., Karius-Fischer, J., Rauch, P., Setz, C., Korn, K., Henklein, P., Fossen, T., & Schubert, U. (2018). The N-terminus of the HIV-1 p6 gag protein regulates

susceptibility to degradation by IDE. *Viruses*, *10*(12), 1–23. https://doi.org/10.3390/v10120710

Schur, F. K. M., Obr, M., Hagen, W. J. H., Wan, W., Jakobi, A. J., Kirkpatrick, J. M., Sachse, C., Kräusslich, H., & Briggs, J. A. G. (2016). An atomic model of HIV-1 capsid-SP1 reveals structures regulating assembly and maturation. *Science*, *353*(6298), 506–508.

Schwartz, O., Maréchal, V., Danos, O., & Heard, J. M. (1995). Human immunodeficiency virus type 1 Nef increases the efficiency of reverse transcription in the infected cell. *Journal of Virology*, *69*(7), 4053–4059. https://doi.org/10.1128/jvi.69.7.4053-4059.1995

Sheehy, A. M., Gaddis, N. C., Choi, J. D., & Malim, M. H. (2002). Isolation of a human gene that inhibits HIV-1 infection and is suppressed by the viral Vif protein. *Nature*, *418*, 646–650. https://doi.org/10.1038/nature00969.Published

Sheehy, A. M., Gaddis, N. C., & Malim, M. H. (2003). The antiretroviral enzyme APOBEC3G is degraded by the proteasome in response to HIV-1 Vif. *Nature Medicine*, *9*(11), 1404–1407. https://doi.org/10.1038/nm945

Strack, B., Calistri, A., Craig, S., Popova, E., & Göttlinger, H. G. (2003). AIP1/ALIX is a binding partner for HIV-1 p6 and EIAV p9 functioning in virus budding. *Cell*, *114*(6), 689–699. https://doi.org/10.1016/S0092-8674(03)00653-6

Swaminathan, R., Hoang, C. P., & Verkman, A. S. (1997). Photobleaching recovery and anisotropy decay of green fluorescent protein GFP-S65T in solution and cells: Cytoplasmic viscosity probed by green fluorescent protein translational and rotational diffusion. *Biophysical Journal*, *72*(4), 1900–1907. https://doi.org/10.1016/S0006-3495(97)78835-0

Takata, M. A., Gonçalves-Carneiro, D., Zang, T. M., Soll, S. J., York, A., Blanco-Melo, D., & Bieniasz, P. D. (2017). CG dinucleotide suppression enables antiviral defence targeting non-self RNA. *Nature*, *550*(7674), 124–127. https://doi.org/10.1038/nature24039

To, T. L., Schepis, A., Ruiz-González, R., Zhang, Q., Yu, D., Dong, Z., Coughlin, S. R., & Shu, X. (2016). Rational Design of a GFP-Based Fluorogenic Caspase Reporter for Imaging Apoptosis In Vivo. *Cell Chemical Biology*, *23*(7), 875–882. https://doi.org/10.1016/j.chembiol.2016.06.007

Toh, H., Masao, O., Kaoru, S., & Takashi, M. (1985). Retroviral protease-like sequence in the yeast transposon Ty 1. *Nature*, *315*(20), 691.

Toohey, K., Wehrly, K., Nishio, J., Perryman, S., & Chesebro, B. (1995). Human immunodeficiency virus envelope V1 and V2 regions influence replication efficiency in macrophages by affecting virus spread. *Virology*, *213*(1), 70–79. https://doi.org/10.1006/viro.1995.1547

Tritch, R. J., Cheng, Y. E., Yin, F. H., & Erickson-Viitanen, S. (1991). *Mutagenesis of Protease Cleavage Sites in the Human Immunodeficiency Virus Type 1 gag Polyprotein*. *65*(2), 922–930.

UNAIDS. (2019). *Fact Sheet--Global AIDS Update 2019*. https://www.unaids.org/sites/default/files/media_asset/UNAIDS_FactSheet_en.pdf

Varmus, H. (1988). Retroviruses. *Science*, *240*(4858), 1427–1435.

Von Schwedler, U. K., Stuchell, M., Müller, B., Ward, D. M., Chung, H. Y., Morita, E., Wang, H. E., Davis, T., He, G. P., Cimbora, D. M., Scott, A., Kräusslich, H. G., Kaplan, J., Morham, S. G., & Sundquist, W. I. (2003). The protein network of HIV budding. *Cell*, *114*(6), 701–713. https://doi.org/10.1016/S0092-8674(03)00714-1

Votteler, J., Ogohara, C., Yi, S., Hsia, Y., Nattermann, U., Belnap, D. M., King, N. P., & Sundquist, W. I. (2016). Designed proteins induce the formation of nanocage-containing extracellular vesicles. *Nature*, *540*(7632), 292–295. https://doi.org/10.1038/nature20607

Wehrly, K., & Chesebro, B. (1997). P24 Antigen Capture Assay for Quantification of Human Immunodeficiency Virus Using Readily Available Inexpensive Reagents. *Methods: A Companion to Methods in Enzymology*, *12*(4), 288–293. https://doi.org/10.1006/meth.1997.0481

Welker, R., Cardel, B., Kräusslich, H. G., & Harris, M. (1998). Virion incorporation of human immunodeficiency virus type 1 Nef is mediated by a bipartite membrane-targeting signal: Analysis of its role in enhancement of viral infectivity. *Journal of Virology*, *72*(11), 8833–8840.

Welker, R., Kottler, H., Kalbitzer, H. R., & Kräusslich, H. G. (1996). Human immunodeficiency virus type 1 Nef protein is incorporated into virus particles and specifically cleaved by the viral proteinase. *Virology*, *219*(1), 228–236. https://doi.org/10.1006/viro.1996.0240

Wollert, T., Wunder, C., Lippincott-Schwartz, J., & Hurley, J. H. (2009). Membrane scission by the ESCRT-III complex. *Nature*, *458*(7235), 172–177. https://doi.org/10.1038/nature07836

Wu, X., Liu, H., Xiao, H., Conway, J. A., Hunter, E., & Kappes, J. C. (1997). Functional RT and IN incorporated into HIV-1 particles independently of the Gag/Pol precursor protein. *EMBO Journal*, *16*(16), 5113–5122. https://doi.org/10.1093/emboj/16.16.5113

Wu, X., Liu, H., Xiao, H., Conway, J. A., & Kappes, J. C. (1996). Inhibition of human and simian immunodeficiency virus protease function by targeting Vpx-protease-mutant fusion protein into viral particles. *Journal of Virology*, *70*(6), 3378–3384.

Yu, H. J., Reuter, M. A., McDonald, D., Hyun, J. Y., Reuter, M. A., & McDonald, D. (2008). HIV traffics through a specialized, surface-accessible intracellular compartment during trans-infection of T cells by mature dendritic cells. *PLoS Pathogens*, *4*(8). https://doi.org/10.1371/journal.ppat.1000134

Yu, Q., Ottmann, M., Pechoux, C., Le Grice, S., & Darlix, J.-L. (1998). Mutations in the Primer Grip of Human Immunodeficiency Virus Type 1 Reverse Transcriptase Impair Proviral DNA Synthesis and Virion Maturation. *Journal of Virology*, *72*(9), 7676–7680. https://doi.org/10.1128/jvi.72.9.7676-7680.1998

Yu, X., Yu, Y., Liu, B., Luo, K., Kong, W., Mao, P., & Yu, X. F. (2003). Induction of APOBEC3G Ubiquitination and Degradation by an HIV-1 Vif-Cul5-SCF Complex. *Science*, *302*(5647), 1056–1060. https://doi.org/10.1126/science.1089591

Zamborlini, A., Usami, Y., Radoshitzky, S. R., Popova, E., Palu, G., & Göttlinger, H. (2006). Release of autoinhibition converts ESCRT-III components into potent inhibitors of HIV-1 budding. *Proceedings of the National Academy of Sciences of the United States of America*, *103*(50), 19140–19145. https://doi.org/10.1073/pnas.0603788103

Zhang, H., Yang, B., Pomerantz, R. J., Zhang, C., Arunachalam, S. C., & Gao, L. (2003). The cytidine deaminase CEM15 induces hypermutation in newly synthesized HIV-1 DNA. *Nature*, *424*(6944), 94–98. https://doi.org/10.1038/nature01707

Zhang, J., Wang, X., Cui, W., Wang, W., Zhang, H., Liu, L., Zhang, Z., Li, Z., Ying, G., Zhang, N., & Li, B. (2013). Visualization of caspase-3-like activity in cells using a genetically encoded fluorescent biosensor activated by protein cleavage. *Nature Communications*, *4*, 1–13. https://doi.org/10.1038/ncomms3157